

Université de Montréal

**Conception et Caractérisation de Nanoparticules Polymères
Théragnostiques Destinées au Traitement des Tumeurs Cérébrales**

par

Hoda Besheir

Faculté de Pharmacie

Thèse présentée à la Faculté des études supérieures en vue de l'obtention du grade de Maîtrise
(M.Sc.) en Sciences Pharmaceutiques option Technologie Pharmaceutique

Août, 2016

© Hoda Besheir, 2016

Résumé

L'intérêt de développer de nouvelles applications de la nanotechnologie pharmaceutique dans les soins de santé augmente année après année. Le rôle des nanosystèmes est devenu évident, surtout après que certains d'entre eux aient contribué à des solutions révolutionnaires dans des maladies graves. Dans notre projet, nous avons cherché à synthétiser des nanoparticules (NPs) intelligentes capables de livrer, de façon sélective, des agents anticancéreux. Les NPs ont été synthétisées afin de cibler des cellules cérébrales atteintes par le glioblastome multiforme (GBM), un cancer du cerveau présentant un mauvais pronostic et un taux de survie médian très faible. À cet effet, nous avons planifié de synthétiser et analyser ces nanoparticules et également d'étudier les preuves de concept de leur efficacité.

Tout d'abord, nous avons sélectionné avec soin, la procédure de formulation ainsi que les polymères avant d'optimiser les caractéristiques physico-chimiques des nanogels (NGs) formulés à base de chitosane.

Après l'optimisation de la taille, du PDI et du potentiel de surface des NGs, nous avons synthétisés des NGs chargés en substance active. Deux molécules thérapeutiques ont été retenues. La première était la doxorubicine HCl (DOX) qui est trop hydrophile pour passer la BHE, bien qu'ayant démontré une efficacité *in vitro* contre le GBM. Le deuxième médicament était le témozolomide (TMZ) qui est déjà utilisé dans le traitement de GBM, comme adjuvant à la radiothérapie, après l'intervention chirurgicale. Les méthodes d'analyses ont ensuite été développées pour déterminer l'efficacité du taux d'encapsulation (EE%) et l'efficacité de chargement de médicament (DLE%) des deux médicaments.

Pour la préparation des nanogels théranostiques, nous avons suivi les mêmes procédures après l'addition de l'agent de contraste USPIO, durant la synthèse des NGs.

Ensuite, nous avons besoin d'assurer la qualité de nos NGs lors du stockage à long terme. Pour atteindre cet objectif, nous avons développé une procédure de lyophilisation en utilisant différents sucres de nature et de concentrations variables. Les sucres ont été ajoutés pour cryoprotéger les NGs contre les contraintes mécaniques et physiques mises en jeu lors de la lyophilisation. Les sucres qui ont démontré des résultats satisfaisants avec NGs vides ont été utilisés, par la suite, dans la cryoprotection des NGs chargées de médicament au cours de leur lyophilisation.

Finalement, nous avons étudié la libération de la DOX à partir des NGs chargées avant et après lyophilisation. Cette étude, en particulier avait deux objectifs. Le premier était de comparer l'effet de la lyophilisation sur le comportement de la libération de DOX des NGs, en observant l'impact de cette procédure sur la cinétique de libération. Le deuxième but de l'étude de relargage était de tester la capacité des NGs à libérer leur contenu à trois pH différents : 5.8 (pH intracellulaire des cellules tumorales), 6.8 (espace interstitiel de la tumeur) et 7.4 (plasma sanguin).

Mots clés: GBM, doxorubicine, nanoparticules, nanogels, chitosane, lyophilisation, cryoprotecteurs.

Abstract

The interest in developing new applications of nanotechnology in the pharmaceutical health care increases year after year. The role of nanosystems became clearer, especially after some of them contributed to revolutionary solutions in serious diseases. In our project, we sought to synthesize ‘intelligent’ nanoparticles (NPs) capable of selectively delivering anticancer agents. NPs were synthesized to target brain cells affected by glioblastoma multiforme (GBM), a brain cancer with a poor prognosis and a very low rate of median survival. To this end, we planned to synthesize and analyze these nanoparticles and also to study the proof-of-concept of their efficiency.

First, we carefully selected the formulation process and the polymers prior to optimize physicochemical characteristics of the nanogels (NGs) formulated with chitosan.

After optimization of the NGs size, PDI and surface potential, we synthesized NGs loaded with active substances. Two therapeutic molecules were selected. First we chose doxorubicin HCl (DOX) which is too hydrophilic to cross the BBB, whereas demonstrating in vitro efficacy against GBM. The second drug was temozolomide (TMZ), already used in the treatment of GBM as an adjuvant to radiotherapy after surgery. Analytical methods were then developed to determine the encapsulation efficiency (EE %) and drug loading efficiency (DLE %) of both drugs.

For the preparation of theranostic nanogels, we followed the same procedures after the addition of the USPIO contrast agent during the NGs synthesis.

Next, we needed to ensure the quality of our NGs during long-term storage. To achieve this goal, we developed a freeze-drying process using different kind of sugar cryoprotectants at varying concentrations, in order to protect NGs against mechanical and physical stresses at play during freeze-drying. Most promising sugars used with unloaded NGs were subsequently used to cryoprotect DOX-loaded NGs.

Finally, we studied the release of DOX from DOX-loaded NGs before and after freeze-drying. This study in particular had two objectives. The first was to compare the effect of the freeze-drying process on the behavior of the DOX-loaded NGs, observing the impact of this procedure on the release kinetics. The second purpose of the release study was to test the ability of NGs to release their contents at three different pH: 5.8 (intracellular pH of tumor cells), 6.8 (interstitial space of the tumor) and 7.4 (blood plasma).

Keywords: GBM, doxorubicin, nanoparticles, nanogels, chitosan, freeze-drying, cryoprotectants.

Contents

Résumé	ii
Abstract	iii
List of tables	vii
List of figures	viii
List of abbreviations	ix
Contributions of coauthors	xiii
Acknowledgements	xiv
Chapter one	1
Introduction	1
1. Glioblastoma (GBM)	2
1.1 Background	2
1.2 Primary versus Secondary glioblastomas	3
Primary GBM:	3
Secondary GBMs:	3
1.3 Understanding the poor prognosis of GBM from a pathological point of view	3
1.4 Epidemiology	5
1.5 Symptoms	6
1.6 Diagnosis	6
1.6.1 Pathological reports produced to initially differentiate 1 ^{ry} from 2 ^{ry} GBMs, Immunohistochemistry (IHC) tests	6
1.6.2 Diagnosis using imaging techniques used to localize the tumor in the brain	7
2. Current treatments:	10
2.1 Currently available treatment strategies for GBMs	10
2.1.1 Surgical intervention	11
2.1.2 Post-operative treatment	11
2.1.3 <i>In vivo</i> and <i>in vitro</i> -effective drug entities in treating GBM	12
2.2 Multidrug resistance (MDR)	17
2.3 Understanding the blood-brain barrier (BBB)	18
3. Novel treatment strategies	20
3.1 Pharmaceutical nanotechnology	20
3.1.1 Polymers and materials used in NP synthesis	21
3.1.2 Different generations of nanoparticles	23

3.1.3	Promising role of pharmaceutical nanotechnology in brain cancer treatment.....	28
3.1.4	Examples of overcoming formulation challenges by pharmaceutical nanotechnology.....	28
3.1.5	Theranostic nanoparticles	31
3.2	Hypothesis and specific objectives	32
4.	References.....	35
5.	Techniques used in physicochemical characterization of NPs:	42
5.1.1	<i>Dynamic light scattering, DLS:</i>	42
5.1.2	<i>Electrophoretic light scattering, ELS:</i>	43
6.	Techniques used in investigating NPs stability:.....	45
6.1.1	<i>Differential scanning calorimetry, DSC:</i>	45
6.1.2	<i>Fourier Transform Infrared Spectroscopy, FTIR:</i>	47
6.1.3	<i>Freeze-drying, FD:</i>	49
Chapter two	51
	Introduction to the reported results.....	51
	Part one	54
	Article	54
▪	Materials and Methods.....	57
1.1.	<i>Materials</i>	57
1.2.	<i>Methods</i>	57
1.3.	<i>Synthesis of blank and DOX-loaded NGs</i>	57
1.4.	<i>NG purification</i>	57
1.5.	<i>NG freeze-drying process</i>	57
1.6.	<i>NG physicochemical characterization</i>	58
1.7.	<i>Doxorubicin quantification</i>	59
1.8.	<i>Doxorubicin release study before and after freeze-drying</i>	59
1.9.	<i>Degradation kinetics of DOX</i>	60
▪	Results.....	60
1.10.	<i>NG physicochemical characterization</i>	60
1.11.	<i>Thermal Analysis (Differential Scanning Calorimetry, DSC)</i>	61
1.12.	<i>Fourier Transform Infrared (FT-IR) analysis</i>	62
1.13.	<i>Freeze-drying (FD) process</i>	63
1.14.	<i>Degradation kinetics of DOX</i>	65
1.15.	<i>Doxorubicin release study before and after freeze-drying</i>	65

▪ Discussion.....	66
▪ Conclusion.....	69
Supporting information	73
Part two.....	76
Materials.....	76
Method	76
Results& discussion.....	78
Part three	82
General discussion	82
References.....	87
Conclusion.....	96
Perspectives	99

List of tables

Table 1. Different grades of glioma according to classification by world health organization (WHO).....	2
Table 2. Median age at diagnosis and age-adjusted average annual (1998–2002) incidence rates of adult gliomas	5
Table 3. Positive results are shown in percentage after applying each of the six immunostains to biopsies from both types of GBMs.....	7
Table 4. Results observed from different clinical studies aimed to investigate efficacy and safety of TMZ	14
Table 5: Results obtained for DLS/ELS characterization for TMZ-loaded nanogels using HMW-CH, USPIO-loaded nanogels, USPIO/Dox- and USPIO/TMZ-loaded nanogels,.....	80

List of figures

Figure 1. Comparing different pathways due to normal and mutant IDH1	4
Figure 2a. CT scan image showing the brain affected by GBM.....	8
Figure 2b. Computed tomography: acquisition with one single slice (left) and multislice CT with four active acquisition channels.....	8
Figure 3. Illustrations showing an overview on magnetic resonance imaging.....	9
Figure 4. MRI images before and after (left) of GBM-affected brain.....	10
Figure 5. Chemical structures of different chemotherapeutics.....	13
Figure 6. An illustration of the BBB structure showing its different components.....	19
Figure 7. A simple diagram illustrating the different stages of drug-loaded nanoparticle development to improve their target specificity	24
Figure 8. The EPR effect in the tumor tissue	25
Figure 9. pH-sensitive chitosan conjugated nanocarrier interactions	27
Figure 10. A hypothetical structure of the final drug-loaded chitosan/hyaluronic acid-based theranostic nanogels.....	32
Figure 11. Illustrations for DLS technique.....	42
Figure 12. A typical DLS graph showing a single population of NPs.....	43
Figure 13. Cuvette for Zeta potential (ZP) measurements containing two opposite electrodes...	44
Figure 14. Zeta Potential of chitosan-based NPs measured by the ELS technique	45
Figure 15. The heat excess and DSC measurement technique for sample and reference	46
Figure 16. Thermogram of chitosan powder.....	47
Figure 17. A scheme showing FTIR Michelson technique	48
Figure 18. Chitosan IR spectrum	49
Figure 19 Schemes of different troubles encountered the process of freeze-drying.....	50

List of abbreviations

2-HG	2-hydroxy glutarate
ABC	ATP-binding cassette
ALPs	alkyl-lysophospholipids
ATP	Adenosine tri-phosphate
BBB	Blood brain barrier
BCNU	Carmustine
BCRP	Breast cancer resistant proteins
BEV	Bevacizumab
CAM	Cell adhesion molecule
CBTRUS	Central brain tumor registry of the United States
CCNU	Lumostine
CH	Chitosan
CIMP	CpG island methylator phenotype
CK	Cytokeratine
CpG	DNA sequence where a cytosine base is followed by a guanine one
CT	Computed tomography
Da	Dalton
DC	Dendritic cells
DDS	Drug delivery system
DLE%	Percentage of drug loading efficiency
DLS	Dynamic light scattering
DNA	Deoxyribonucleic acid
DOX	Doxorubicin
DSC	Differential scanning calorimetry
EE%	Percentage of encapsulation efficiency
EGFR	Epidermal growth factor receptors
ELS	Electric light scattering
EPR	Enhanced permeation retention
ET	Edelfosine
FD	Freeze-drying
FDA	US Food and Drug Administration
FTIR	Fourier Transform Infrared
GBM	Glioblastoma multiforme
Gd³⁺	Gadolinium
GFAP	Glial fibrillary acidic protein
GFP	Green fluorescent protein
GST	Glutathione-S-transferase
HA	Hyaluronic acid
IDH	Isocitrate dehydrogenase
IgG	Immunoglobulin G
IHC	Immunohistochemistry
LC/MS-MS	Liquid Chromatography - Mass Spectrometry and Liquid Chromatography - Tandem Mass Spectrometry
LMW	Low molecular weight

mAbs	Monoclonal antibodies
MDM	Murine double minute
MDR	Multi drug resistance
MGMT	Methyl guanine methyl transferase
mo	Month (unit used to measure mPFS & mOS)
mOS	Median overall survival
mPFS	Median progression-free survival
MPS	Mononuclear phagocytes system
MR	Magnetic resonance
MRI	Magnetic resonance imaging
MRPs	Multi-drug resistance associated proteins
mTOR	Mechanistic target of rapamycin
mV	Milli volt
MWCO	Molecular weight cut-off
NG	Nanogel
nm	Nanometer
nM	Nanomolar
NOS	Not otherwise specified
NP	Nanoparticle
PCL	Poly (epsilon-caprolactone)
PdI	Polydispersity index
PdI_f	Final polydispersity index (i.e. after FD)
PdI_i	Initial polydispersity index (i.e. prior to FD)
PEG	Polyethylene glycol
PEO-PCL	Poly(ethylene oxide)-modified poly(epsilon-caprolactone)
p-gp	P-glycoprotein
PLGA	poly(lactic-co-glycolic acid)
PNGs	Plasmonic nanogels
PY%	Percentage of production yield
ref	Reference
RF	Radiofrequency
S_f	Final size (i.e. after FD)
S_i	Initial size (i.e. prior to FD)
t_{1/2}	Half-life time
TAA_s	Tumor associated antigens
Tg'	Glass transition temperature
TMZ	Temozolomide
TMZ-NP	Temozolomide-loaded nanoparticles
TPP	Tripolyphosphate
TSA_s	Tumor specific antigens
TTF_s	Tumor treating fields
UK	United Kingdom
US/USA	United States of America
USPIO	Ultra-small super paramagnetic iron oxide
V	Volt
vs	Versus

WHO
ZP

World Health Organization
Zeta potential

To the soul of Mahmoud Abdel-aziz, R.I.P.

Contributions of coauthors

This thesis is based on two chapters. Part one of chapter two is an article containing the major part of our project. The contribution of each author to the article is described as below:

Chapter two (part one): Recoverability of freeze-dried doxorubicin-loaded, chitosan-based nanogels: a physicochemical study

Hoda Besheir¹, Hugo Alarie¹, Martin Jutras², V. Gaëlle Roullin^{1, 2*}

The NG synthesis, physicochemical characterization as well as their freeze-drying is a team work of Hoda Besheir and Hugo Alarie. The DSC, FT-IR experiments and release study were accomplished by Hoda Besheir. LC-MS/MS method development in the DOX quantification to obtain encapsulation efficiency as well as determining remaining DOX concentrations in the release study was done by Martin Jutras. The work follow up and review was done by the director of research prof. V. Gaëlle Roullin.

Acknowledgements

First of all I would like to thank my supervisor, Prof. V. Gaëlle Roullin, for the patient guidance, encouragement and advice she has provided throughout my time as her student.

I would also like to thank the members of my advisory committee, Prof. Jeanne Leblond-Chain and Prof. Grégoire Leclair, for their generosity and for taking the time to evaluate my work.

Special thanks to my coworkers and coauthors:

- Martin Jutras, B.Sc., HPLC-MS/MS specialist, platform of biopharmacy, for his great help in developing methods to analyze our samples.
- Hugo Alarie, 3rd year biopharmacy student, for the contributions he made to my project particularly his work in the freeze-drying process and release kinetics experiments
- Dounia Boumahni, B.Sc. in biopharmacy, for helping us in the NGs synthesis and their freeze-drying.

Great thanks to my colleagues in the laboratory of pharmaceutical nanotechnology, Valéry Aoun (Post-Doc.), Soudeh Tehrani (Ph.D. candidate) and Florian Bernard (Ph.D. candidate) as well as all members of department of formulation and analysis for their guidance and for answering my inquiries whenever I asked for their help.

Thanks to Mary Salib, student in D.E.S.S drug development, B.Sc. biopharmaceutical sciences for editing the French summary.

Chapter one

Introduction

1. Glioblastoma (GBM)

1.1 Background

Glioma is a general term used to describe brain tumors which affect glial cells, the glue-like supportive tissue of the brain.(1) A subtype of gliomas is the astrocytic tumors or so-called astrocytomas. Astrocytomas are named after the astrocytes, the star-shaped cells they grow from.(2) According to their degree of aggressiveness, astrocytomas are classified, following an ascending order into 4 grades from I to IV, grade I being the least aggressive while grade IV is the most aggressive one.(3) This classification also reflects the degree of growth and tendency of the tumor to recur.(3) For example, grades I and II are low-grade astrocytomas that grow relatively slowly and are considered benign tumors manageable by surgical excision. Both grades III and IV are malignant types and require more aggressive treatment strategies.(3, 4) Grade IV glioma, also called glioblastoma (GBM), is a fast-growing tumor with very low prognosis, hence its high degree of malignancy and aggressiveness. It also has a very short median survival rate (14.9 months).(5) Main characteristics of each glioma type are outlined in table 1.

Table 1: Different grades of glioma according to classification by world health organization (WHO).*Adapted from reference (3)*

WHO grade	Histologic Characteristics
Grade I	Includes lesions with low proliferative potential and a frequently discrete nature; surgical resection is the main treatment.
Grade II	Includes lesions that are generally infiltrating and low in mitotic activity but recur. Some tumor types tend to progress to higher grades of malignancy.
Grade III	Includes lesions with histologic evidence of malignancy, generally in the form of mitotic activity, clearly expressed infiltrative capabilities, and anaplasia.
Grade IV	Includes lesions that are mitotically active with vascular proliferation, necrosis-prone, and generally associated with a rapid preoperative and postoperative evolution of disease.

Unfortunately GBM is not only the most aggressive and malignant tumor among the four types of astrocytomas but also the most common one, affecting about 3 cases per 100,000 person-years.(6) Another cause that contributes to the aggressiveness of GBM is the infiltrating features it bears,(6) mainly because of the star shape of the affected astrocytes. Affecting such types of cells with high-grade, fast-growing tumors generates a characteristic invasive nature of the tumor; therefore the surgical procedure is not enough. Sometimes it is even challenging to achieve the complete tumor resection due to the tumor existence near parts of the brain responsible for essential body functions.

1.2 Primary versus Secondary glioblastomas

All grades II, III and IV astrocytomas are also known as diffuse gliomas. GBM (grade IV glioma) alone accounts for 45-50% of all primary intrinsic brain tumors.(7) Brief definitions for both are provided below to understand the main differences:

Primary GBM: Represents the vast majority of GBMs and is defined as the one which arises *de novo* in the brain without clinical or histological evidence of a lesser malignant precursor lesion.(8)

Secondary GBMs: are brain tumors which develop due to evolution of pre-existing lower-grade gliomas.(8)

1.3 Understanding the poor prognosis of GBM from a pathological point of view

From a histological point of view, both primary and secondary GBM are very indistinguishable but fortunately they differ in their genetic and epigenetic profiles. In 1940, Scherer, a young German neuropathologist scientist was, for the first time, able to enlighten the differences between both types.(9, 10) According to him, it is very important to distinguish primary from secondary glioblastomas as the latter ones are the cause of most of glioblastomas with long clinical duration.(9) The main differences between primary and secondary astrocytomas lie in their biological behaviors. In fact the answer was found after the discovery of IDH gene mutations. IDH

gene, with two subtypes IDH1 & IDH2, encodes for the enzyme isocitrate dehydrogenase, which catalyzes the conversion of isocitrate to alpha-ketoglutarate (Figure 1).

Mutations of both subtypes occur in glioblastomas.(10, 11) However, IDH2 mutations occur less frequently than IDH1.(10) The wild type IDH, non-mutant type, catalyzes the conversion of isocitrate to alpha-ketoglutarate. IDH mutant types follow an alternative procedure and catalyze the conversion of alpha-ketoglutarate to 2-hydroxy glutarate (2-HG) (Figure 1). 2-HG is an oncometabolite which accumulates at high levels, inhibiting alpha-ketoglutarate-dependent enzymes. It inhibits histone demethylase leading to the synthesis of a hypermethylated DNA resulting in a tumor called G-CIMP or what is known as Glioma CpG Island.(12) Actually what makes IDH1 mutant a reliable tool of differentiation between primary and secondary GBM is its abundance in the later with a percentage of >80% vs. <5% in primary GBM.(13-16)

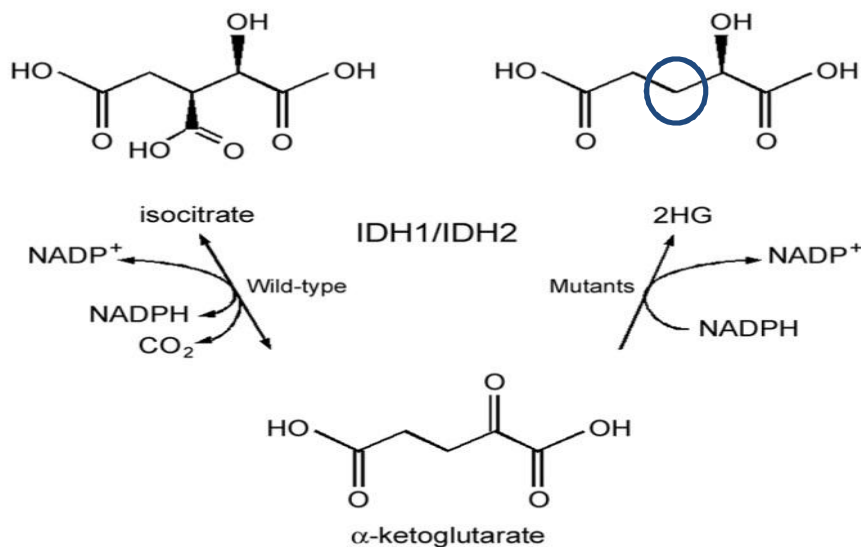


Fig. 1. Comparing different pathways due to normal and mutant IDH1

The normal IDH1 enzyme converts isocitrate into alpha-ketoglutarate. The mutant IDH1 enzyme converts alpha-ketoglutarate into 2-hydroxyglutarate (2-HG). “Originally published by {Mellai M, Caldera V, Annovazzi L, Schiffer D. The Distribution and Significance of IDH Mutations in Gliomas 2013 2013-02-27}. Available from: Ref. (17)

1.4 Epidemiology

According to different reports, GBM has a higher incidence in Caucasian than in African or Asian populations.(18) Males are at higher risk of developing GBM than in case of females. Statistics in Canada showed in 2012 that the estimated distribution rates of new cases per 100,000 population tested for brain cancer was 1.6 in males and 1.4 in females.(19) Although these data are relatively low, especially when compared to the same statistics for prostate and breast cancers, 27.2 and 25.6 respectively,(19) the total estimated numbers to be diagnosed and die from primary brain tumors alone, in the same year, were 2,800 and 1,850 cases respectively which were still high numbers and should not be ignored.(20)

Incidence of grade IV glioma, i.e. GBM, is fourfold higher in countries like Canada and US than in regions with lower incidence such as India and Philippines.(21) According to a report issued in 2012 by the Alberta Health Services, results showed that GBM alone accounted for 40 percent of all malignant brain tumors. In USA, among all tumors, GBM is the most commonly reported one after meningioma, 15.4% and 36.1% respectively.

Table 2 gives an idea about GBM relative high incidence, age group, gender-difference occurrence as well as its general total rate of incidence comparing to other types of astrocytomas.

Table 2 *Median age at diagnosis and age-adjusted average annual (1998–2002) incidence rates of adult gliomas stratified by sex. Reported in CBTRUS 2005–2006 Statistical Report: Primary Brain Tumors in the United States, 1998–2002.*

These results are obtained from studies performed in the US

Adult glioma by major histologic subtype	No of Cases	Median age at diagnosis (years)	Total rate ^a	Male rate ^a	Female rate ^a
Glioblastoma	12,943	64	3.05	3.86	2.39

^aRates are per 100,000 population, age-adjusted to the 2000 US (19 age-groups) standard, and based on data from the following registries: Arizona, Colorado, Connecticut, Delaware, Idaho, Maine, Massachusetts, Minnesota, Montana, New Mexico, New York, North Carolina, Rhode Island, Texas, Utah and Virginia. Abbreviation: NOS, not otherwise specified.

1.5 Symptoms

Although malignant gliomas, including GBM, are the most common primary brain tumors affecting adults, only few studies give information on the early symptoms. The silent development of GBM can partially explain why GBM is still difficult to notice at the beginning. For high-grade gliomas, symptoms like focal neurological deficits, epilepsy and cognitive dysfunction are prominent and can be observed at any stage of the disease.(22) Generally symptoms of glioma vary and they greatly depend on the patient's age as well as the tumor histopathological class.(23)

1.6 Diagnosis

There are always several techniques and laboratory tests needed to be performed before providing certain information about the type of glioma affecting the brain. Some are histological laboratory tests which are performed mainly to give initial pathological reports. These tests are based on Immunohistochemistry (IHC) which uses small biopsies specifically extracted for diagnosis and which, despite being expensive and relatively time-consuming, are considered one of the most reliable tests used for accurate differentiation between the metastatic malignant carcinoma (secondary GBM) and primary GBMs. Imaging techniques of diagnosis such as computed tomography (CT-scan) and magnetic resonance imaging (MRI) are usually performed directly on the patient's body to specifically localize the regions affected by the tumor in the brain.(24)

1.6.1 Pathological reports produced to initially differentiate 1^{ry} from 2^{ry} GBMs, Immunohistochemistry (IHC) tests

This kind of laboratory tests is performed using a brain biopsy tested by a panel of immunostains before determining the accurate diagnosis depending on the obtained results.(25) According to a publication in 1999 by David OH *et. al.* (25) whose study was performed on biopsies from 45 patients, among who 23 had GBM. Table 3 shows the results of immunoreactivity obtained by different stains when applied to biopsies from both primary and secondary GBM.(25)

Table 3 Positive results are shown in percentage after applying each of the six immunostains to biopsies from both types of GBMs. Adapted from ref (25)

Immunostain	% Observed immunoreactivity in 1^{ry} GBM biopsies	% Observed immunoreactivity in 2^{ry} GBM biopsies
Fibrillary acid protein (GFAP)	100%	13.6%
Ber-EP4*	0%	50%
Antikeratin monoclonal antibodies AE1/3	95.7%	100%
Antibodies to CAM 5.2	4.3%	100%
Cytokeratin 7 (CK7)	4.3%	77.3%
Cytokeratin 20 (CK20)	4.3%	40.9%

*Ber-EP4 is a monoclonal antibody that reliably labels epithelial tissues.(26)

Table 3 results suggest that, to distinguish poorly-differentiated secondary from primary GBMs, a combination of immunostains including GFAP and cytokeratins CAM 5.2 should be the best method to use. Their diagnostic capability is mainly due to fully stain, by 100%, one type of GBM with almost negligible effect on the other type. However, because a significant number of GBMs stains are labeled with antikeratin monoclonal antibodies (AE1/3), such markers should not be used to differentiate between the two types of glioblastomas due to their lack of specificity.(25)

1.6.2 Diagnosis using imaging techniques used to localize the tumor in the brain

1.6.2.1 Computed Tomography (CT-scan)

CT-scan was introduced to the field of medical examination in the late of 1980s.(27) In this diagnostic imaging procedure, X-rays are used to give an image of the biological material (figure 2-a). Briefly, the principle depends on reconstructing cross-section images of the body after measuring how much an X-ray beam is attenuated as it crosses the tissue under examination. Data acquisition is preformed either by uni- or multi-slice detectors (figure 2-b).(27) Despite having advantages such as being non-invasive and quick, CT scan sensitivity in detecting cancer tissues was found to be significantly less than other imaging techniques such as MRI.(28) In addition to

this, CT scan bears the risk of developing cancer in the future due to being an increasing source of radiation.(29)

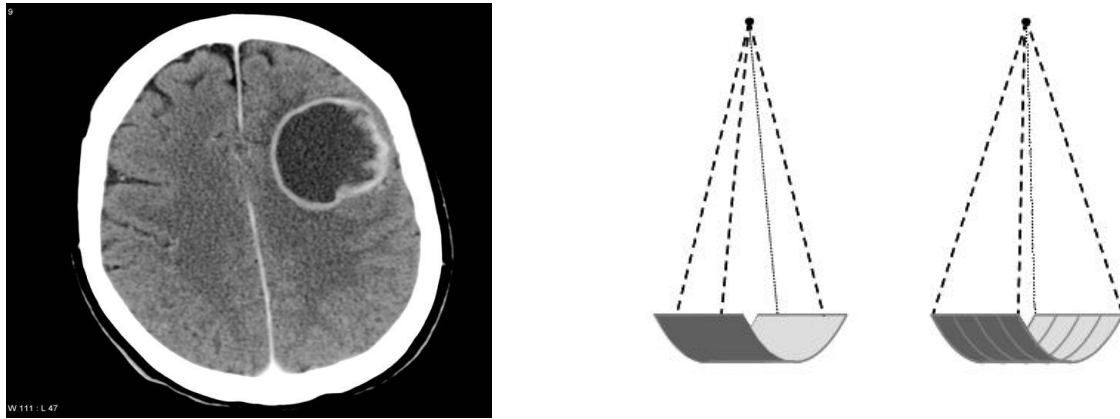


Fig. 2. (a) A CT scan image showing the brain affected by GBM. Case courtesy of A. Prof Frank Gaillard, "<http://radiopaedia.org/>>Radiopaedia.org. From the case "<http://radiopaedia.org/cases/4756/>>rID: 4756 (b) Computed tomography: acquisition with one single slice (left) and multislice CT with four active acquisition channels. Reproduced from.(30) by G. Bongartz, S. J. Golding, A. G. Jurik, M. Leonardi, E. van Persijn van Meerten, R. Rodríguez, K. Schneider, A. Calzado, J. Geleijns, K. A. Jessen, W. Panzer, P. C. Shrimpton, G. Tosi European Guidelines for Multislice Computed Tomography Funded by the European Commission Contract number FIGM-CT2000-20078-CT-TIP March 2004

N. B. (we chose to explain the second technique, magnetic resonance imaging (MRI), in more details because the diagnostic features of our nanoparticle formula will mainly depend on this principle).

1.6.2.2 Magnetic Resonance Imaging (MRI)

MRI is a technique that takes advantage of the magnetic properties found in atomic nuclei. A typical example of these nuclei is the protons found in hydrogen atoms of water molecules (H_2O) which are abundant in all tissues of the human body.(31, 32) Those protons act as tiny magnets because of the positive charge they carry in addition to their fast spinning (figure 3-a). Since these protons are oriented randomly in the human body, their magnetic fields do not sum up but they

rather cancel out. Nevertheless, in the presence of a strong constant external magnetic field (B_0), the spinning nuclei of hydrogen atoms undergo precession, i.e. a change in the orientation of their rotation axis. Of course some of them still cancel out but most of them will tend to align with the applied magnetic field in direction Z and this results in a net magnetization (Figure 3-b).(31)

The net magnetization is the source of magnetic resonance (MR) that is used to produce the images. To guarantee the efficient transfer of energy, protons are allowed to constantly oscillate by applying radio waves (B_1 field) perpendicular to the previously applied magnetic field. The applied radiofrequency energy (RF pulse), which comes in the form of rapidly changing magnetic and electric fields generated by electrons, causes the protons to oscillate back and forth (Figure 3-c). The time these protons take to reach the equilibrium state, after RF is stopped, is interpreted in terms of signals T_1 & T_2 signals.(31)

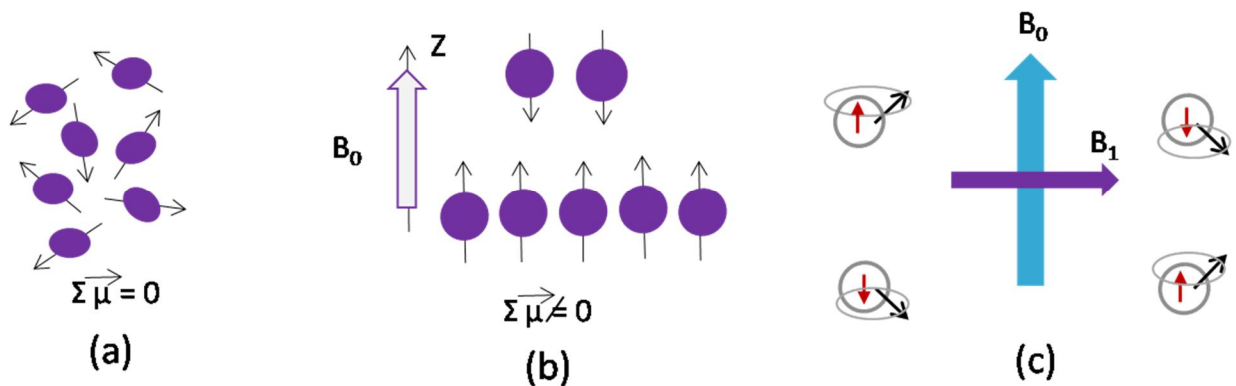


Fig. 3. Illustrations showing an overview on magnetic resonance imaging

(a) Random spinning of hydrogen protons: their net magnetization is zero because they are tiny magnets that do not sum but they rather cancel out. (b) Applying an external magnetic field (B_0) to the randomly spinning protons will cause most of them to precess and change the orientation of their axes. Protons will still spin about their axes but aligned to the direction of B_0 , direction Z. The system now shows net magnetization. (c) Radiofrequency energy (B_1) is applied perpendicular to the external magnetic field (B_0) causing the protons oscillation back and forth.

MRI technique is now accompanied by the use of contrast agents. Best examples of these are chelates using ions such as Gadolinium (Gd^{3+}) and USPIO (Ultra Small super Paramagnetic Iron Oxide). The first ones shorten the T_1 relaxation time and cause the part affected by the tumor to appear brighter than its surroundings. Gd^{3+} chelates are therefore called positive contrast agent (figure 4-a). On the contrary, USPIO shorten the T_2 relaxation time and produce an image in which the tumor-affected part looks darker than the rest of the brain. Hence they are known as negative contrast agents (figure 4-b). *In vivo* distribution and pharmacokinetic properties of both agents vary widely depending on their chemical composition, molecular structure and overall size.(33)

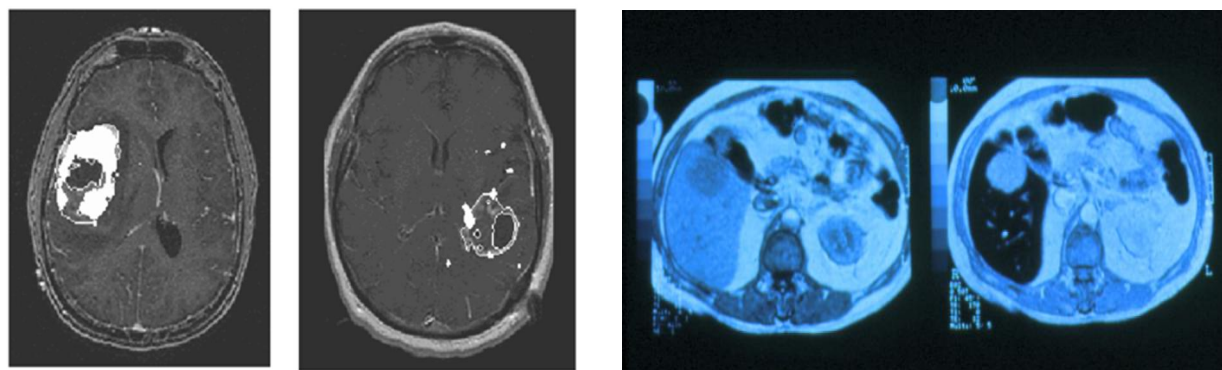


Fig. 4. MRI images before (right) and after (left) injection of a contrast agent, in a GBM-affected brain. (a) MRI image using a Gd^{3+} chelate as a contrast agent. Affected part is shown brighter than its surroundings. (b) MRI image using USPIO as a contrast agent. Affected part is shown darker than its surroundings.(34)

(a) This image was originally published in JNM. Kristin R. Swanson, Gargi Chakraborty, Christina H. Wang, Russell Rockne, Hana L.P. Harpold, Mark Muzi, Tom C.H. Adamsen, Kenneth A. Krohn and Alexander M. Spence. Complementary but Distinct Roles for MRI and ^{18}F -Fluoromisonidazole PET in the Assessment of Human Glioblastomas. *J Nucl Med.* 2009; 50:36-44. © by the Society of Nuclear Medicine and Molecular Imaging, Inc.

(b) This image was originally published in Neurospin Saclay website

2. Current treatments:

2.1 Currently available treatment strategies for GBMs

The treatment of patients with high-grade gliomas, either primary or secondary glioblastomas, has always represented a challenge to both neurosurgeons and drug researchers. Each line and option

of treatment has its own degree of success, restrictions and sometimes consequences. Each one of the currently available treatment options is discussed below in details.

2.1.1 Surgical intervention

Surgery is a first-line procedure to follow in the treatment strategy of GBM, whenever possible.

However, there is still a controversy regarding the extent of the tumor that needs to be removed and whether it participates to an increase in the median survival rate of the patient or not.(35)

The recommendations by many neurosurgeons to perform the tumor resection as extensively as possible, were further supported by studying the critical effect of the percentage of tumor removal on the increase in median survival rate.(35) Summarizing the study results, in which they compared a group of patients who underwent $< 98\%$ removal of the diagnosed tumor to a second group who underwent $\geq 98\%$ removal of their tumor, the results showed that the second group of patients demonstrated a significant increase in median survival rates, around 19 months compared to 10.9 months in people with lower percentage of tumor resection.(35)

Surgery as an only option for the high-grade glioma is never enough, since, as we previously mentioned the characteristic infiltrating feature of GBM and its potential presence next to essential brain parts restrict the 100% tumor elimination by surgical intervention.

2.1.2 Post-operative treatment

Although for many years surgery has been considered the initial treatment that ensured maximal safety and the highest degree of tumor elimination in GBM, clinical research was pursued to find postoperative treatment options that could help in increasing the median survival rate. For this reason therapists chose to resort to **radiotherapy** which increased the survival from 4-5 months to 9-12 months.(36) There were also results to support the role of using **corticosteroids** in controlling symptoms (mainly postoperative edema) although there was no information about their oncolytic

effects.(37) Starting from the early 1980s many scientists became more encouraged to study, discuss and publish the advantages of **concomitant additive chemotherapeutics** that could be used in combination with radiotherapy.(35) Nitrosoureas (Carmustine BCNU, Lumostine CCNU and others) remained included as first-line adjuvant therapy after surgery and they were combined with radiotherapy either alone or in a combination of Lumostine and procarbazine.(38) In 1999 published results proved the necessity to use Temozolomide (TMZ) as a first-line agent because of displaying better toxicity profiles than nitrosoureas.(39, 40) Since then, those were used as a second-line option.(38) The poor prognosis of GBM, jointly with the tumor recurrence inevitably after a median survival rate of 32 to 36 weeks,(41) motivated the researchers to look for more effective drug molecules. In the next part, we will discuss some of the promising chemotherapeutic agents which demonstrated efficacy against GBM either *in vivo* or *in vitro*.

2.1.3 *In vivo* and *in vitro*-effective drug entities in treating GBM

2.1.3.1 *Nitrosoureas*

They are also DNA alkylating agents with a high degree of lipophilicity, allowing them to cross the BBB and exert their cytotoxic effects on brain tumors.(38) Before 1999 nitrosoureas (e.g. Carmustine (BCNU), Lumostine (CCNU) or Nimustine (figures 5-c, 5-d and 5-e respectively) were always included in first-line treatments of GBM.(39, 40)

That was before studies started to reveal the higher efficacy of TMZ especially for patients with recurrent GBM who had not received more than one course of nitrosourea treatment.(38) Another study also recommended TMZ over BCNU especially for patients with recurrent GBM due to better toxicity profiles of the former.(41) All this contributed to changing nitrosoureas from first-line treatments to second-line options. Acting by the same mechanism as BCNU, TMZ causes the emergence of the same resistance mechanisms during treatment with BCNU, leading to cross

resistance interaction between both agents.(41) However, they are still used as secondary-line treatment when TMZ has failed.(38)

Nitrosoureas monotherapy phase II and phase III clinical trials were performed to investigate the side effect profiles of drugs from this group.(42-44) Hematologic and long-lasting hepatic and pulmonary toxicity were found to be the predominant side effects when using BCNU or CCNU in recurrent GBM patients who had received TMZ before.(42-44) For nimustine the side effects reported were hematologic but no pulmonary fibrosis was observed.(45) The best findings were obtained when Fotemustine (figure 5-f), another nitrosourea agent which was administered continuously after TMZ administration as first line treatment. There were the characteristic grades 3 & 4 hematologic toxicities but the report rates were much less than with other agents.(46) Despite having cytotoxic effects on tumor cells, their toxicity side effects made them undesirable agents and greatly limit their use in cancer treatment.

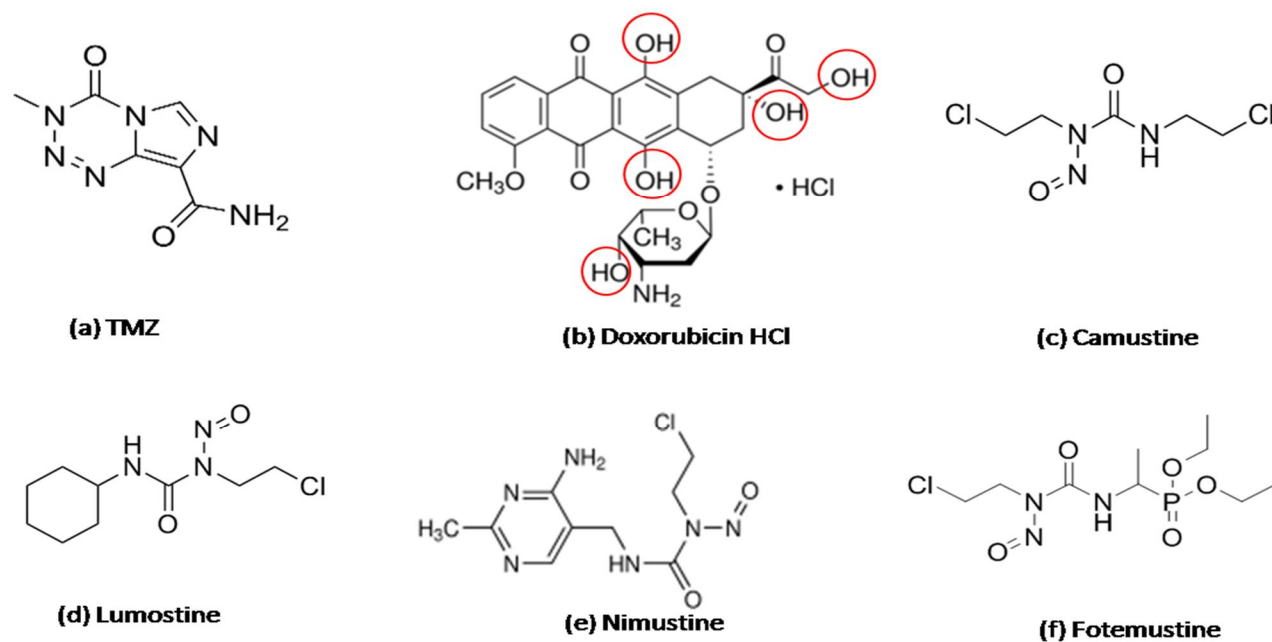


Fig. 5. Chemical structures of different chemotherapeutics (a) Temozolomide, TMZ. (b) Doxorubicin HCl (c) Carmustine, BCNU (d) Lumostine, CCNU. (e) Nimustine (f) Fotemustine.

2.1.3.2 Temozolomide (TMZ) (Figure 5-a)

TMZ is a highly lipophilic DNA alkylating agent prodrug which exhibits antitumor activity.(47) Due to its favourable efficacy and safety profiles, it became the drug of choice for GBM starting from 2005.(48) The mode of action of this drug is to deliver a methyl group to purine bases of DNA in the tumor cells leading to a defected hypermethylated DNA followed by eventual apoptosis of the affected cell.(47) A critical problem of TMZ therapy is the inherent, as well as acquired, resistance by tumor cells to this drug.(49) Resistance is mainly caused by therapy neutralization by MGMT (Methyl guanine methyl transferase) which is a DNA repair protein generated by GBM tumor cells. Several studies investigated TMZ safety and efficacy.(49) First, it was investigated in TMZ-naïve patients who were pre-treated either by nitrosoureas or by a combination of surgery and radiation. In a second group TMZ rechallenge was evaluated in TMZ-pretreated patients.(38) Table 4 is an attempt to summarize all results obtained in TMZ-naïve patients

Table 4: Results observed from different clinical studies aimed to investigate efficacy and safety of TMZ. Table was adapted from ref. (38)

TMZ-treatment Naïve Patients			
Treatment cycle	No. Of studies	Results	Side effects
75 mg/m ² /d for 21 d q28d	3	mPFS (mo)* = 3.8 mOS (mo)** = 9.3	Grade 3&4 hematologic toxicity occurred in a limited proportion of patients as thrombocytopenia, leukopenia, and neutropenia. Usually the toxicity resolved with one dose level reduction.
75 mg/m ² /d for 42 d q70d	3	mPFS (mo) = 2.3 mOS (mo) = 7.7	
150 mg/m ² 1-week-on/1-week-off schedule	1	mPFS (mo)= NA mOS (mo)= 7	
150-200 mg/m ² , 5-day cycles of 28 day cycle	5	mPFS (mo) = 2.1 mOS (mo) = 5.4	

*mPFS (mo) = median progression free survival in months.

**mOS (mo) = median overall survival in months.

Across all 9 studies PFS* ranged between 18-48% and median OS** was 5.4–9.9 months.

When considering 6 studies performed on TMZ-pretreated patients,(50-55) a variety of similar dosing strategies as in table 3 were evaluated. PFS ranged from 23 to 53% while median OS ranged between 5.1 – 13 months. Toxicity following TMZ use as monotherapy in TMZ re-challenge studies was due to grade 3 and 4 hematologic adverse events but no data for cumulative toxicity was reported. Stupp *et. al.* demonstrated in their study that the addition of a chemotherapeutic agent such as Temozolomide significantly increased the median survival rates among patients recently diagnosed with GBM. The observed median survival increase was a factor of 2.5 months, from 10% with radiotherapy alone to 27% when the combination therapy was used.(56) Therefore, a combination of radiotherapy and temozolomide has been recommended, for higher efficacy, over radiation monotherapy as postoperative surgical treatment of GBM.(56)

2.1.3.3 Doxorubicin (figure 5-b)

Doxorubicin (DOX) is a well-known anticancer molecule (already on the market). It is an anthracycline molecule synthesized for the first time in the late 60s from mutation-induced strains of *Streptomyces Peucetius*.(57) It is widely used for the treatment of various peripheral cancers such as leukemia, lymphoma, bladder, stomach, breast and ovarian cancers.(58) It also still exhibits severe side effects which limit its use. For example, in addition to bone marrow suppression, mouth ulcers and alopecia, delayed cardiotoxicity remains a main limitation against the use of DOX.(59) Also the rapid clearance of DOX due to the hydrophilic structure (figure 5-b), reported average $t_{1/2}$ of 5 to 10 minutes,(60) from the body greatly reduces its chances to reach the site of action.(61) Another added challenge to be considered when treating GBM is the crossing of the blood brain barrier (BBB).(62) Free DOX cannot even cross a disrupted BBB. All those problems contributed to the urgency of developing delivery system which is able to safely, effectively and selectively carry DOX to GBM-affected cells. The aimed formulation needed to be one able to hide DOX inside it, so that healthy body organs are protected from its serious side

effects, and at the same time possesses high affinity to cross BBB. A DOX-loaded formula sought to target GBM has also to be sensitive enough to specifically open in the brain tumor cells which are, relatively, highly acidic than interstitial space and surrounding healthy cells.(63)

Resorting to new pharmaceutical technologies such as pharmaceutical nanotechnology allowed resolving, to a great extent, the dilemma of using DOX. Doxil® is an excellent current example of a nanoliposomal system coated with polyethylene glycol (PEG). This coating helped mainly to protect the formula against opsonisation and rapid elimination from the body.(58) Doxil® showed a remarkable success in treating peripheral tumors for more than 20 years.(58) The targeted delivery properties of Doxil® mainly depended on the enhanced permeation retention (EPR) effect. EPR effect, in case of brain tumors, is noticed to be relatively weaker than in other types.(58, 64) Therefore while Doxil® is suitable for the treatment of peripheral tumors, a DOX formula that is more specific and sensitive to brain tumors has not been yet well-developed. Many clinical trials were performed using combination treatment of both temozolomide and PEGylated liposomal DOX.(65) Moreover many publications reporting the encapsulation of doxorubicin into chitosan-based nanoparticles showed that it can help overcoming DOX post-administration problems.(66) Progress of these trials will be discussed in a later section in an introductory context to our hypothesis.

2.1.3.4 Antiangiogenic agents

The most common example of this group is Bevacizumab (BEV), which is a human recombinant monoclonal antibody to vascular endothelial growth factor mediating tumor neoangiogenesis. It is suggested that antiangiogenic agents reorganize the blood vessels back to normal.(67) These agents displayed more efficacies in progressive disease than in newly diagnosed patients. In 2009

BEV was approved by the US Food and Drug Administration (FDA) for recurrent GBM based on uncontrolled phase II trials after showing 6-month improvement of progression-free survival.(67)

2.1.3.5 Novel chemotherapeutics

Generally, they can be categorized into two main approaches. The first one, which is known as targeted molecular therapy, alters the tumor growth pathways. For example some agents alter receptor tyrosine kinase pathway(68, 69) while others alter p53 pathway which is a tumor suppressor gene mutated in up to 85% of GBM.(67, 70) Another approach of novel chemotherapeutics is immunotherapy which mainly affects the tumor microenvironment through targeting tumor specific antigens (TSAs) and tumor associated antigens (TAAs).(71, 72) Immune response of the patient is not strong enough to destroy these antigens.(73)

2.1.3.6 Other alternative strategies (physical methods)

Based on a phase III trial, FDA approved NovoTTF-100A system (Novocure Ltd., Haifa, Israel) for recurrent GBM.(74) The concept of therapy is to deliver tumor treating fields (TTFs) in the form of low-amplitude, alternating electrical fields that disrupt cell division and tumor development. Fields are transferred to patient through electrodes fixed to the head for 20 -24 hrs daily. The use of TTF is now being tested in the treatment of newly diagnosed GBM. Preliminary results showed higher mOS and PFS data when using TTF plus TMZ compared to using TMZ alone in patients after receiving their initial radiotherapy.(75) There are still concerns regarding the price, the need to wear the device for a long time and also having to carry the source of energy in a backpack.(67)

2.2 Multidrug resistance (MDR)

MDR occurs mainly as a cross-resistance of a wide range of agents after antineoplastic treatment.(76) Drug resistance of tumor cells is conditioned by multiple factors, e.g. glutathione-S-transferase (GST), MGMT, p-glycoprotein (p-gp) and multi-drug resistance associated proteins

(MRPs).(76) All of them protect tumor cells from cytotoxic agents by different mechanisms. For example the role the BBB plays in brain homeostasis is regulated by actions of active-efflux transporters of the ATP-binding cassette (ABC) family including (p-gp), MRPs and breast cancer resistant proteins (BCRP).(77) All these proteins are overexpressed by high-grade gliomas.(77)

A candidate drug designed to cross the BBB has to possess both lipid solubility and affinity to the transporters on the BBB.(78) Many of the aforementioned substrates are substrates for these transporters e.g. MRPs & BCRP. Therefore, they compete with the drug to these pathways causing drug accumulation outside the brain.(78) A lot of anticancer drugs face MDR when they try to reach tumor tissues. Examples of these are doxorubicin, daunorubicin, docetaxel, epirubicin, etoposide, idarubicin, methotrexate, mitoxantrone, paclitaxel, teniposide, vinblastine, vincristine, etc(78)

Recently many molecules showed promising efficacy results when tested *in-vitro* on tumor cells. However, crossing physiological barriers such as the BBB always stood against their delivery in effective concentrations. Before explaining how to improve drug delivery systems to overcome this challenge, we will firstly give a detailed explanation of the BBB structure.

2.3 Understanding the blood-brain barrier (BBB)

Normally the blood capillary wall thickness in human body is about one cell thick with three exceptions.(79) Those exceptions are the placental barrier, blood-testicular barrier and the BBB. The BBB is a complex physiological structure, challenging many drug therapies and usually standing as a major obstacle against their crossing to the intended sites of action. Endothelial tissue of the capillary bed all over the human body shows fenestrations.(79) Those fenestrations are absent in the entire Circle of Willis,(79) a circulatory anastomosis (i.e. connection of two blood vessels) that supplies blood to the brain, and its surrounding structures.(80) There are rather tight

junctions between the adjacent endothelial cells.(79) Those junctions restrict the paracellular pathways. Thus, the endothelial continuous walls of the microcellular vessels act as a highly lipophilic barrier.(79) In addition to endothelial cells, the BBB is composed of a basement membrane, astrocytes end-feet ensheathing the vessels and pericytes which are embedded in the basement membrane.(79) They are thought to play an important role in angiogenesis. Microglia are glial cells found in the brain and spinal cord and they act as resident macrophages (figure 6).(79)

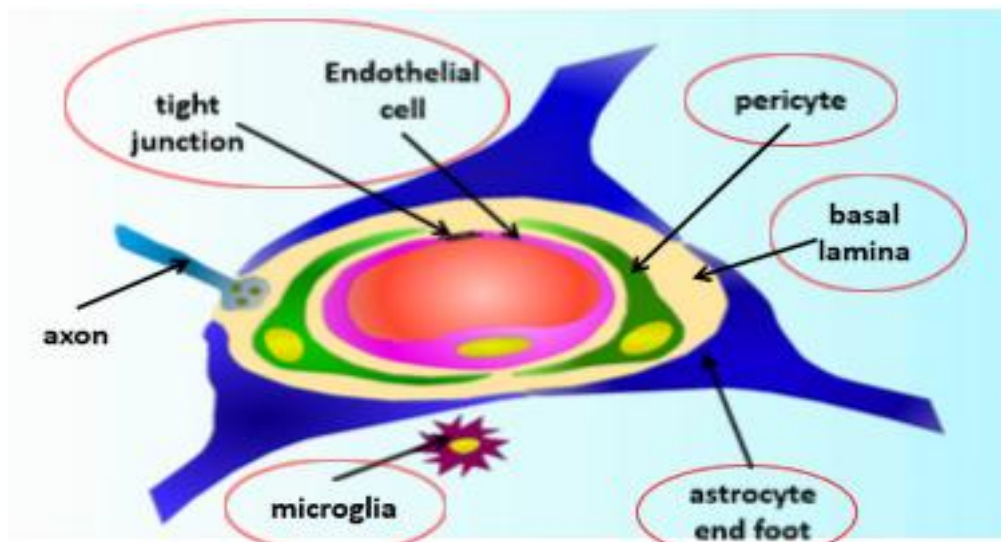


Fig. 6: An illustration of the BBB structure showing its different components such as the tightened adjacent endothelial cells, astrocyte end-foot and the resident macrophages(microglia).(81)Reproduced with permission.

The whole protective structure of the BBB aims at protecting the brain from harmful substances that can be found in the periphery. There are efflux transport systems included in the BBB to regulate the entrance of some essential substances such as glucose.(79) Therefore, drug uptake into the brain only relies on a certain degree of lipophilicity, small size and affinity to transporters located on the BBB and blood-cerebrospinal fluid interfaces.(81)

3. Novel treatment strategies

Because the current therapeutic strategies are still away from safely and effectively eliminating GBM tumors, researchers are always moving forward to discover newly modified drug delivery systems and new drug entities. A very promising area of research is pharmaceutical nanotechnology. A historical background, principles and nanosystems which are currently under investigation are discussed below in details.

3.1 Pharmaceutical nanotechnology

Throughout the last two decades pharmaceutical nanoparticles started to be considered, in research scale, one of the evolutionary mechanisms of drug delivery. In fact the considered promising effects of this technique can be attributed to the advantageous features they have over other drug delivery systems (DDS). Among those unique features is a very small size (< 1000 nm) while, at the same time, the significant large surface-to-mass ratio of a NP compared to other entities. Another advantage is their quantum properties which facilitate their adsorption and the effective carrying of other drug molecules.(82)

A subtype of solid NPs is nanogels which are hydrogels synthesized in a nanoscale. Hydrogels were best described as hydrophilic three-dimensional polymer networks able to take up large amounts of water or physiological fluid, while maintaining their internal network structure.(83) Research has been focused on adapting NGs for *in vivo* applications, trying to make a benefit from the biocompatibility/biodegradability of certain polymers.(60) When such polymers are used in the synthesis of self-assembled NGs, an added advantage of safety, in addition to the previously mentioned ones, is warranted. The modifiable surface of NGs allows the incorporation of ligands to it and the subsequent target delivery of the encapsulated drug, thus reducing harm to healthy cells while maximizing efficacy of the dosage form.(84) Another important key feature is the immediate response to environmental factors such as pH and temperature changes, all thanks to

nanosize as well as the chemical properties of the polymers used in NG synthesis.(84) This type of NGs, known as stimuli-responsive, is being researched extensively as it is considered to exhibit promising selectivity in drug delivery. Examples of this NG type will be explained later in details.

3.1.1 Polymers and materials used in NP synthesis

Nanoparticles can be prepared from a variety of materials such as lipids, proteins, polysaccharides and synthetic polymers. Selection of the material to be used in the synthesis depends widely on the required size, release profile aimed for the drug, final site to target, drug physicochemical characteristics and also on the degree of biodegradability, biocompatibility and toxicity of the selected polymers.(85)

Another important factor which seems to play a great role in selecting polymers is the mechanism by which NPs are intended to be prepared. Among different approaches used in the preparation of NPs, nanoprecipitation and ionic gelation are two major ones.

In **nanoprecipitation**, or so called **solvent displacement**, NPs are prepared by dissolving both polymer and drug in a water-miscible solvent. The prepared solution is then added, drop by drop, to a nonsolvent to the polymer which is usually water. This addition will allow the diffusion of the organic phase into the aqueous one and vice versa. The result will be supersaturation and precipitation of the polymeric NPs with drug entrapped inside them.(86) Poly (d,l-lactide-co-glycolide) (PLGA) and polycaprolactone (PCL) are typical examples of polymers used in the nanoprecipitation method.

Another major approach for synthesizing NPs, particularly NGs, is ionic gelation. The mechanism of this method depends mainly on ionic bond formation. The bond is formed between the protonated amino acid groups in polymers like chitosan and the negatively-charged phosphate groups of a crosslinker such as tripolyphosphate. For this reaction to occur, pH adjustment of the

medium is critical because protons are required to be present at the amino groups of the selected polymer.(87, 88)

Chitosan, a very popular polymer in the NG synthesis, is a natural biodegradable polysaccharide derived from chitin.(89) It contains units from both glucosamine and N-acetyl-D-glucosamine (NAG). Chitosan is characterized by a ratio of glucosamine to NAG higher than one. Chitosan has wide contributions in food and pharmaceutical industries as an excipient that is able to help in tablet compression and disintegration. In addition to its role as an excipient, chitosan has attracted attention as a main component in NGs formulation thanks to its unique physicochemical properties. The acidic pKa of chitosan, ~6.3, allowed it to gain a proton in a medium of pH <5.5, thus turning chitosan into a positively-charged molecule that can easily form an ionic bond with negative phosphate groups of TPP.(89) Other polymers such as alginic acid can undergo the same mechanism (but with reverse negative charges) and get crosslinked with CaCO₃ to form calcium alginate. However, the resulting chitosan gels appear to be more stable compared to those synthesized by calcium alginate especially in phosphate buffers. Therefore chitosan gels are expected to have longer life span.(90) Another potential component in NG synthesis is hyaluronic acid (HA) which is a polysaccharide composed of NAG and D-glucuronic acid. HA is an endogenous substance that exhibits excellent biocompatibility and biodegradability properties.(91) The structure of HA also includes carboxylic groups available for a reaction with protonated amino groups of chitosan, when both molecules are combined together.(92) In this way, incorporating HA into NG structure provide extra support to the matrix. In addition to this, CD4, a HA receptor abundant in tumor cells, facilitates the intracellular uptake of HA-based NGs into their target cells.(93)

3.1.2 Different generations of nanoparticles

Nanoparticles can be classified into four generations so far, according to their degree of 'intelligence', i.e. ability to act safely and effectively.

3.1.2.1 First generation

Those are conventional nanoparticles with a surface remaining unmodified. They are naïve drug carriers that are easily recognized by blood components (opsonins) such as IgG, complement C3 components (figure 7-a). These opsonins adsorb onto the nanoparticle surface, mostly a hydrophobic surface which favours opsonin adherence. As a consequence nanoparticles are massively cleared from the bloodstream, together with their carried drug, by macrophages of the mononuclear phagocytes system (MPS) such as liver, spleen, lungs and bone marrow.(94)

3.1.2.2 Second generation

They were developed from the first generation to produce long-circulating drug delivery systems. This was mainly achieved by surface modification of the conventional nanoparticles so they were not recognized by the circulating opsonins (figure 7-b). The modification is made either by a) surface-coating of the nanoparticles using specific adsorption of hydrophilic polymers/surfactants or b) grafting hydrophilic segments to the surface, example of these hydrophilic segments are polyethylene glycols (PEG), poloxamers, poloxamines and polysorbates.(94)

A good example of this is the PEGylation of liposomal DDS which were proved to avoid the *in vivo* uptake by MPS. Some of these 'stealth' systems are currently marketed e.g. Doxil[®] (doxorubicin-loaded PEGylated liposomes) and Abraxane[®] (albumin-bound paclitaxel nanoparticles) both used for the treatment of metastatic breast cancer.(95)

Nanoparticles from the first and second generations reach their site of action by passive targeting,(95) a pathway which benefits from angiogenesis abnormalities of tumor tissues to enhance the drug permeability. For better understanding, we will explain the tumor tissue lining

structure. Tumor tissue walls are characterized by angiogenesis abnormalities in which new blood vessels are generated to supply nourishment to the over-grown tumor cells.(96) This causes the tumor vascular lining to lose the smooth muscle layer and to have highly defective endothelial cells with wider fenestrations. Also permeability enhancing factors such as nitric oxide, prostaglandins, bradykinins, vascular permeability factor are overexpressed and they cause extravasation of the tumor tissue walls allowing the passage of macromolecules, a phenomenon known as enhanced permeability and retention effect (EPR) (Figure 8).(64)

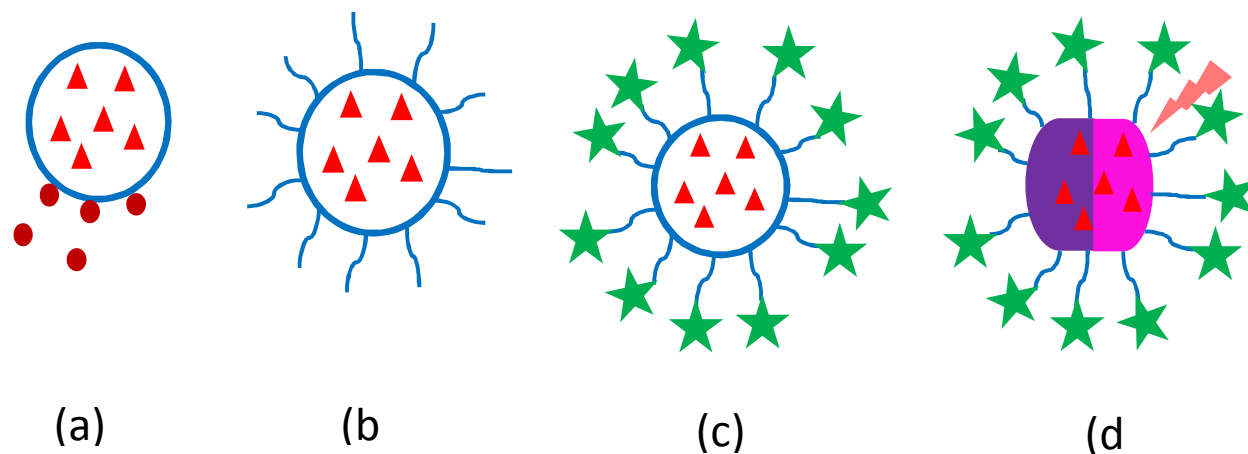


Fig. 7: A simple diagram illustrating the different stages of drug ▲-loaded nanoparticle development to improve their target specificity. (a) first generation, conventional and non-modified surface nanoparticles easily recognized by opsonins ●, (b) second generation modified-surface nanoparticles successfully avoided blood-circulating opsonins, (c) third generation nanoparticles in which ligands ★ are grafted to their surfaces making them able to target specific cell receptors, (d) fourth generation nanoparticles, they are highly intelligent and sensitive to triggers ⚡ in the tumor environment.

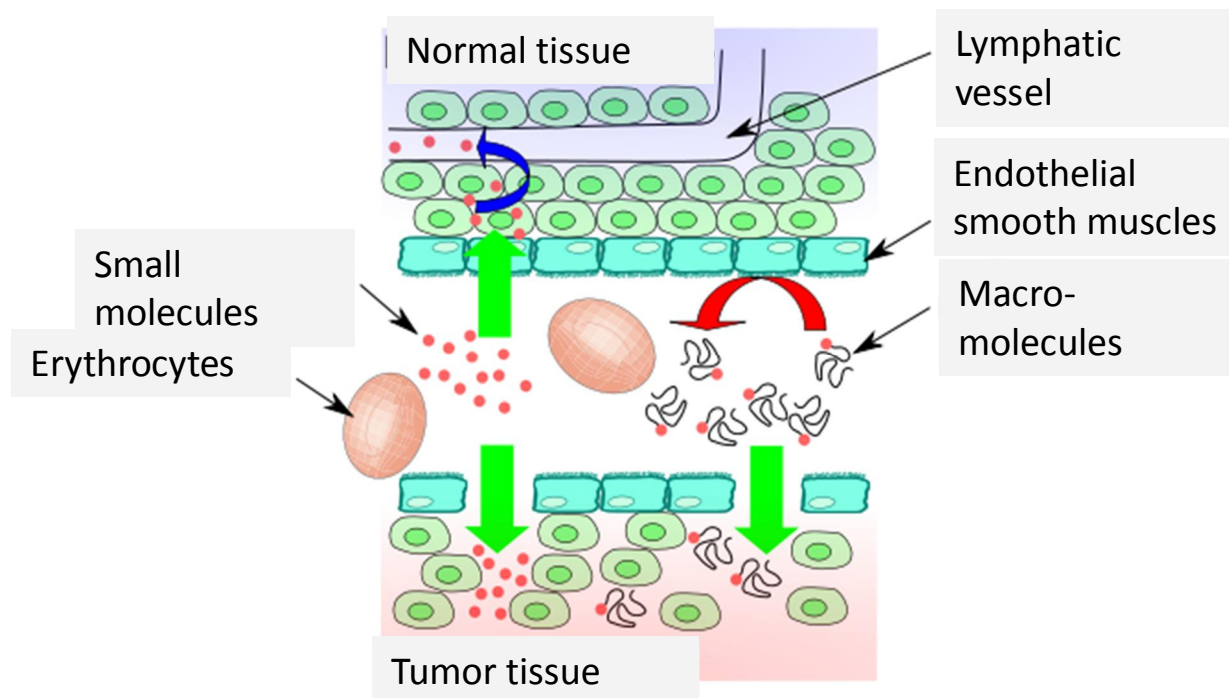


Fig. 8: *The EPR effect in the tumor tissue.*

A comparison between the intact endothelial smooth muscle structure lining the normal tissues and the loose one lining the tumor tissues which results in EPR effect and allowing accumulation of the drug inside. Reproduced from www.wikipedia.org

The abnormal structure also allows for drug molecules to favour the accumulation in tumor tissues exerting their therapeutic effects.

Increasing the drug circulation period in the body by avoiding opsonisation and depending on the efficiency of the EPR effect provides a more controlled release of the drug. However, there is still a random drug delivery of the drug. For example, tumor vascularisation does not only vary in its degree of porosity but also EPR phenomenon is not restricted to tumor tissues and extends to normal tissues although with much lower degree.(95) In fact when it comes to brain tumor, the noticed EPR effect is relatively weak. For instance, the macromolecules and nanoparticles need to be less than 100 nm to significantly extravasate from the tumor vasculature. These particles also

need to be higher than 20 nm to be able to remain in the tumor environment and not inefficiently get back to the circulation or undergo rapid renal filtration.(97)

Therefore, closely looking at the degree of intelligence of first and second generations of nanoparticles, one can easily conclude that the specific targeting of the site of action by nanocarriers is not yet achieved. As a result developing nanocarriers continued for the purpose of achieving specific targeting.

3.1.2.3 Third generation (Active targeting)

In this generation nanoparticle surface was subjected to further modification. Ligands were grafted to the outer surface of the nanoparticles to enable active targeting of the tumor cells (figure 7-c). The whole concept depends on an efficient interaction, active targeting, between the grafted ligand and the receptor at the tumor cell membrane.(95) Some tumor cells are known for overexpressing some specific antigens or receptors on their surfaces.(95) Example of moieties that can be grafted to target specific cell receptors are proteins (mainly antibodies and their fragments), peptides, nucleic acids (aptamers), small molecules, or others (vitamins or carbohydrates).(95)

Although they seem to be relatively highly specific in targeting the tumor cell, the third generation nanoparticles are limited by many factors. These factors include the extent of the selective expression of the target cell receptor relative to non-target cells, the receptor availability on the target cell surface, the rate of internalization vs. shedding of that surface receptor following ligand binding, etc.(98) Moreover the expression of a promising tumor-targeting receptor may not be occurring homogenously throughout the whole tumor. Therefore, the need to produce nanoparticles with higher degree of intelligence necessitated the quest for identifying conditions that are highly specific to tumor tissues alone and not the healthy ones.

3.1.2.4 Fourth generation (dynamic or self-triggered nanoparticles)

Fourth generation nanoparticles are highly ‘intelligent’ (i.e. ‘smart’) nanosystems demonstrating target-specificity characteristics. Moreover, in these systems, the drug release effect at the target site is mostly triggered by factors that could be either internal or external (figure 7-d). Examples of internal factors are enzymes or low pH of the tumor environment, while external factors could be light, temperature, magnetic field, and ultrasound.(98)

Example of self-triggered nanoparticles is pH-sensitive nanocarriers which are able to stabilize the drugs inside their nanoparticles at the physiological pH while releasing it in the tumor tissues, in which a higher degree of acidity is normally caused by glycolysis-upregulated hypoxia. Solid tumors have an acidic pH of 5 – 6.8. Chitosan, a polysaccharide polymer used to synthesize pH-sensitive nanogels, has a pKa of 6.3. Since the interstitial space of solid tumors has a pH in a range of 6.8 – 7.2, chitosan-based nanogels should be able to specifically release their encapsulated drug in the microenvironment of the tumor tissue (figure 9).(96)

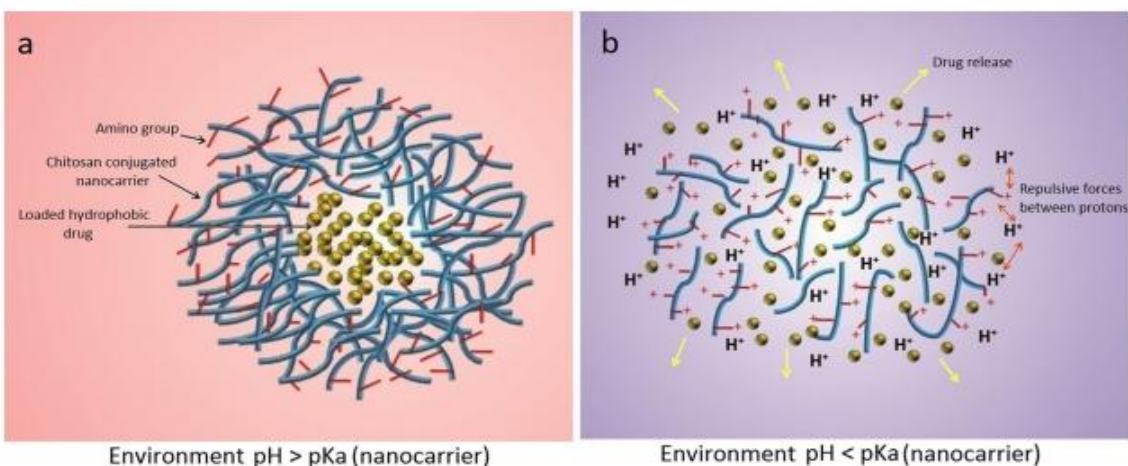


Fig. 9: pH-sensitive chitosan conjugated nanocarrier interactions: (a) aggregated form of nanocarrier in blood or natural tissues. (b) Swollen form in the acidic sites. Repulsion between protonated amino group on the chitosan skeleton and protons leads to release the anti-tumor drugs. Reproduced with permission from (96)

USPIO, magnetized iron oxide synthesized as nanoparticles and used as diagnostic agents, represent another good example of an ideal fourth generation. These NPs consist of a coated magnetized iron oxide core, the coated surface usually being PEG. Their average hydrodynamic diameter measures around 10 nm.(99) The hydrophilic nature of the coating protects USPIO against opsonisation and makes them long-circulating particles. In addition to this, the magnetic properties of the core allowed its specific delivery in response to the application of an extra magnetic field. Thus, after iv infusion of USPIO-containing micro-bubbles in healthy mice, the accumulation of diagnostic USPIO were visualized and quantified using MRI. By the same technique the co-delivery of anticancer drug can be rendered specific.(100)

3.1.3 Promising role of pharmaceutical nanotechnology in brain cancer treatment

A safe and effective drug delivery system (DDS) needs to be able to control the fate of the drug. Many academic researches were started to investigate the safety and efficacy of pharmaceutical nanotechnology as DDSs. There are several challenges that stand against the drug delivery in therapeutic concentrations to the specific site of actions. These challenges are faced by the drug throughout its journey starting from administration until its elimination from the body. Among these encountered problems are poor solubility, crossing the BBB, increased resistance to the drug and nonspecific targeting resulting in the drug accumulation in healthy tissues causing serious side effects.(101)

3.1.4 Examples of overcoming formulation challenges by pharmaceutical nanotechnology

The following are some, but not all, general examples about how pharmaceutical nanotechnology could overcome the potential problems encountered during the drug journey to its site of action.

3.1.4.1 *Improving bioavailability of poorly soluble drug*

Solubility is crucial for both drug formulation and bioavailability following its administration. Pharmaceutical nanotechnology played a role in increasing bioavailability of many drugs either

hydrophilic or hydrophobic. Around 40% molecules recognized to be active substances are limitedly used because of their poor water solubility and consequent difficulty to be formulated.(102) A good example of this is the hydrophobic anticancer camptothecin which was successfully delivered to cancer cells and induced their death after its loading into mesoporous silica nanoparticles.(103) Thanks to their small size, NPs can be administered intravenously for targeted delivery. Also targeting moieties can be conjugated to their surfaces for further increase of therapeutic efficiency of the drug.(104) Testing chitosan-based NGs loaded with temozolomide showed that drug release was specifically enhanced in response to pH changes.(105) Further *in vitro* cytotoxicity experiments proved their efficacy compared to the unloaded NGs.(106) Chitosan NGs also gave an advantage to DOX by turning the latter in to an orally bioavailable molecule. Such experiments offered a proof of chitosan absorption-enhancing properties.(107)

3.1.4.2 *Increasing the half-life time of drug in the body*

Delivery of hydrophilic drugs to brain tumors remains a great challenge in the field of pharmaceutical formulation. Many hydrophilic molecules, e.g. methotrexate (MTX) and DOX exhibited *in vitro* cytotoxic effects to isolated brain tumors. However, they still have limited or no *in vivo* application because of their short half-life time. Chitosan polymer and its derivatives as main components of NGs offer the advantage of having modifiable surfaces. A recent *in vivo* trial compared results after iv administration of free MTX solution, nanodispersions of unmodified MTX-loaded chitosan NGs (UMNGs) as well as polysorbate-80-modified-MTX-loaded chitosan NGs (MNGs). Both UMNGs and MNGs produced 2.33- and 8.52-fold area under the plasma concentration–time curve within the test time period (AUC_{0-t}) compared with the free MTX. This observation was suggested to be due to some drug preserving mechanism(s), e.g. physical masking, exerted by the nanoparticles on the loaded MTX. This physical masking protected the

drug molecules against being rapidly eliminated by natural elimination mechanisms of the body.(108)

Another example is a doxorubicin-loaded dextrin-based nanogels which showed higher sustained release compared to doxorubicin-poly lactide nanoparticles over 72 h.(109)

3.1.4.3 Decreasing the resistance of tumor cells to anti-cancer drugs

MDR remains a major challenge against the chemotherapeutic efficacy in cancer cells. As previously mentioned, many factors are involved in MDR. These include decreased drug uptake, enhanced DNA repair, overexpression of drug transporters such as P-gp, MRP1, MRP2, and (BCRP). Polymeric nanoparticles have been investigated as vectors to overcome drug resistance by diverting ABC-transporter mediated drug efflux mechanisms.(110) A famous example of this is free DOX which is resisted by MCF-7 cell lines in breast cancer cells. After loading DOX into chitosan-coated magnetic NPs, the drug was investigated by fluorescence microscopy in comparison to free DOX. Unlike the free drug which did not sufficiently accumulate in DOX-resistant MCF-7, the loaded one showed higher accumulation rates similar to those found in sensitive cells.(111) A similar approach was the targeting specificity of chlorotoxin-conjugated nanoparticles.(112) This formula significantly reduced IC_{50} compared to TMZ-NP and free TMZ which means a decrease in GBM resistance to TMZ therapy.(112)

Although pharmaceutical nanotechnology is relatively a new science, it still has a lot of secrets to reveal especially in challenging conditions such as GBM. In our work, we tried to benefit from the previously mentioned advantages trying to prove the below hypothesis by setting and applying the objectives mentioned after.

Currently many efforts have been concentrating on combining both therapeutic and diagnostic approaches in one particle. This system is referred to by the term theranostics.

3.1.5 Theranostic nanoparticles

They are nanoparticles which contain both diagnostic and therapeutic agents designed mainly to exhibit simultaneous diagnostic and therapeutic properties. Therefore, treating affected tissues as early as possible while the disease is still curable.(113) The theranostic mechanism of nanocomposite NGs greatly varies depending on the contents of their core.(106) However, the desired functions of these NGs as novel delivery systems are generally more or less the same. To understand different advantages of theranostic nanoparticles, the following are recently published examples of this type. The first example is nanocomposite nanoparticles described as multicomponent pH-responsive nanogels. Similar to other theranostic nanoparticles, this type also tries to approach cancer cells from different angles by carrying both therapeutic and diagnostic properties. However, pH-responsiveness and hence a selective rupture can be also guaranteed depending on component pKa and pH adjustment of the media. For example chitosan has pKa of 6.3 and it becomes ionized in a relatively acidic pH, 5.1 which is tumor intracellular pH, releasing the drug inside the tumor cell. This unique pH-sensitivity can be utilized to selectively deliver chemotherapeutic agents, for instance doxorubicin, to cancer cells while not affecting adjacent healthy ones.(114) A similar example of theranostic NGs using the same chitosan polymer was the co-encapsulation of the drug prednisolone phosphate (PLP) and the negatively charged diagnostic agent Gd-DOTP. The distribution of both PLP and Gd-DOTP was guided by their net charges as well as those of the NGs components. Inside the NG structure, the negatively charged Gd-DOTP was ionically linked to chitosan positive amino groups, while amphiphilic PLP was mostly located at the interface with the perfluoropentane core. The co-encapsulation was successfully achieved with an overall encapsulation efficiency of 78%. The high encapsulation was suggested to be due to the structural flexibility of the NPs components, including chitosan. The encapsulation did not affect the core-shell structure of the nanoparticles.(115)

3.2 Hypothesis and specific objectives

From all the innovative strategies developed to treat GBM, we reckon that the use of nanoparticles loaded with efficient anticancer drugs would improve the disease outcome. The pKa values of chitosan and how its ionization changes in response to changes in pH; can be utilized in synthesizing pH-sensitive chitosan/hyaluronic acid-based nanogels (NGs). Chemotherapeutic agents with anti-GBM effect, either *in vitro* like DOX or *in vivo* like TMZ, can be encapsulated into the pH-sensitive NGs. Either of these agents can also be co-encapsulated with a contrast agent into the same NGs. Thus, synthesizing theranostic NGs capable of simultaneous diagnosis and exerting a cytotoxic effect to the tumor-affected cells without harming the healthy cells (Figure 10).

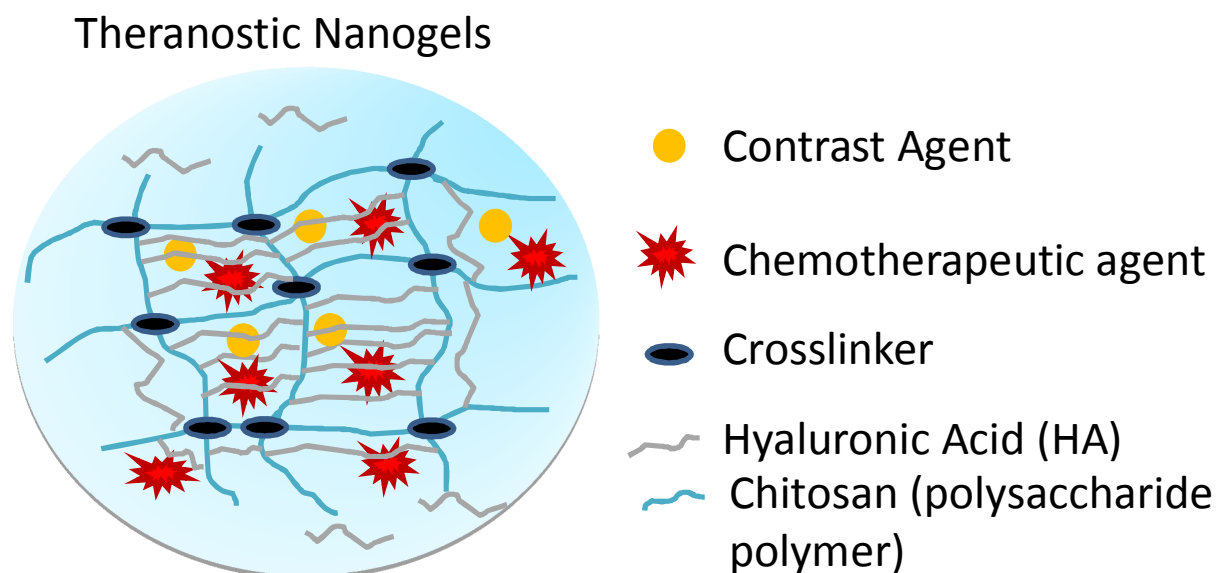


Fig. 10: A hypothetical structure of the final drug-loaded chitosan/hyaluronic acid-based theranostic nanogels showing a chemotherapeutic agent (either doxorubicin or temozolomide) co-encapsulated with a diagnostic agent (USPIO)

To demonstrate this hypothesis, we have divided our work into the following objectives:

- **Objective 1: Synthesizing drug- (DOX)-loaded NGs and determining their physicochemical characteristics:**

For that purpose the following were conducted:

1.1. Blank NGs were optimized for their size and surface charge.

(NGs were synthesized using ionic gelation method before being tested for their size, PDI and Zp using DLS/ELS techniques).

Other techniques of characterization were also applied such as: differential scanning calorimetry (DSC) and Fourier-transformed infrared (FTIR) analysis.

1.2. Synthesis of drug-loaded NGs:

After synthesizing blank NGs with optimal PDI, size and ZP, the same polymers at the same concentrations were used to encapsulate DOX into the NGs.

The produced formulas were also characterized using the aforementioned techniques in addition to determination of their encapsulation efficiency (EE%), production yield PY% and drug-loading efficiency DLE%.

- **Objective 2: Studying release profile of DOX from NGs before and after freeze-drying**

For that purpose the following steps were carried out:

2.1. Freeze-drying of the drug-loaded formula:

To achieve this step; sugars, of different types and concentrations were used to cryoprotect blank NGs. The best cryoprotectants were then selected to repeat the freeze-drying process to the DOX-loaded NGs.

The produced formulas were also characterized using the aforementioned techniques in addition to determination of their EE%, PY% and DLE%.

2.2. Testing the release profile of DOX from the synthesized NGs

For this purpose batches of DOX-loaded NGs, with and without freeze-drying, were incubated in release media. Those media were prepared so that they almost simulated physiological conditions.

Release patterns were then monitored at three different pH values 5.8, 6.8 and 7.4.

Apparent results were corrected using K_d values of DOX to compensate for the first order degradation of the later.

Objective 3: Preliminary trials to synthesize theranostic NGs

To achieve this goal, the following batches were prepared and characterized.

3.1. Synthesizing TMZ-loaded NGs

TMZ-loaded NGs were optimized for the desired physicochemical characteristics.

TMZ was also quantified to determine EE% of TMZ-loaded NGs.

3.2. Synthesizing theranostic NGs

The same procedures of drug encapsulation were used to prepare TMZ/USPIO- and DOX/USPIO-Co-loaded NGs. These were preliminary investigations to prepare theranostic NGs.

NGs were checked for their physicochemical characteristics using DLS/ELS techniques.

4. References

1. Gromeier M, Lachmann S, Rosenfeld MR, Gutin PH, Wimmer E. Intergeneric poliovirus recombinants for the treatment of malignant glioma. *Proceedings of the National Academy of Sciences of the United States of America*. 2000;97(12):6803-8.
2. Liu Z, Yao Z, Li C, Lu Y, Gao C. Gene Expression Profiling in Human High-Grade Astrocytomas. *Comparative and Functional Genomics*. 2011;2011.
3. Louis DN, Ohgaki H, Wiestler OD, Cavenee WK, Burger PC, Jouvet A, et al. The 2007 WHO Classification of Tumours of the Central Nervous System. *Acta Neuropathologica*. 2007;114(2):97-109.
4. R. Stupp JCTonn. High-grade malignant glioma: ESMO Clinical Practice Guidelines for diagnosis, treatment and follow-up.
5. Jackson M, Hassiotou F, Nowak A. Glioblastoma stem-like cells: At the root of tumor recurrence and a therapeutic target. *Carcinogenesis*. 2014.
6. Mason WP, Maestro RD, Eisenstat D, Forsyth P, Fulton D, Laperrière N, et al. Canadian recommendations for the treatment of glioblastoma multiforme. *Current Oncology*. 2007;14(3):110-7.
7. M. Stephen Mahaley J, Curtis Mettlin, Nachimuthu Natarajan, Edward R. Laws J, Barbara B. Peace. National survey of patterns of care for brain-tumor patients. *Journal of Neurosurgery*. 1989;71(6):826-36.
8. Ohgaki H, Dessen P, Jourde B, Horstmann S, Nishikawa T, Di Patre P-L, et al. Genetic Pathways to Glioblastoma: A Population-Based Study. *Cancer Research*. 2004;64(19):6892-9.
9. Scherer HJ. Cerebral Astrocytomas and Their Derivatives. *The American Journal of Cancer*. 1940;40(2):159-98.
10. Ohgaki H, Kleihues P. The Definition of Primary and Secondary Glioblastoma. *Clinical Cancer Research*. 2013;19(4):764-72.
11. Narahara K, Kimura S, Kikkawa K, Takahashi Y, Wakita Y, Kasai R, et al. Probable assignment of soluble isocitrate dehydrogenase (IDH1) to 2q33.3. *Human Genetics*. 1985;71(1):37-40.
12. Turcan S, Rohle D, Goenka A, Walsh LA, Fang F, Yilmaz E, et al. IDH1 mutation is sufficient to establish the glioma hypermethylator phenotype. *Nature*. 2012;483(7390):479-83.
13. Balss J, Meyer J, Mueller W, Korshunov A, Hartmann C, von Deimling A. Analysis of the IDH1 codon 132 mutation in brain tumors. *Acta Neuropathologica*. 2008;116(6):597-602.
14. Watanabe T, Nobusawa S, Kleihues P, Ohgaki H. IDH1 Mutations Are Early Events in the Development of Astrocytomas and Oligodendrogliomas. *The American Journal of Pathology*. 2009;174(4):1149-53.
15. Yan H, Parsons DW, Jin G, McLendon R, Rasheed BA, Yuan W, et al. IDH1 and IDH2 Mutations in Gliomas. *New England Journal of Medicine*. 2009;360(8):765-73.
16. Nobusawa S, Watanabe T, Kleihues P, Ohgaki H. IDH1 Mutations as Molecular Signature and Predictive Factor of Secondary Glioblastomas. *American Association for Cancer Research*. 2009;15(19):6002-7.
17. Mellai M, Caldera V, Annovazzi L, Schiffer D. The Distribution and Significance of IDH Mutations in Gliomas 2013 2013-02-27.
18. Ohgaki H. Epidemiology of Brain Tumors. In: Verma M, editor. *Cancer Epidemiology. Methods in Molecular Biology*. 472: Humana Press; 2009. p. 323-42.
19. Canadian Cancer Society SC, Provincial territorial Cancer Registries, Public Health Agency of Canada. *Canadian Cancer Statistics 2012*.
20. Glioblastoma: Alberta Health Services, CLINICAL PRACTICE GUIDELINE CNS-001 version 3; 2012. 15 p.
21. Schwartzbaum JA, Fisher JL, Aldape KD, Wrensch M. Epidemiology and molecular pathology of glioma. *Nat Clin Pract Neuro*. 2006;2(9):494-503.

22. Sizoo EM, Braam L, Postma TJ, Pasman HRW, Heimans JJ, Klein M, et al. Symptoms and problems in the end-of-life phase of high-grade glioma patients. *Neuro-Oncology*. 2010;12(11):1162-6.
23. Posti JP, Bori M, Kauko T, Sankinen M, Nordberg J, Rahi M, et al. Presenting symptoms of glioma in adults. *Acta Neurologica Scandinavica*. 2015;131(2):88-93.
24. Brat DJ, Prayson RA, Ryken TC, Olson JJ. Diagnosis of malignant glioma: role of neuropathology. *Journal of Neuro-Oncology*. 2008;89(3):287-311.
25. David Oh, Richard A. Prayson. Evaluation of Epithelial and Keratin Markers in Glioblastoma Multiforme. *Archives of Pathology & Laboratory Medicine*. 1999;123(10):917-20.
26. Beer TW, Shepherd P, Theaker JM. Ber EP4 and epithelial membrane antigen aid distinction of basal cell, squamous cell and basosquamous carcinomas of the skin. *Histopathology*. 2000;37(3):218-23.
27. Goldman LW. Principles of CT: Multislice CT. *Journal of Nuclear Medicine Technology*. 2008;36(2):57-68.
28. Achiam MP, Løgager VB, Skjoldbye B, Møller JM, Lorenzen T, Rasmussen VL, et al. Preoperative CT versus diffusion weighted magnetic resonance imaging of the liver in patients with rectal cancer; a prospective randomized trial. *PeerJ*. 2016;4:e1532.
29. Brenner DJ, Hall EJ. Computed Tomography — An Increasing Source of Radiation Exposure. *New England Journal of Medicine*. 2007;357(22):2277-84.
30. Bongartz G. Technical principles of MSCT: European Guidelines for Multislice Computed Tomography; 2004 March 2004. 13 p.
31. Pooley RA. Fundamental Physics of MR Imaging. *RadioGraphics*. 2005;25(4):1087-99.
32. Scherzinger AL, Hendee WR. Basic Principles of Magnetic Resonance Imaging—An Update. *Western Journal of Medicine*. 1985;143(6):782-92.
33. Gustav J. Strijkers WJMM, Geralda A. F. van Tilborg and Klaas Nicolay. MRI Contrast Agents: Current Status and Future Perspectives. 15 p.
34. Aime S, Castelli DD, Crich SG, Gianolio E, Terreno E. Pushing the Sensitivity Envelope of Lanthanide-Based Magnetic Resonance Imaging (MRI) Contrast Agents for Molecular Imaging Applications. *Accounts of Chemical Research*. 2009;42(7):822-31.
35. Michel Lacroix, Dima Abi-Said, Daryl R. Fourney, Ziya L. Gokaslan, Weiming Shi, Franco DeMonte, et al. A multivariate analysis of 416 patients with glioblastoma multiforme: prognosis, extent of resection, and survival. *Journal of Neurosurgery*. 2001;95(2):190-8.
36. Julka PK. Postoperative treatment of glioblastoma multiforme with radiation therapy plus concomitant and adjuvant temozolomide : A mono-institutional experience of 215 patients. *Can Res Ther*. 2013;9:381-6.
37. Walker MD, Green SB, Byar DP, Alexander E, Batzdorf U, Brooks WH, et al. Randomized Comparisons of Radiotherapy and Nitrosoureas for the Treatment of Malignant Glioma after Surgery. *New England Journal of Medicine*. 1980;303(23):1323-9.
38. Weller M, Cloughesy T, Perry JR, Wick W. Standards of care for treatment of recurrent glioblastoma—are we there yet? *Neuro-Oncology*. 2013;15(1):4-27.
39. Yung WKA, Albright RE, Olson J, Fredericks R, Fink K, Prados MD, et al. A phase II study of temozolomide vs. procarbazine in patients with glioblastoma multiforme at first relapse. *British Journal of Cancer*. 2000;83(5):588-93.
40. Brada M, Hoang-Xuan K, Rampling R, Dietrich P-Y, Dirix LY, Macdonald D, et al. Multicenter phase II trial of temozolomide in patients with glioblastoma multiforme at first relapse. *Annals of Oncology*. 2001;12(2):259-66.
41. Reithmeier T, Graf E, Piroth T, Trippel M, Pinsker M, Nikkhah G. BCNU for recurrent glioblastoma multiforme: efficacy, toxicity and prognostic factors. *BMC Cancer*. 2010;10(1):30.

42. van den Bent MJ, Brandes AA, Rampling R, Kouwenhoven MCM, Kros JM, Carpentier AF, et al. Randomized Phase II Trial of Erlotinib Versus Temozolomide or Carmustine in Recurrent Glioblastoma: EORTC Brain Tumor Group Study 26034. *Journal of Clinical Oncology*. 2009;27(8):1268-74.
43. Brandes AA, Tosoni A, Amistà P, Nicolardi L, Grosso D, Berti F, et al. How effective is BCNU in recurrent glioblastoma in the modern era?: A phase II trial. *Neurology*. 2004;63(7):1281-4.
44. Wick W, Puduvalli VK, Chamberlain MC, van den Bent MJ, Carpentier AF, Cher LM, et al. Phase III Study of Enzastaurin Compared With Lomustine in the Treatment of Recurrent Intracranial Glioblastoma. *Journal of Clinical Oncology*. 2010;28(7):1168-74.
45. Happold C, Roth P, Wick W, Steinbach J, Linnebank M, Weller M, et al. ACNU-based chemotherapy for recurrent glioma in the temozolomide era. *Journal of Neuro-Oncology*. 2009;92(1):45-8.
46. Addeo R, Caraglia M, De Santi MS, Montella L, Abbruzzese A, Parlato C, et al. A new schedule of fotemustine in temozolomide-pretreated patients with relapsing glioblastoma. *Journal of Neuro-Oncology*. 2011;102(3):417-24.
47. Fan CH, Liu WL, Cao H, Wen C, Chen L, Jiang G. O6-methylguanine DNA methyltransferase as a promising target for the treatment of temozolomide-resistant gliomas. *Cell Death Dis*. 2013;4:e876.
48. Stupp R, Hegi ME, Mason WP, van den Bent MJ, Taphoorn MJB, Janzer RC, et al. Effects of radiotherapy with concomitant and adjuvant temozolomide versus radiotherapy alone on survival in glioblastoma in a randomised phase III study: 5-year analysis of the EORTC-NCIC trial. *The Lancet Oncology*. 2009;10(5):459-66.
49. Messaoudi K, Clavreul A, Lagarce F. Toward an effective strategy in glioblastoma treatment. Part I: resistance mechanisms and strategies to overcome resistance of glioblastoma to temozolomide. *Drug Discovery Today*. 2015;20(7):899-905.
50. Franceschi E, Omuro AMP, Lassman AB, Demopoulos A, Nolan C, Abrey LE. Salvage temozolomide for prior temozolomide responders. *Cancer*. 2005;104(11):2473-6.
51. Kong, Lee, Kim, Son, Lim, Kim, et al. A pilot study of metronomic temozolomide treatment in patients with recurrent temozolomide-refractory glioblastoma. *Oncology Reports*. 2006;16(5):1117-21.
52. Berrocal A, Perez Segura P, Gil M, Balaña C, Garcia Lopez J, Yaya R, et al. Extended-schedule dose-dense temozolomide in refractory gliomas. *Journal of Neuro-Oncology*. 2010;96(3):417-22.
53. Perry JR, Bélanger K, Mason WP, Fulton D, Kavan P, Easaw J, et al. Phase II Trial of Continuous Dose-Intense Temozolomide in Recurrent Malignant Glioma: RESCUE Study. *Journal of Clinical Oncology*. 2010;28(12):2051-7.
54. Kong D-S, Lee J-I, Kim JH, Kim ST, Kim WS, Suh Y-L, et al. Phase II trial of low-dose continuous (metronomic) treatment of temozolomide for recurrent glioblastoma. *Neuro-Oncology*. 2010;12(3):289-96.
55. Norden AD, Lesser GJ, Drappatz J, Ligon KL, Hammond SN, Lee EQ, et al. Phase 2 study of dose-intense temozolomide in recurrent glioblastoma. *Neuro-Oncology*. 2013;15(7):930-5.
56. Stupp R, Mason WP, van den Bent MJ, Weller M, Fisher B, Taphoorn MJB, et al. Radiotherapy plus Concomitant and Adjuvant Temozolomide for Glioblastoma. *New England Journal of Medicine*. 2005;352(10):987-96.
57. Arcamone F, Cassinelli G, Fantini G, Grein A, Orezzi P, Pol C, et al. Adriamycin, 14-hydroxydaimomycin, a new antitumor antibiotic from *S. Peucetius* var. *caesius*. *Biotechnology and Bioengineering*. 1969;11(6):1101-10.
58. Barenholz Y. Doxil® — The first FDA-approved nano-drug: Lessons learned. *Journal of Controlled Release*. 2012;160(2):117-34.
59. O'Brien MER, Wigler N, Inbar M, Rosso R, Grischke E, Santoro A, et al. Reduced cardiotoxicity and comparable efficacy in a phase III trial of pegylated liposomal doxorubicin HCl (CAELYX™/Doxil®) versus conventional doxorubicin for first-line treatment of metastatic breast cancer. *Annals of Oncology*. 2004;15(3):440-9.

60. PubChem Compound Database; [Internet]. [cited accessed Apr. 1, 2016].
61. Rahman A, Carmichael D, Harris M, Roh JK. Comparative Pharmacokinetics of Free Doxorubicin and Doxorubicin Entrapped in Cardiolipin Liposomes. *Cancer Research*. 1986;46(5):2295-9.
62. Bigotte L, Olsson Y. Cytofluorescence localization of adriamycin in the nervous system. *Acta Neuropathologica*.58(3):193-202.
63. Gerweck LE, Seetharaman K. Cellular pH Gradient in Tumor versus Normal Tissue: Potential Exploitation for the Treatment of Cancer. *Cancer Research*. 1996;56(6):8.
64. Greish K. Enhanced permeability and retention of macromolecular drugs in solid tumors: A royal gate for targeted anticancer nanomedicines. *Journal of Drug Targeting*. 2007;15(7-8):457-64.
65. Ananda S, Nowak AK, Cher L, Dowling A, Brown C, Simes J, et al. Phase 2 trial of temozolomide and pegylated liposomal doxorubicin in the treatment of patients with glioblastoma multiforme following concurrent radiotherapy and chemotherapy. *Journal of Clinical Neuroscience*. 2011;18(11):1444-8.
66. Yousefpour P, Atyabi F, Vasheghani-Farahani E, Movahedi A-AM, Dinarvand R. Targeted delivery of doxorubicin-utilizing chitosan nanoparticles surface-functionalized with anti-Her2 trastuzumab. *International Journal of Nanomedicine*. 2011;6:1977-90.
67. Kang JH, Adamson C. Novel chemotherapeutics and other therapies for treating high-grade glioma. *Expert Opinion on Investigational Drugs*.0(0):1-19.
68. Thomas AA, Brennan CW, DeAngelis LM, Omuro AM. EMerging therapies for glioblastoma. *JAMA Neurology*. 2014;71(11):1437-44.
69. Dresemann G. Imatinib and hydroxyurea in pretreated progressive glioblastoma multiforme: a patient series. *Annals of Oncology*. 2005;16(10):1702-8.
70. Brennan CW, Verhaak RGW, McKenna A, Campos B, Noushmehr H, Salama SR, et al. The Somatic Genomic Landscape of Glioblastoma. *Cell*. 2013;155(2):462-77.
71. Ettinghausen S, Rosenberg S. The adoptive immunotherapy of cancer using lymphokine activated killer cells and recombinant interleukin-2. *Springer Semin Immunopathol*. 1986;9(1):51-71.
72. Wei J, Barr J, Kong L-Y, Wang Y, Wu A, Sharma AK, et al. Glioma associated cancer-initiating cells induce immune suppression. *Clinical cancer research : an official journal of the American Association for Cancer Research*. 2010;16(2):461-73.
73. Forrester JV, Xu H, Lambe T, Cornall R. Immune privilege or privileged immunity? *Mucosal Immunol*. 2008;1(5):372-81.
74. Stupp R, Wong ET, Kanner AA, Steinberg D, Engelhard H, Heidecke V, et al. NovoTTF-100A versus physician's choice chemotherapy in recurrent glioblastoma: A randomised phase III trial of a novel treatment modality. *European Journal of Cancer*. 2012;48(14):2192-202.
75. Swanson KD, Lok E, Wong ET. An Overview of Alternating Electric Fields Therapy (NovoTTF Therapy) for the Treatment of Malignant Glioma. *Current Neurology and Neuroscience Reports*. 2016;16:8.
76. Leweke F, Damian MS, Schindler C, Schachenmayr W. Multidrug Resistance in Glioblastoma: Chemosensitivity Testing and Immunohistochemical Demonstration of P-Glycoprotein. *Pathology - Research and Practice*. 1998;194(3):149-55.
77. Tivnan A, Zakaria Z, O'Leary C, Kogel D, Pokorny JL, Sarkaria JN, et al. Inhibition of Multidrug resistance protein 1 (MRP1) improves chemotherapy drug response in primary and recurrent glioblastoma multiforme. *Frontiers in Neuroscience*. 2015;9.
78. Loscher W, Potschka H. Drug resistance in brain diseases and the role of drug efflux transporters. *Nat Rev Neurosci*. 2005;6(8):591-602.
79. McKinnon. *Towards Precriving Practice: The blood-brain barrier*. 6 ed2007. 5:6 p.
80. Uston C. NEUROwords Dr. Thomas Willis' Famous Eponym: The Circle of Willis. *Journal of the History of the Neurosciences*. 2005;14(1):16-21.

81. Abbott NJ, Patabendige AAK, Dolman DEM, Yusof SR, Begley DJ. Structure and function of the blood–brain barrier. *Neurobiology of Disease*. 2010;37(1):13-25.
82. De Jong WH, Borm PJA. Drug delivery and nanoparticles: Applications and hazards. *International Journal of Nanomedicine*. 2008;3(2):133-49.
83. Raemdonck K, Demeester J, De Smedt S. Advanced nanogel engineering for drug delivery. *Soft Matter*. 2009;5(4):707-15.
84. Soni G, Yadav KS. Nanogels as potential nanomedicine carrier for treatment of cancer: A mini review of the state of the art. *Saudi Pharmaceutical Journal*. 2016;24(2):133-9.
85. Caraglia. *Nanotech Revolution for the Anti-Cancer Drug Delivery through Blood- Brain-Barrier*. Bentham Science. 2012;12(3):186-96.
86. Reisch A, Runser A, Arntz Y, Mély Y, Klymchenko AS. Charge-Controlled Nanoprecipitation as a Modular Approach to Ultrasmall Polymer Nanocarriers: Making Bright and Stable Nanoparticles. *ACS Nano*. 2015;9(5):5104-16.
87. Shirsat AE, Chitlange SS. Application of quality by design approach to optimize process and formulation parameters of rizatriptan loaded chitosan nanoparticles. *Journal of Advanced Pharmaceutical Technology & Research*. 2015;6(3):88-96.
88. Brunel F, Véron L, Ladavière C, David L, Domard A, Delair T. Synthesis and Structural Characterization of Chitosan Nanogels. *Langmuir*. 2009;25(16):8935-43.
89. Kiang T, Wen J, Lim HW, Leong KW. The effect of the degree of chitosan deacetylation on the efficiency of gene transfection. *Biomaterials*. 2004;25(22):5293-301.
90. Wukasz RF. *Proceedings of the 49th Industrial Waste Conference Purdue University, May 1994*: Taylor & Francis; 1994.
91. Mironov V, Kasyanov V, Zheng Shu X, Eisenberg C, Eisenberg L, Gonda S, et al. Fabrication of tubular tissue constructs by centrifugal casting of cells suspended in an in situ crosslinkable hyaluronan-gelatin hydrogel. *Biomaterials*. 2005;26(36):7628-35.
92. Tan H, Chu CR, Payne KA, Marra KG. Injectable in situ forming biodegradable chitosan–hyaluronic acid based hydrogels for cartilage tissue engineering. *Biomaterials*. 2009;30(13):2499-506.
93. Lee H, Mok H, Lee S, Oh Y-K, Park TG. Target-specific intracellular delivery of siRNA using degradable hyaluronic acid nanogels. *Journal of Controlled Release*. 2007;119(2):245-52.
94. Mohanraj. Nanoparticles—a review. *Tropical Journal of Pharmaceutical Research*. 2006;5:561-73.
95. Yu MK, Park J, Jon S. Targeting Strategies for Multifunctional Nanoparticles in Cancer Imaging and Therapy. *Theranostics*. 2012;2(1):3-44.
96. Ghaz-Jahanian M, Abbaspour-Aghdam F, Anarjan N, Berenjian A, Jafarizadeh-Malmiri H. Application of Chitosan-Based Nanocarriers in Tumor-Targeted Drug Delivery. *Mol Biotechnol*. 2015;57(3):201-18.
97. Prabhakar U, Maeda H, Jain RK, Sevick-Muraca EM, Zamboni W, Farokhzad OC, et al. Challenges and key considerations of the enhanced permeability and retention (EPR) effect for nanomedicine drug delivery in oncology. *Cancer research*. 2013;73(8):2412-7.
98. Bae YH, Park K. Targeted drug delivery to tumors: Myths, reality and possibility. *Journal of Controlled Release*. 2011;153(3):198-205.
99. Di Marco M, Sadun C, Port M, Guilbert I, Couvreur P, Dubernet C. Physicochemical characterization of ultrasmall superparamagnetic iron oxide particles (USPIO) for biomedical application as MRI contrast agents. *International Journal of Nanomedicine*. 2007;2(4):609-22.
100. Lammers T, Koczera P, Fokong S, Gremse F, Ehling J, Vogt M, et al. Theranostic USPIO-Loaded Microbubbles for Mediating and Monitoring Blood-Brain Barrier Permeation. *Advanced functional materials*. 2015;25(1):36-43.
101. Liang X-J, Chen C, Zhao Y, Wang PC. Circumventing Tumor Resistance to Chemotherapy by Nanotechnology. *Methods in molecular biology (Clifton, NJ)*. 2010;596:467-88.

102. Merisko-Liversidge EM, Liversidge GG. Drug Nanoparticles: Formulating Poorly Water-Soluble Compounds. *Toxicologic Pathology*. 2008;36(1):43-8.
103. Lu J, Liong M, Zink JJ, Tamanoi F. Mesoporous Silica Nanoparticles as a Delivery System for Hydrophobic Anticancer Drugs. *Small*. 2007;3(8):1341-6.
104. Park JH, Saravanakumar G, Kim K, Kwon IC. Targeted delivery of low molecular drugs using chitosan and its derivatives. *Advanced Drug Delivery Reviews*. 2010;62(1):28-41.
105. Chan M, Almutairi A. Nanogels as imaging agents for modalities spanning the electromagnetic spectrum. *Materials Horizons*. 2016;3(1):21-40.
106. Sierra-Martin B, Fernandez-Barbero A. Multifunctional hybrid nanogels for theranostic applications. *Soft Matter*. 2015;11(42):8205-16.
107. Feng C, Sun G, Wang Z, Cheng X, Park H, Cha D, et al. Transport mechanism of doxorubicin loaded chitosan based nanogels across intestinal epithelium. *European Journal of Pharmaceutics and Biopharmaceutics*. 2014;87(1):197-207.
108. Azadi A, Rouini M-R, Hamidi M. Neuropharmacokinetic evaluation of methotrexate-loaded chitosan nanogels. *International Journal of Biological Macromolecules*. 2015;79:326-35.
109. Das D, Patra P, Ghosh P, Rameshbabu AP, Dhara S, Pal S. Dextrin and poly(lactide)-based biocompatible and biodegradable nanogel for cancer targeted delivery of doxorubicin hydrochloride. *Polymer Chemistry*. 2016.
110. Kapse-Mistry S, Govender T, Srivastava R, Yergeri M. Nanodrug delivery in reversing multidrug resistance in cancer cells. *Frontiers in Pharmacology*. 2014;5:159.
111. Unsoy G, Khodadust R, Yalcin S, Mutlu P, Gunduz U. Synthesis of Doxorubicin loaded magnetic chitosan nanoparticles for pH responsive targeted drug delivery. *European Journal of Pharmaceutical Sciences*. 2014;62:243-50.
112. Fang C, Wang K, Stephen ZR, Mu Q, Kievit FM, Chiu DT, et al. Temozolomide Nanoparticles for Targeted Glioblastoma Therapy. *ACS Applied Materials & Interfaces*. 2015;7(12):6674-82.
113. Kelkar SS, Reineke TM. Theranostics: Combining Imaging and Therapy. *Bioconjugate Chemistry*. 2011;22(10):1879-903.
114. Wang C, Ravi S, Garapati US, Das M, Howell M, MallelaMallela J, et al. Multifunctional Chitosan Magnetic-Graphene (CMG) Nanoparticles: a Theranostic Platform for Tumor-targeted Co-delivery of Drugs, Genes and MRI Contrast Agents. *Journal of materials chemistry B, Materials for biology and medicine*. 2013;1(35):4396-405.
115. Cavalli R, Argenziano M, Vigna E, Giustetto P, Torres E, Aime S, et al. Preparation and in vitro characterization of chitosan nanobubbles as theranostic agents. *Colloids and Surfaces B: Biointerfaces*. 2015;129:39-46.
116. Pecora R. Dynamic Light Scattering Measurement of Nanometer Particles in Liquids. *Journal of Nanoparticle Research*. 2000;2(2):123-31.
117. Goodman JW. Some fundamental properties of speckle*. *J Opt Soc Am*. 1976;66(11):1145-50.
118. Josefowicz J, Hallett FR. Homodyne Electrophoretic Light Scattering of Polystyrene Spheres by Laser Cross-Beam Intensity Correlation. *Appl Opt*. 1975;14(3):740-2.
119. Privalov PL, Potekhin SA. Scanning microcalorimetry in studying temperature-induced changes in proteins. *Methods Enzymol*. 1986;131:4-51.
120. Haines PJ, Reading M, Wilburn FW. Chapter 5 - Differential Thermal Analysis and Differential Scanning Calorimetry. In: Michael EB, editor. *Handbook of Thermal Analysis and Calorimetry*. Volume 1: Elsevier Science B.V.; 1998. p. 279-361.
121. Gill P, Moghadam TT, Ranjbar B. Differential Scanning Calorimetry Techniques: Applications in Biology and Nanoscience. *Journal of Biomolecular Techniques : JBT*. 2010;21(4):167-93.
122. Hariharan P, Hariharan P. 16 - Fourier Transform Spectroscopy. *Basics of Interferometry (Second edition)*. Burlington: Academic Press; 2007. p. 145-51.

123. Griffiths PR, De Haseth JA, Winefordner JD. *Fourier Transform Infrared Spectrometry*: Wiley; 2007.
124. Abdelwahed W, Degobert G, Stainmesse S, Fessi H. Freeze-drying of nanoparticles: Formulation, process and storage considerations. *Advanced Drug Delivery Reviews*. 2006;58(15):1688-713.
125. Lee MK, Kim MY, Kim S, Lee J. Cryoprotectants for freeze drying of drug nano-suspensions: Effect of freezing rate. *Journal of Pharmaceutical Sciences*. 2009;98(12):4808-17.
126. Fonte P, Soares S, Costa A, Andrade JC, Seabra V, Reis S, et al. Effect of cryoprotectants on the porosity and stability of insulin-loaded PLGA nanoparticles after freeze-drying. *Biomatter*. 2012;2(4):329-39.
127. Kumar S, Gokhale R, Burgess DJ. Sugars as bulking agents to prevent nano-crystal aggregation during spray or freeze-drying. *Int J Pharm*. 2014;471(1–2):303-11.
128. Michael JP. *Mechanisms of Protein Stabilization during Freeze-Drying and Storage*. *Freeze-Drying/Lyophilization Of Pharmaceutical & Biological Products*, Third Edition. *Drugs and the Pharmaceutical Sciences*: Informa Healthcare; 2004.

5. Techniques used in physicochemical characterization of NPs:

5.1.1 Dynamic light scattering, DLS:

DLS is a technique in physics used in measuring size (hydrodynamic diameter, D_H) and size distribution (Polydispersity Index, PDI) of nanoparticles in a suspension.(116)

Briefly, a monochromatic light source, i.e. a laser (generally about 630 nm) is shot through a polarizer before hitting the particles of a sample (Figure 11a). The light is then scattered in all directions and interferes with each other either constructively or destructively (speckle patterns). This process is repeated at short time intervals with analyzing the resulting patterns by an autocorrelator to compare the light intensity at each spot over time.(117) Since particles are submitted to the Brownian motion, the scattered light intensity varies with the nanoparticle speed in their medium. If the particles are large, the scattered light will present a high intensity level but few variations (the particles do not move fast in this case). If the particles are small, they will move faster but the light will scatter less. Therefore, the intensity pattern will be low but with a high variability (fig. 11 b).

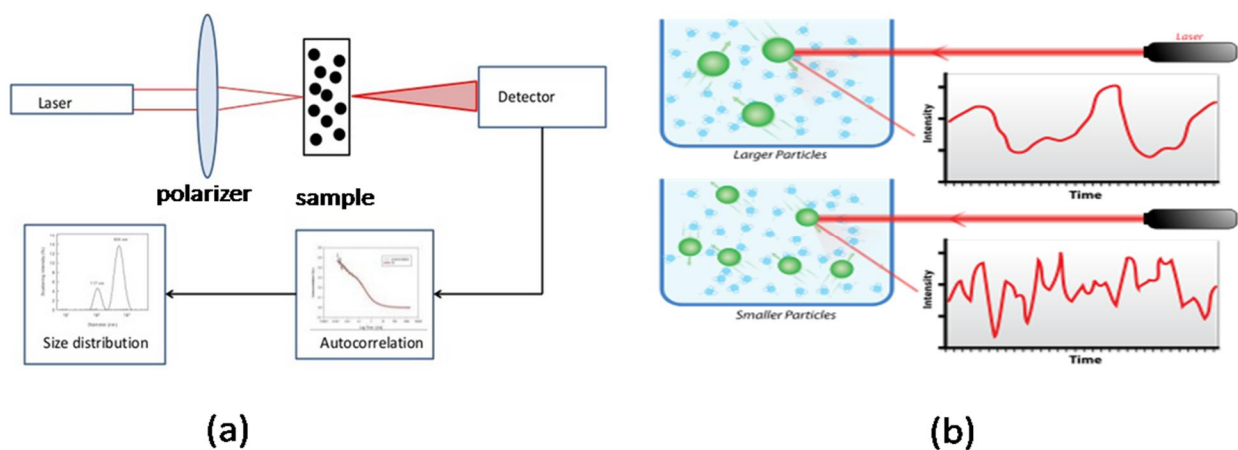


Fig 11. a- Arrangement of the DLS measuring technique in which a laser beam is polarized before hitting the sample particles. The light then gets scattered in all directions resulting in constructive and destructive interferences with the scattered beams. **b-** Impact of particle size on the intensity of a scattered light where the large slowly-moving particles produce high-intensity scattered light while the smaller faster-moving particles produce lower-intensity scattered light.

Therefore, using the Stoke-Einstein equation, the average hydrodynamic diameter can be deduced from the diffusion coefficient, itself deduced from the mean intensity of scattered light. This calculation assumes that all particles are spheres.

Procedure. Samples were diluted in 3 folds their volume with MilliQ water. This dilution produced an attenuation factor of 6 or 7. To ensure reproducibility, each sample was analyzed in triplicates of 25 cycles. Laser position was determined automatically and samples were measured at 20°C at a scattering angle of 173°. DLS data were expressed in both % Intensity in order to detect the potential presence of aggregates in the nanoparticle suspensions. A typical graph of size vs intensity % is given in Figure 12.

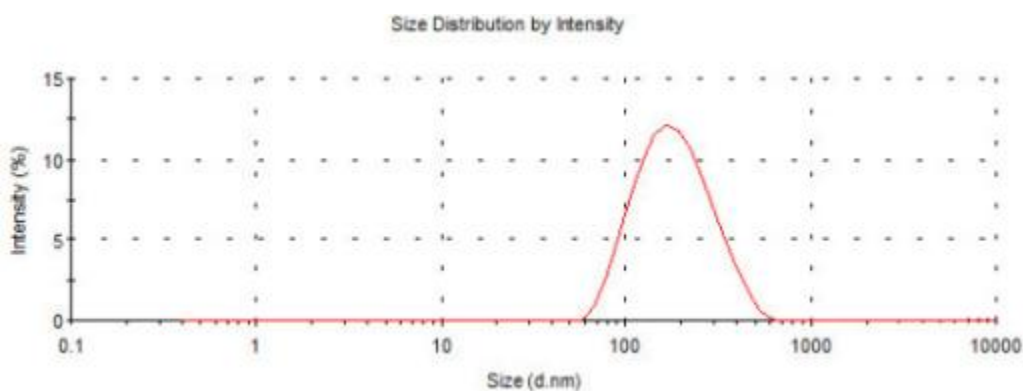


Fig 12. A typical DLS graph showing a single population of NPs with an average hydrodynamic diameter around 200 nm.

5.1.2 Electrophoretic light scattering, ELS:

ELS is based on the same concept of DLS where the frequency shift of incident laser beam depends on the mobility of dispersed particles. However, the particle movement in ELS technique is caused by an oscillating electric field. In an instrument such as Malvern Zetasizer NanoZS (the one we used), the cell in which the sample was measured contained two electrodes. Once the electrical field is applied to the electrodes, the charged particles migrate to the electrode with the opposite

charge. This migration takes place at different velocities that are proportional to the net charge on the surface of each particle. The velocity of each is calculated and mathematically interpreted into a net charge (Figure 13). Results are then interpreted through a photomultiplier to measure the mean electrophoretic mobility then calculating zeta potential (ZP) to get information about the surface charge of a particle.(118)

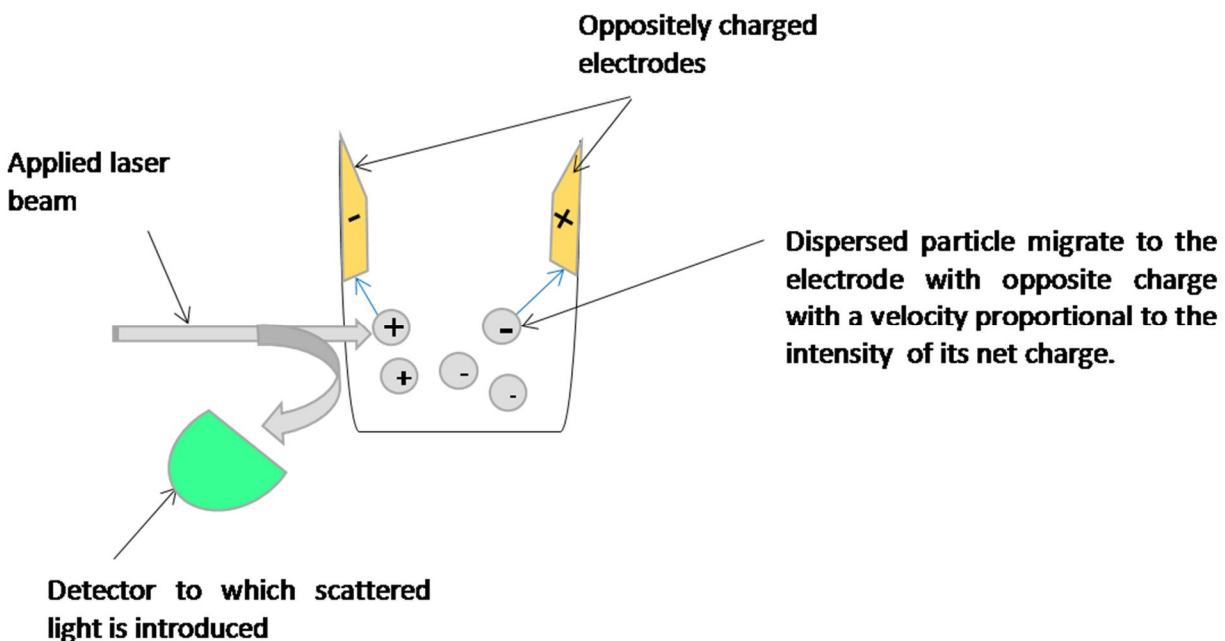


Fig 13. Cuvette for Zeta potential (ZP) measurements containing two opposite electrodes. When an electric current is applied, each particle is then attracted to the electrode displaying the opposite charge. The velocity by which a particle migrates is directly proportional to how much charge it carries. The incident laser beam is then scattered when hitting the mobile migrating parts and the scattered light is determined by photomultiplier.

Procedure. Samples were diluted in 3 folds their volume of MilliQ water. Instrument settings were adjusted at 20°C, 150 V. The instrument was calibrated with a Malvern - 42 mV standard prior to each set of measurements. Each sample was measured 3 times allowing 40 runs for each measurement. For all kinds of measurements pure water, water/

citric acid mixture or sugar-based solutions were used as a reference dispersing medium according to the situation of each sample. Figure 14 shows the ZP analysis of chitosan NPs.

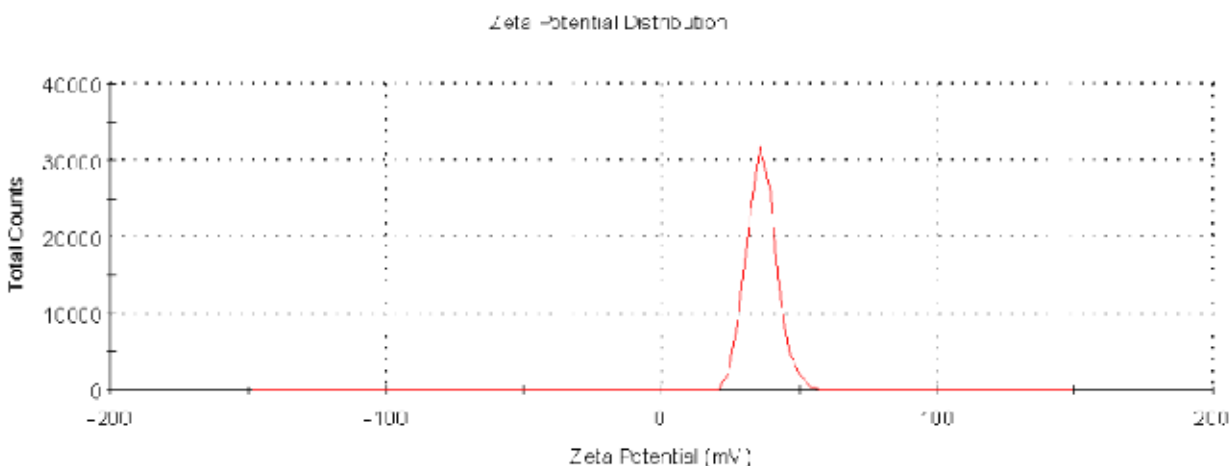


Fig 14. Zeta Potential of chitosan-based NPs measured by the ELS technique. The mean value is displayed in the positive range indicating a positive net surface charge of the chitosan NPs.

6. Techniques used in investigating NPs stability:

6.1.1 Differential scanning calorimetry, DSC:

Generally, calorimetry is a primary technique which measures the thermal properties of materials and establishes a relation between temperature and specific physical properties of substances.(119) DSC can be defined as a thermodynamic tool directly assessing the heat energy uptake which occurs in a sample in response to regular increase or decrease in temperature. Calorimetry is applied in this setting mainly to monitor the phase transitions.

In a DSC experiment, equal amounts of energy, in the form of heat (at the same flow) are introduced into both sample and reference cells at the same time. The difference in the input energy required to match the temperature of the sample to that of the reference would be the amount of excess heat absorbed or released by the molecule in the sample (during an endothermic or exothermic process, respectively). The energy required to bring the sample to the same temperature as the reference, due to the presence of molecule(s) of interest in the sample, is expressed as heat excess. A thermal analysis instrument determines the temperature and heat flow associated with

material transitions as a function of time and temperature.(120) Radiated or absorbed heat quantity is measured on the basis of a difference between the sample and the reference material.(120, 121) as seen in Figure 15.

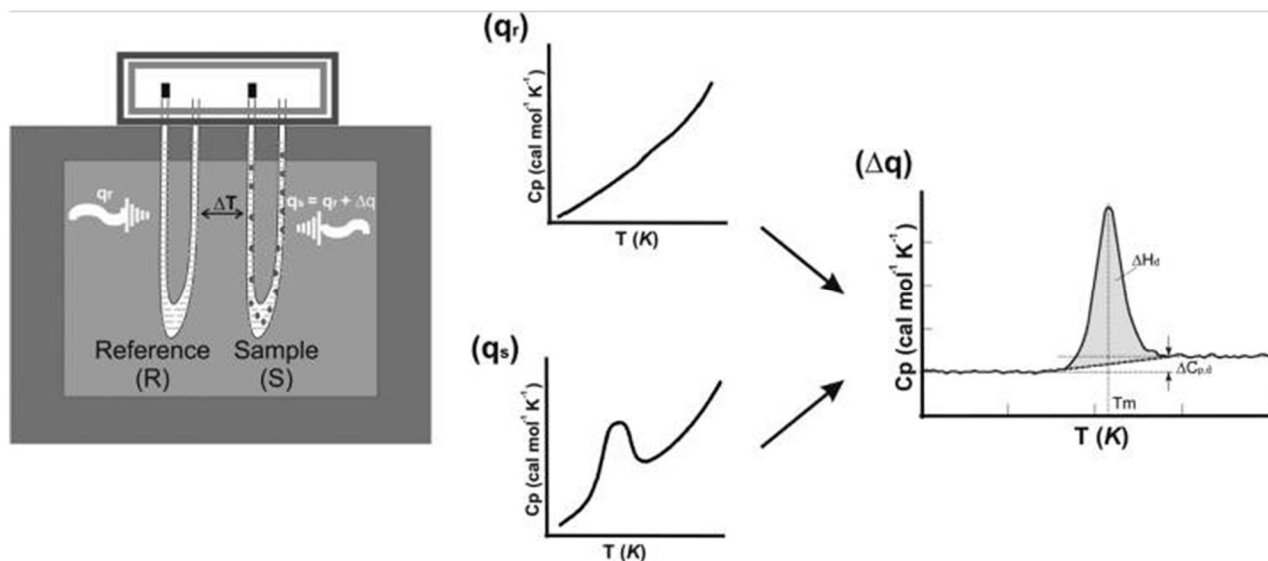


Fig 15. The heat excess (Δq) is the difference between q_s (amount of heat in the sample) and q_r (amount of heat in the reference). This heat excess corresponds to the difference in temperature required to bring the sample to the same temperature as the reference. When the reference DSC scan is subtracted from that one of the sample, the resulting plot shows how this heat excess (Δq) changes as a function of temperature T .

C_p : heat capacity of the sample, T_m : transition and melting point, T (K): Temperature, kelvin, ΔH_d : change in enthalpy.

Procedure. Using a Perkin Elmer DSC 4000 equipped with a VWR vacuum pump, and under N_2 gas purged at 20 mL/min, the thermal behaviour of various powders was determined against Zn reference (figure 16).

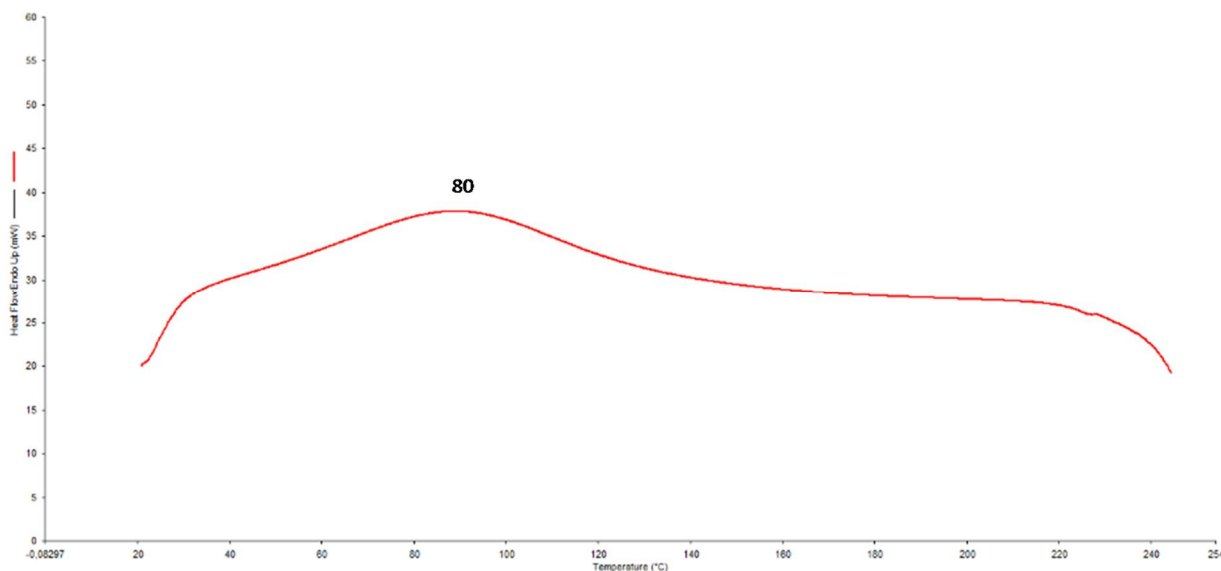


Fig 16. A thermogram of chitosan powder has undergone a phase transition in response to an increase in temperature, as can be observed by the large endothermic peak culminating at 80 °C corresponding to the melting point of the crystalline region.

6.1.2 Fourier Transform Infrared Spectroscopy, FTIR:

Chemical structures and functional groups of raw materials and NGs were confirmed by the FT-IR technique. From a broadband light source a beam with many frequencies of light at once shines and is applied to the sample. The light hits a mirror which is part of the Michelson Interferometer and which is moved by a motor. When the mirror moves, each wavelength of the light is blocked and transmitted periodically. The intonation of different wavelengths at different rates is responsible for the fingerprinted nature of the resulting spectrum (figure 17).(122) The process is repeated many times. Final results are interpreted as wavenumbers (cm^{-1}) plotted against % transmittance.(123)

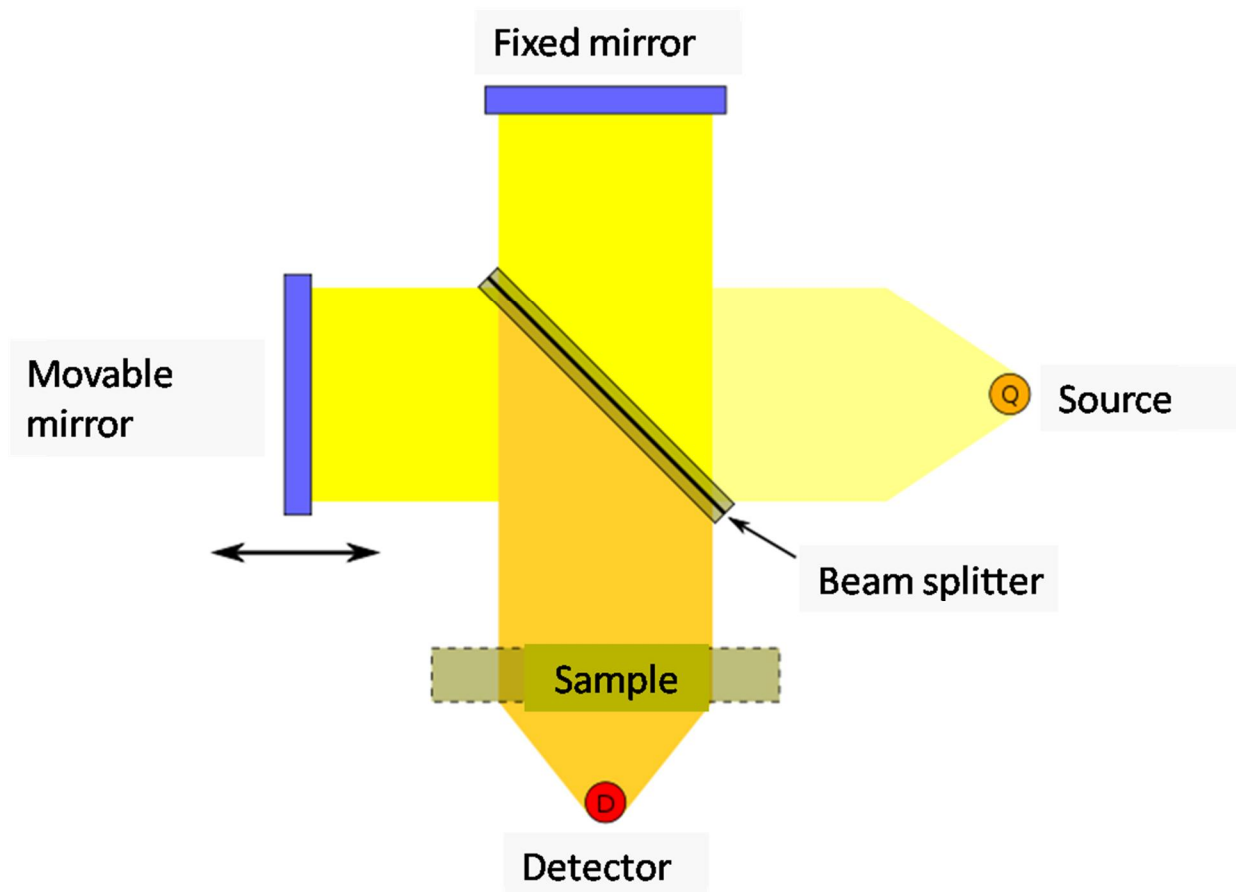


Fig. 17. A scheme showing the Michelson-based FTIR technique. The projected light is splitted by a beam splitter and part of it is reflected to a fixed mirror while the other part is reflected to a movable one. At the beam splitter, a recombination of the reflected beams occurs. These beams are furtherly reflected towards the sample. Absorption of some parts of the modulated energy from the interferometer may occur and a detector records the intensity of energy modulated to produce an interferogram.

Procedure. A very small amount of chitosan powder (typically 5-10 mg) was placed in the IR spectrometer (FTIR; Thermo Nicolet Nexus 6700, US). Average values of 32 scans were recorded, with a $4000\text{--}400\text{ cm}^{-1}$ wavelength scanning range. The functional groups of chitosan are interpreted in the spectrum peaks (figure 18).

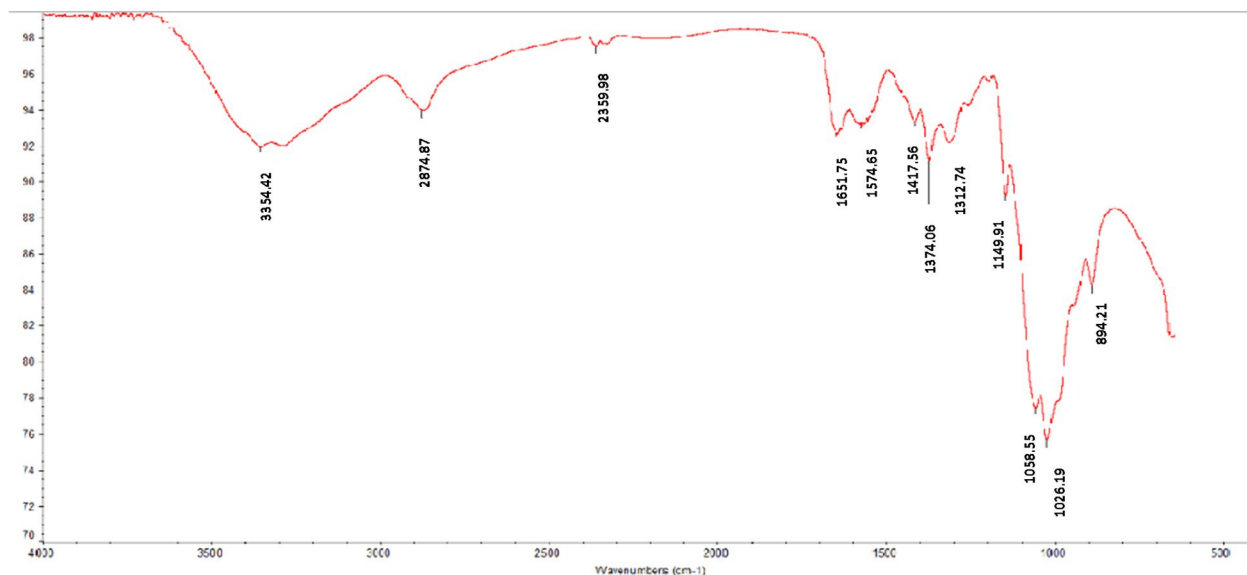


Fig. 18. An IR spectrum of chitosan showing that the broad absorption band from 3100 to 3650 cm^{-1} can be related to O-H stretching. In this area, two stretching vibrations of N-H of the primary amines can also be distinguished at 3300 and 3354 cm^{-1} . This characteristic primary amine function is also fingerprinted by two NH_2 scissoring bands at 1652 and 1575 cm^{-1} .

6.1.3 Freeze-drying, FD:

Freeze-drying, also known as lyophilization, is an industrial process which allows removing water from a frozen sample by sublimation and desorption under vacuum.(124) FD remains the process of choice to stabilize many dosage forms, including NPs, thus contributing to the production of NPs eligible for long-term storage. However, freeze-drying manifests its own issues due to freezing and dehydration and other mechanical stresses generated during the process (Figure 19).(124) A detailed explanation of the technique follows in the introduction of part one (article). To overcome these effects, cryoprotectants- especially sugars- are usually added prior to the freeze-drying process to form a glassy matrix in which the NPs are immobilized and protected against aggregation.(125-128)

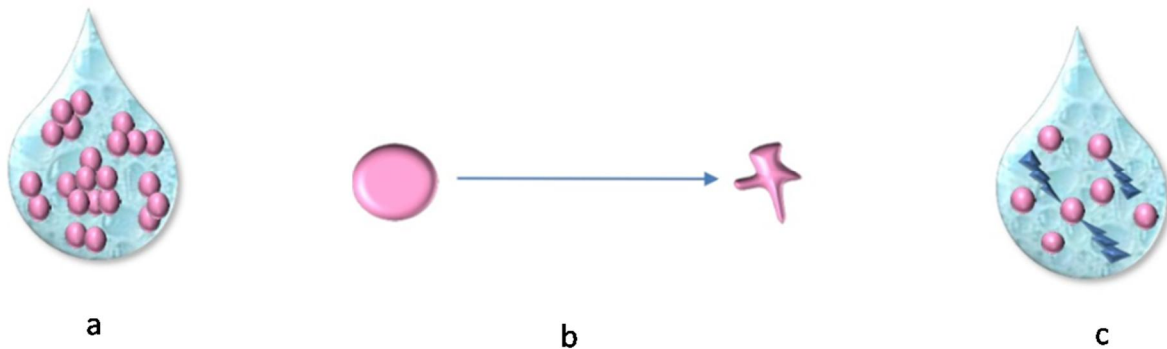


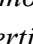


Fig. 19 Schemes of different troubles encountered in the process of freeze-drying. a) phase separation occurs in response to sudden solidification of colloidal solution following freezing. The formation of solid phase triggers NPs  to aggregate and form another separate phase. b) the dehydration stress induces NPs to shrink  due to sudden freezing and initial volume shrinkage. Both a & b are included under a more general problem known as freezing stress. c) mechanical stress showing the ice crystals exerting a mechanical pressure  to the NPs, a process which can lead to rupture of the NPs and further leakage of their contents.

Procedure. The sugar-based NGs were subjected to brutal freezing in liquid nitrogen at -180°C for 10 minutes before being stored at -80°C for 48 hrs until freeze-drying. Frozen samples were then freeze-dried at -51°C , 1.8 mBar for 24 – 48 hrs (Modulyo, Thermo Electron corporation).

Chapter two

Introduction to the reported results

The following experimental section is sub-divided in three parts.

The first part is constituted by a scientific article, entitled '*Recoverability of freeze-dried doxorubicin-loaded, chitosan-based nanogels: a physicochemical study*' and co-authored by Hugo Alarie, Martin Jutras & V Gaëlle Roullin. This manuscript relates the study of the entrapment mechanisms of doxorubicin, as a model hydrophilic anticancer drug, into chitosan-based nanogels. Based on previously published results,(129) we studied the influence of some formulation parameters onto the physicochemical characteristics of blank nanogels, such as hydrodynamic diameter, polydispersity index, zeta potential and production yield. Then we loaded the optimized nanogels with doxorubicin, a model hydrophilic drug. Following interesting results of entrapment efficiencies, we hypothesized that positively-charged DOX molecules were co-trapped with positively-charged chitosan by electrostatic bridging of the 5-times negatively charged ionic crosslinker, sodium tripolyphosphate. This assumption was investigated through analytical techniques, namely DSC and FT-IR. In parallel, a freeze-drying process was optimized in order to extend the nanogel shelf-life, while maintaining adequate physicochemical characteristics.

The second part of this manuscript is dedicated to the study of encapsulation of TMZ, USPIO, DOX-USPIO or TMZ-USPIO. Slight modifications of the optimized protocol were introduced to guarantee adequate encapsulation rates. Due to structural similarities, TMZ was assumed to be trapped by the same electrostatic mechanisms than DOX molecules into the hydrophilic nanogels. Similar results for TMZ than for DOX were observed, accordingly reinforcing this hypothesis. Negatively-charged USPIO were used to be successfully loaded into chitosan-based nanogels and subsequent theranostic nanogels were also prepared. The preliminary physicochemical

characterization was, however, not entirely completed, due to the delay in purchasing and installing one of the required equipments, namely a 60-MHz relaxometer.

A general discussion, as well as a conclusive overview and some perspectives, complete this manuscript.

Part one

Article

Recoverability of freeze-dried doxorubicin-loaded, chitosan-based nanogels: a physicochemical study

Hoda Besheir^{1#}, Hugo Alarie^{1#}, Martin Jutras², V Gaëlle Roullin^{1, 2*}

1. Laboratoire de Nanotechnologies Pharmaceutiques (LNP), faculté de pharmacie
2. Plateforme de biopharmacie, faculté de pharmacie

*Corresponding author

these authors equally contributed to this manuscript.

Université de Montréal, CP6128, succursale Centre-ville, Montreal QC, H3C 3J7, Canada.

Phone: (514) 343-6111 ext 0687

Email: vg.roullin@umontreal.ca

Key-words: nanogels, chitosan, doxorubicin, freeze-drying, cryoprotectant, *in vitro* release.

Introduction

Doxorubicin (DOX) is an anthracycline molecule synthesized for the first time in the late 60s from mutation-induced strains of *Streptomyces Peucetius*.(130) It is best described as a double-edged sword. DOX was found to be more active than many drugs, including molecules from the same family such as daunorubicin, against a wide variety of tumors in mice. It also exhibited severe side effects which limited its use in cancer treatment. For instance, in addition to bone marrow suppression, mouth ulcers and alopecia, delayed cardiotoxicity remained a main limitation against its use.(59) Moreover the rapid plasma clearance of DOX greatly reduces its chances to reach the site of action.(61) Another observed challenge with this agent is the crossing of biological barriers, especially the blood brain barrier (BBB). Free DOX cannot even cross a disrupted BBB as other compounds do.(131) All these problems contributed to the urgency of developing delivery systems able to safely, effectively and selectively carry DOX to tumor cells.

Resorting to new pharmaceutical technologies such as pharmaceutical nanotechnology allowed resolving, to a great extent, the dilemma of using DOX. Doxil® is an excellent current example of a nanoliposomal system coated with polyethylene glycol (PEG). This coating helps mainly to protect the formula against opsonisation and rapid elimination from the body.(58) Doxil® showed a remarkable success in treating peripheral tumors for more than 20 years.(58) The targeted delivery properties of Doxil® mainly depended on the enhanced permeation retention (EPR) effect.(64) In this effect the abnormal defective structure of solid tumors helps the specific drug accumulation inside this type of cells. However, accumulation into brain cells depends also on the amount of drug which can cross BBB. This explains limited benefits for EPR-dependent formulas if used in brain cancer. Also defected cell structure is extended to normal cell as well which indicates a lack of specificity for this mechanism.(95)

Another worth-mentioning strategy is the development of pH-responsive DOX formulas. These nanocarriers, mostly nanoparticles, selectively disrupt to release the drug in acidic pH, such as the intracellular pH of tumor cells, whilst remaining intact at higher pH values (corresponding to pH values of tumor interstitial space and healthy cells).(96) Applications of this concept were recently illustrated by the pH-responsive DOX/laponite hybrids, as well as by chitosan-based nanogels.(96, 132-134) Chitosan-based nanosystems are especially attractive for biomedical applications. Chitosan (CH), a glucosamine polymer produced by N-deacetylation of chitin, is a biocompatible and biodegradable polymer.(135, 136) Displaying a pKa around 6.5, its amino groups can become protonated in acidic pH(137, 138), thus becoming available for ionic interactions and being crosslinked by

negatively charged sodium tripolyphosphate (TPP). This reaction is known as ionic gelation.(139, 140) Incorporation of the endogenous biopolymer hyaluronic acid (HA) into the nanogel structure enhances their uptake and target specificity, mainly through the specific HA- CD44 receptor interaction, the latter being overexpressed by many cancer cells.(141)

However appealing, ionically-crosslinked nanogels suffer from a major drawback, namely a stability problem. Those nanogel suspensions are subjected to physical and/or chemical instability, resulting in aggregation, particle fusion, polymer hydrolysis, drug loss from the nanocarriers and chemical reactivity of the drug.(140) Freeze-drying is the process of choice to stabilize formulas and render them eligible for long-term storage. Nonetheless, freeze-drying presents its own issues caused by freezing, dehydration and mechanical stresses generated during the process itself.(124) For instance these stresses can cause cryoconcentration of nanoparticles in one phase, which can, in turn, lead to particle aggregation. Moreover, the mechanical stress exerted by forming ice crystals on the nanoparticles can lead to their denaturation and further leakage of the drug.(124)

To overcome these effects, cryoprotectants and especially sugars, are usually added prior to the freeze-drying process to form a glassy matrix in which the nanoparticles are immobilized and protected against aggregation(125-128) Many sugars were screened for their cryoprotective capacity of polymeric nanoparticles, such as PLGA(142, 143). However, not so many were investigated in the case of ionically-crosslinked, chitosan-based nanogels. Also several studies researched the release profiles of DOX from freeze-dried NPs other than chitosan NGs. An extensive study was required to understand how freeze-drying and/or pH responsiveness of chitosan polymer controlled the release of DOX from chitosan-based NGs.

In this study, we hypothesized that chitosan-based nanogels could be used to carry significant amounts of Doxorubicin and deliver them in a pH-dependant manner. Moreover, by optimizing a standard freeze-drying process, the shelf life of DOX-loaded nanogels should be greatly extended, while preserving their physicochemical properties. To that extent, chitosan/hyaluronic acid based-nanogels loaded with doxorubicin were prepared and characterized. Following promising results of entrapment efficiencies, we investigated the DOX loading mechanisms by Differential Scanning Calorimetry (DSC) as well as Fourier Transform Infrared (FTIR) experiments. We also screened five sugars, at three different concentrations, for their cryoprotective capacity. Finally, a release study was designed and performed on both fresh and reconstituted nanogels to establish the impact of the freeze-drying process on the nanogel overall release capacity.

▪ Materials and Methods

1.1. *Materials*

Unless otherwise stated, starting materials were obtained from commercial suppliers and used without further purification. Citric acid was purchased from A&C (American Chemicals LTD, Montreal (Qc), Canada). Sodium tripolyphosphate (TPP) was purchased from Alfa Aesar (Ward Hill (MA), USA). All other chemicals, including doxorubicin HCl (DOX), were purchased from Sigma Aldrich (St. Louis, MO, USA). Milli-Q water was used for all experiments.

1.2. *Methods*

Due to degradation properties of DOX, all DOX samples (either solutions, fresh or freeze-dried powders) were continuously protected from light and stored at temperature not higher than 4 °C.(144)

1.3. *Synthesis of blank and DOX-loaded NGs*

Blank (unloaded) and DOX-loaded nanogels (NGs) were obtained through ionic gelation as previously reported.(129) Briefly, 9 mL of a cationic phase were prepared by dissolving 22.5 mg of chitosan (CH) in 10%(w/v) citric acid at room temperature until complete dissolution. To this, 4.5 mL of an anionic phase consisting of 0.8 mg. mL⁻¹ HA and 1.2 mg. mL⁻¹ TPP in Milli-Q water were added dropwise. The turbid nanosuspensions were then left 10 min under moderate stirring for a maximal nanogel formation. To prepare DOX-loaded NGs, the exact same procedure was followed, except that DOX was added to the cationic phase at a concentration of 0.188 mg. mL⁻¹.

1.4. *NG purification*

Nanoparticle suspensions were purified using the membrane dialysis method (SpectraPor®6 dialysis membrane, MWCO = 25000 KDa) at a 1:100 volume ratio against Milli-Q water for at least 6 hours. The external phase was exchanged every 2 h, as a minimum, for 3 times.

1.5. *NG freeze-drying process*

Different types of sugars were tested for their cryoprotectant capacity: trehalose, sucrose, glucose, lactose and LMW dextran (average= 74,200 Da). Each sugar was used at three different concentrations, namely 5, 10 & 20 %w/v. Briefly sugars were weighed in Eppendorf tubes before mixing them by means of a vortex with volumes of 1.5 mL purified NG suspensions. Then, the sugar-based NGs were subjected to brutal freezing in liquid nitrogen at -180°C for 10 minutes before storing them at -80°C for 48 hrs until further freeze-drying. Frozen samples were then freeze-dried at -51°C, 1.8 mBar for 24 – 48 hrs (Modulyo, Thermo Electron corporation).

Finally, freeze-dried powders were reconstituted by slow and gradual addition of purified water (200-500 μL), to allow proper wetting of the lyophilisates, followed by 45-sec vortexing, until the initial volumes (1.5 mL) were reached.

1.6. NG physicochemical characterization

Size and surface charge. Dynamic light scattering (DLS) was used for measurement of average hydrodynamic diameters (D_h) and polydispersity indexes (PdI) (Malvern Zetasizer Nano-ZS, Malvern Instruments, UK). Samples were diluted in 3 folds their volume of MilliQ water. This dilution produced an attenuation factor of 6-7. To assure reproducibility each sample was analyzed in triplicates of 25 cycles. Laser position was determined automatically and samples were measured at 20°C at a scattering angle of 173°. DLS data were expressed in both % Intensity in order to detect the potential presence of aggregates in the nanoparticle suspensions.(129)

ζ -(zeta) potential (ZP) data were collected through electrophoretic light scattering (ELS) at 20°C, 150 V. The instrument was calibrated with a Malvern - 42 mV standard prior to each set of measurements. For all kinds of measurements pure water, water/ citric acid mixture or sugar-based solutions were used as a reference dispersing medium according to the situation of each sample.

To evaluate the freeze-drying efficiency, sugar-cryoprotected NGs before FD as well as reconstituted samples were characterised by DLS/ELS technique for their size, PdI and ZP (taking into account the sugar concentration for corrected medium). Final data (after freeze-drying) were divided by initial ones (before freeze-drying) and results were calculated to get ratios for size, PdI and ZP expressed in the form of S_f/S_i , PdI_f/PdI_i and ZP_f/ZP_i where S_f/S_i : ratio of size after FD to size before FD; PdI_f/PdI_i : ratio of PdI after FD to PdI before FD; ZP_f/ZP_i : ratio of ZP after FD to ZP before FD.

Thermal Analysis (Differential scanning calorimetry). The thermal behaviours of blank and dox-loaded freeze-dried nanogels were determined using DSC (Perkin Elmer, DSC 4000, VWR vacuum pump, N_2 gas purged at 20 mL/min). The obtained thermograms were compared to thermograms of single components of doxorubicin HCl, chitosan, hyaluronic acid and sodium tripolyphosphate. Scanning was performed from 20°C to 250°C, at 20°C/min.

Fourier Transform Infrared (FTIR) analysis. Powder samples, a very small amount of powder (typically 5-10 mg), of both freeze-dried blank, dox-loaded nanogels as well as single components of NGs, were analysed using FTIR technique. Infra spectra were recorded on a Nicolet iS10 FTIR (Thermo-Scientific, Canada) equipped with a SMART iTR attenuated total reflectance (ATR) sampling accessory with a ZnSe plate. Data were acquired and analyzed using the OMNIC® interface. Average values of 32 scans were recorded, with a 4000–400 cm^{-1} wavelength scanning range.

1.7. Doxorubicin quantification

DOX concentrations were determined by LC/MS-MS (Agilent1100 Series coupled to AB/SCIEX 4000 QTRAP) Column: Luna C8, 30 X 2mm, 5 μ m, column temperature adjusted at 45°C, sample temperature adjusted at 5°C). Calibration curves were generated for DOX concentrations between 0 and 400 nM repeated 3 times each and average results were used. Detailed information is given in Figures S1 a, b & c (supporting information).

Production yield (PY%), encapsulation efficiency (EE%) and drug loading efficiency (DLE%)

1.5 mL aliquots of either purified blank or DOX-loaded NGs were centrifuged at 16,000 g for 90 min at 4°C (Eppendorf Centrifuge 5415 R). Supernatants and pellets were treated separately.

Production yield:

Pellets of either blank or DOX-loaded NGs were freeze-dried as previously prescribed. Equation 1 was used to determine the PY% of NG fabrication.

Equation1:

$$PY \% = \frac{\text{weight of freeze - dried NGs (mg)}}{\text{total weight of NG components (mg)}} \times 100$$

where NGs components taken into account were CH, HA, TPP \pm DOX.

Encapsulation efficiency, EE%, & Drug loading efficiency, DLE%:

Appropriate dilutions of supernatants from DOX-loaded NGs were prepared in the mobile phase. DOX was quantified using LC/MS-MS as previously mentioned. Equations 2 and 3 were thereafter used to calculate EE% and DLE% respectively.

Equation2:

$$EE \% = \frac{\text{Initial}[DOX] - [DOX] \text{ supernatant}}{\text{Initial [DOX]}} \times 100$$

Equation 3:

$$DLE \% = \frac{EE \% * \text{initial weight of DOX}}{PY \% * \text{total mass of NG components}} \times 100$$

1.8. Doxorubicin release study before and after freeze-drying

Both fresh and reconstituted freeze-dried NGs were incubated in a dissolution apparatus (Logan instrument, DTB 678, pumb VTC 200, 50 rpm, 37°C) for 72 h in release media of

KH₂PO₄ buffer solutions prepared at three different pH values (5.8, 6.8 & 7.4) according to USP 38-NF 33 (reagents, buffer solutions, see table S1, supporting information). Typically 2 mL samples were incubated into 500-mL buffers. Samples were withdrawn at 0, 0.5, 1, 1.5, 2, 3, 4, 6, 24, 36, 48, 54 and 72 h. Withdrawn samples were centrifuged at 16,000 g, 4°C (Eppendorf Centrifuge 5415 R) for 90 minutes. The supernatants were then quantified by LC/MS-MS using appropriate dilutions with mobile phase, as previously described.

1.9. Degradation kinetics of DOX

Since DOX degrades rapidly when placed in aqueous media (145), free DOX was incubated in the same conditions as DOX-loaded NGs and DOX was quantified as previously described.

Obtained results were plotted against time (h). K_d, degradation rate constant of DOX represented by the slope of each corresponding plot, was calculated using Equation 4.

Equation 4

$$[\text{DOX, nM}] = \exp(-k_d \times t)$$

It was thereafter used to correct the release kinetics of DOX from NGs according to equation 5.(146)

Equation 5:

$$\frac{M_t}{M_\infty} = \exp(-k_d \cdot t) - \frac{6}{\pi^2} \sum_{n=1}^{\infty} \frac{1}{n^2} \cdot \exp\left(-\frac{D \cdot n^2 \cdot \pi^2 \cdot t}{r^2}\right)$$

Where M_t and M_∞ are the released mass of DOX at time t and time infinite respectively, D is the diffusion coefficient of DOX in the NPs and r is the NP radius, as measured by DLS.

■ Results

1.10. NG physicochemical characterization

DLS and ELS techniques were performed to determine size, polydispersity and surface charge of both blank and DOX-loaded NGs. Obtained results are presented in Table 1 together with encapsulation efficiencies in the case of DOX-loaded nanoparticles.

Table 1. Physicochemical characterization for blank and DOX-loaded chitosan NGs (n=3-5 batches, 3 measurements / batch).

		Blank NGs		DOX-loaded NG	
		Before purification	After purification	Before purification	After purification
DLS/ELS	Size (nm)	172 ± 14	165 ± 3	211 ± 3	257 ± 14
	PdI	0.39 ± 0.19	0.27 ± 0.04	0.24 ± 0.02	0.27 ± 0.02
	ZP (mV)	20 ± 2	23 ± 9	47 ± 1	53 ± 1
Synthesis efficiency results	Average EE%	N/A	N/A	90 ± 8	57 ± 9
	Average PY%	N/A	54 ± 2	N/D	68 ± 10
	Average DLE%	N/A	N/A	N/D	4.4 ± 1.0 (Theoretical = 5%)

N/A: not applicable

N/D: not determined.

The encapsulation of DOX resulted in a significant increase in size (> 20%) and in surface charge (+25/30 mV). The purification process (dialysis) caused a significant loss of DOX (- 30%) but the subsequent loading efficiency was still satisfactory compared to the theoretical one (average 88% of the maximum loading capacity).

1.11. Thermal Analysis (Differential Scanning Calorimetry, DSC)

Results from differential scanning calorimetry performed on raw powders and freeze-dried NGs are summarized in thermograms shown in figure 1. Physically mixing chitosan and TPP showed a significant increase in T_g from their individual thermograms (Fig. 1A, lines

CH+TPP vs CH and TPP). Moreover in DOX-loaded NGs, the characteristic peaks of HA and CH were replaced by a single peak with higher T_g (95.5 °C vs 79.0 and 87.5 °C, respectively). The characteristic TPP peak at 114 °C completely disappeared and most probably was merged in the new plateau (179 – 222 °C).

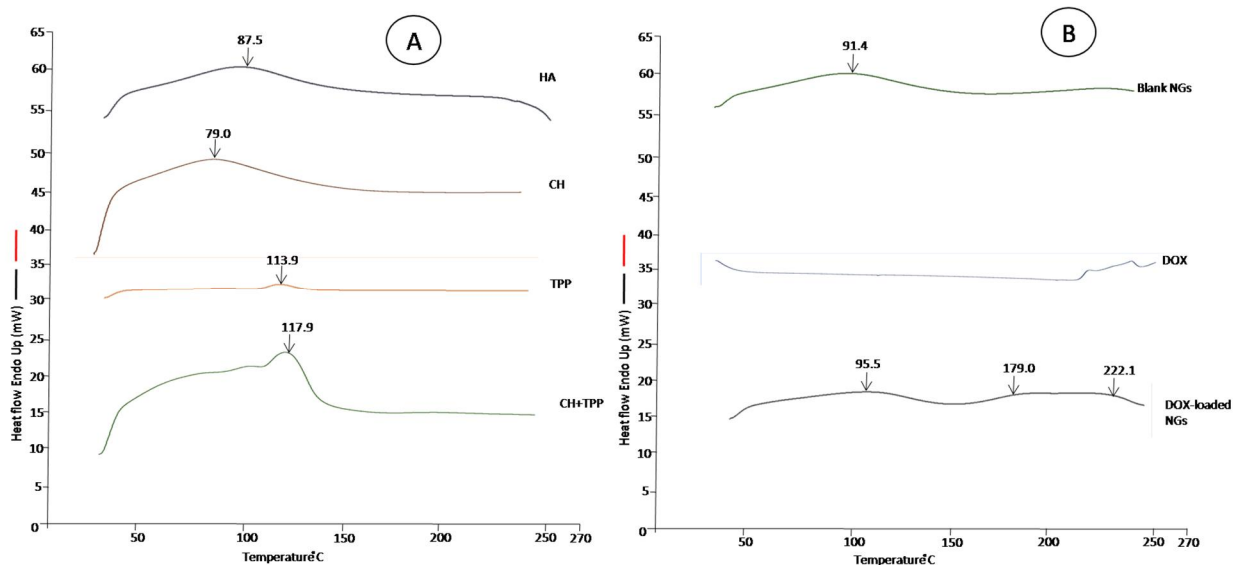


Figure 1. 1A) thermograms of HA, CH, TPP and physical mixtures of CH & TPP.
1B) thermograms of blank NGs, DOX and DOX-loaded NGs.

1.12. Fourier Transform Infrared (FT-IR) analysis

Chemical structures and functional groups of raw materials and nanogels were confirmed by the FT-IR technique (Figure 2). On the chitosan spectrum, the broad absorption band from 3100 to 3650 cm^{-1} can be related to O-H stretching. In this area, two stretching vibrations of N-H of the primary amines can also be distinguished at 3300 and 3354 cm^{-1} . This characteristic primary amine function is also fingerprinted by two NH_2 scissoring bands at 1652 and 1575 cm^{-1} of CH. Overall, a closely similar pattern is found for blank NGs and DOX-loaded NGs, except for the absence of the two stretching vibrations of N-H and attenuated scissoring vibrations of NH_2 . Strong stretching vibrations of phosphates are found in the 1100 – 1200 cm^{-1} region for TPP, but not anymore in the spectra of blank and DOX-loaded NGs. Also the 3300 cm^{-1} peak related to the stretching vibrations of primary amine in DOX spectrum disappeared in DOX-loaded NGs. That behaviour may be because it was engaged in H-bond formation. Finally, the DOX spectrum presents a typical ketone fingerprint at 1712 cm^{-1} , which is unmistakably discernible in the spectrum from DOX-loaded NGs but not from blank NGs.

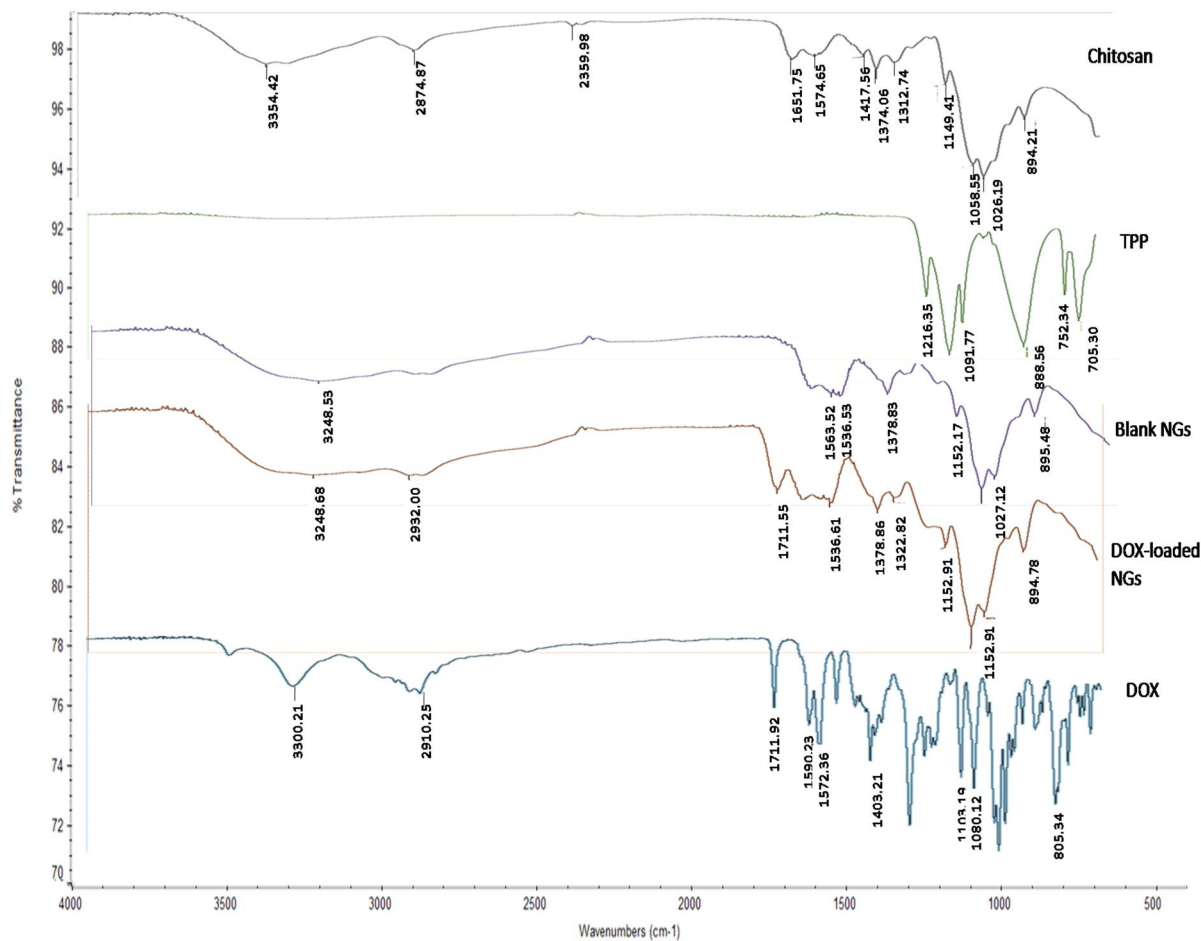


Figure 2. FT-IR spectra of (top to bottom): chitosan, TPP, blank NGs, DOX-loaded NGs and DOX powder.

1.13. Freeze-drying (FD) process

The physicochemical characteristics of NGs before and after freeze-drying were expressed as ratios S_f/S_i and PdI_f/PdI_i where S stands for size, PDI for polydispersity index, f (final or after freeze-drying), i (initial or before freeze-drying). Results of size as well as PDI ratios for freeze-dried, blank (unloaded) NGs are shown in table 2.

Table 2. Influence of FD on size & PDI of both blank and DOX-loaded NGs. Results expressed in ratios S_f/S_i and PdI_f/PdI_i . $n = 3$ batches, 3 measurements / batch.

Nature of sugar	[Sugar] %w/v	Blank NGs	
		S_f/S_i	PdI_f/PdI_i
Trehalose	5	1.79 ±0.20	1.70 ±1.29
	10	1.83 ±1.14	1.15 ±0.65
	20	1.16 ±0.02	0.83 ±0.03
Sucrose	5	1.52 ±0.12	1.24 ±0.36
	10	1.00 ±0.03	0.87 ±0.19
	20	0.97 ±0.00	0.57 ±0.03
Glucose	5	2.36 ±0.67	1.87 ±0.52
	10	1.15 ±0.05	1.14 ±0.35
	20	1.01 ±0.02	0.88 ±0.09
Lactose	5	1.40 ±0.03	1.21 ±0.23
	10	1.30 ±0.29	1.22 ±0.18
	20	2.03 ±1.02	2.4 ±1.3
LMW dextran	5	1.12 ±0.14	1.21 ±0.52
	10	0.66 ±0.59	Not dispersible
	20	1.12 ±0.14	1.03 ±0.01

In the absence of international guidelines or consensus, a 15% deviation around the initial values was set as an acceptable variation after FD, *i.e.* a ($parameter_f/parameter_i$) in the $[1.00 \pm 0.15]$ range. Above this range, nanogels would start aggregating in a way not compatible with parenteral administration. Below this range, nanogels would be partly and irreversibly dehydrated, which would significantly alter the drug release. As observed from Table 2, only the presence of glucose and trehalose was associated with approximate success, for concentrations over 10% w/v. Also good results were observed with LMW dextran and sucrose with concentrations of 20 and 10% w/v respectively. Therefore, glucose and trehalose were selected to investigate the freeze-drying of DOX-loaded NGs. Table 3 shows S_f/S_i as well as PdI_f/PdI_i ratio for DOX-loaded chitosan NGs.

Table 3. S_f/S_i and PdI_f/PdI_i for DOX-loaded NGs freeze-drying using glucose & trehalose 20%w/v

	S_f/S_i	PdI_f/PdI_i
Trehalose 20%	1.27 ±0.20	1.60 ±0.36
Glucose 20%	1.02 ±0.13	1.07 ±0.02

From these results, only glucose 20% was able to provide reconstituted samples with adequate physicochemical characteristics.

There was no significant change in ZP values before and after freeze-drying for both blank and DOX-loaded NGs (data not shown).

1.14. Degradation kinetics of DOX

The degradation rate constant (K_d) of DOX was determined in the three release media to be used later in the release study. DOX exhibits a first order degradation behaviour (145) which can severely interfere with the real values of the released amounts (Table S3). The calculated K_d values were therefore used to correct the apparent DOX concentrations released from NGs (Figure S2). Table 4 shows the calculated K_d values in the 3 release media under investigation. K_d values were calculated using equation 4 as previously mentioned under materials and methods.

Table 4. Degradation constant k_d for DOX in phosphate buffers at pH values of 5.8, 6.8 & 7.4. Temperature maintained at 37°C, protected from light.

pH	5.8	6.8	7.4
K_d (h^{-1})	0.006	0.009	0.012

1.15. Doxorubicin release study before and after freeze-drying

After correcting the apparent concentrations of release study using K_d values from Table 4, the DOX release percentages were plotted against time (h). Figures 3 & 4 show DOX release profiles before and after FD, respectively.

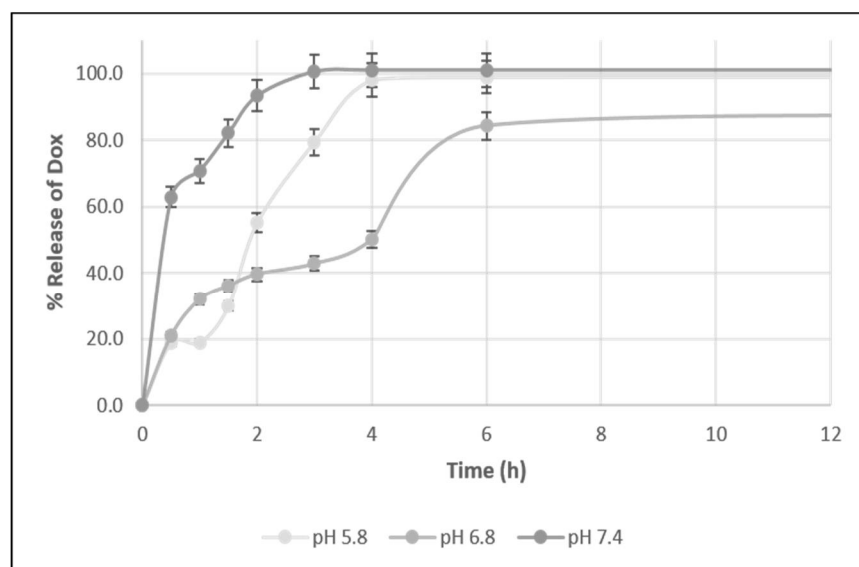


Figure 3. Comparison of DOX release profiles on freshly purified, DOX-loaded NGs, at pH 5.8 (light grey), 6.8 (medium grey) and 7.4 (dark grey). $n=4$ batches / time point.

As shown on this figure, all profiles presented a burst effect within a maximum time of 6 hours followed by a plateau until the end of the 72 h. Comparison of the 3 plots also shows that the drug release is higher at pH 6.8 and 7.4.

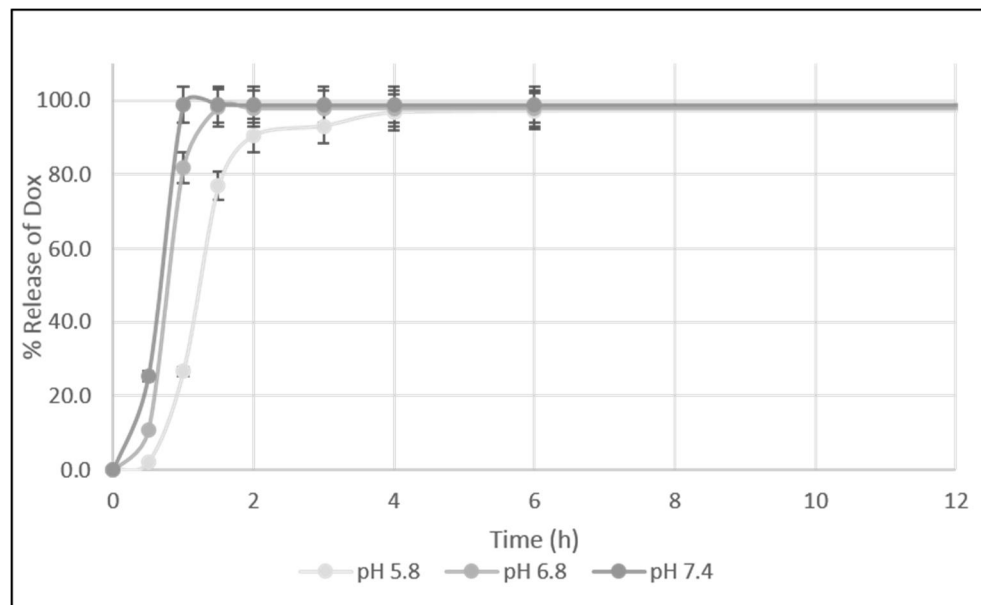


Figure 4. Comparison of DOX release profiles on freeze-dried, DOX-loaded NGs, at pH 5.8 (light grey), 6.8 (medium grey) and 7.4 (dark grey). $n=4$ batches / time point.

As seen on Figure 4, the burst effect for all the formulas was reached faster, 100% DOX was released within 2 hours. The two plateau effects appearing in fresh NGs in figure 3 were no longer seen.

■ Discussion

Nanogels have attracted much attention as performing, biocompatible delivery systems for therapeutic and diagnostic drugs in the last few years.(141) In particular, those synthesized from chitosan, a natural polysaccharide derived from chitin, have been extensively studied for their ability to change conformation and solubility according to the environmental pH.(147) Owing to the slightly acidic pH of the tumoral area, and the more markedly acidic intracellular pH, it is believed that such nanosystems could be used as pH-sensitive nanocarriers, delivering their content into areas of interest.(133) Various synthesis approaches have been reported; among them, ionic gelation is particularly appealing owing to its simplicity, biocompatibility and short synthesis time. It is based on the electrostatic interactions between the cationic chitosan molecules (in acidic conditions) and the negatively-charged crosslinking agent, penta sodium triphosphate (TPP). This self-

assembled network can be reinforced by the presence of anionic hyaluronic acid chains, resulting into spherical nanogels.(141) Because of their hydrophilic nature, these nanogels are especially well-suited to encapsulate hydrophilic molecules, such as contrast agents,(148) peptides and proteins(149) or other smaller molecules, such as anthracyclines.(150)

In articles dealing with the loading of DOX into chitosan nanoparticles, DOX is either grafted to the polymeric backbone of chitosan,(151) or complexed within the nanogels. This resulted in efficient loadings but also in various release kinetics, from a few minutes to several hours.(150, 152) One major pitfall of these systems is their lack of biocompatibility in each process step (use of toxic solvents or high amounts of emulsifiers for instance). In this view, ionic gelation is preferable since it involves mild aqueous conditions.(153) However, the sole use of chitosan and TPP does not allow the efficient retention of DOX into nanogels and a polyanion has to be included into the formulation.(150) Therefore we chose to investigate the encapsulation of DOX into chitosan / hyaluronic acid / TPP nanogels which were successfully used with other molecules.(154)

The encapsulation of DOX through ionic gelation resulted in an increase in hydrodynamic diameter and surface charge, without significantly affecting the nanoparticle size distribution. From the zeta potential results, it can be deduced that a significant part of DOX is entrapped at the nanogel surface since after purification, a markedly more positive surface charge is observed. These physicochemical characteristics were noticed to be higher than others reported recently and suggest better particle stability in terms of surface charge.(155) Generally, our NGs exhibited particle sizes which were smaller and also more uniform with a PDI of 0.27 after purification. Encapsulation efficiency values were found to be slightly higher than those obtained for chitosan/TPP alone (156) or chitosan/carboxymethyl chitosan nanogels.(107) This could be attributed to the incorporation of TPP and HA into the structure of our NGs where the negative phosphate and carboxylic groups could doubly interact with the protonated amino groups of DOX, in a similar mechanism to the one crosslinking chitosan chains. This was revealed by a significantly higher T_g for CH and TPP physical mixture, compared to thermograms of individual powders (Fig. 1). The electrostatic interactions, probably occurring at first thanks to water trace amounts, resulted in a more rigid, denser structure. Similarly, when DOX was added to the system (thermogram of DOX-loaded nanogels, Fig. 1B), the structure was further rigidified. Generally, chitin and chitosan thermograms show an endothermic peak at 70°C ascribed to the loss of water.(157) This confirms that water acts as a plasticizer in chitosan, but also in other biopolymers, such as hyaluronic acid. Water

molecules form intermolecular hydrogen bondings with the biopolymers through amine and hydroxyl groups present in them. This helps in molecular rearrangement which eases the chain mobility in chitosan. Less associated water molecules, such as in a more compact structure, result in an increased T_g. These interactions are further confirmed by FT-IR spectra (Fig. 2) where NH₂ characteristic bands of chitosan tend to disappear, at the same time than distinctive bands of phosphate groups, when considered in the nanogel spectra. The high presence of DOX into the nanogels is, at the same time, visualized by the fingerprinted band of its ketone functions at 1712 cm⁻¹. Therefore, all these favorable conditions could explain the high encapsulation and loading efficiencies we observed compared to other similar formulations.(156)

In order to develop nanoformulations which could translate into actual pharmaceutical products, stability upon storage is of fundamental prominence.(158) Freeze-drying is a natural and widely-spread approach with molecular drugs. Nonetheless, freezing was found a very important step in affecting nanoparticle sizes and distributions. Other previous attempts with nanogels gave mixed results, with either increased sizes (159) or instability following reconstitution.(160) Thus we chose to add a cryoprotectant to enhance stability and preserve physicochemical and morphological features of the DOX-loaded, chitosan-based nanogels.

Size and surface charge preservation of our nanogels during freeze drying mainly depended on the cryoprotective capacity of the used sugars as well as their concentration. In our case, we chose to express results as ratios of size and PDI before and after freeze drying. Ideally these ratios should be as close to 1 as possible. In absence of international guidelines regarding the freeze-drying stability and reconstitution of nanosuspensions, we decided to focus on a 15% variation around the initial values of the selected parameters, *i.e.* hydrodynamic diameters, polydispersity and zeta potentials. Above this range, nanogels would start aggregating in a way not compatible with parenteral administration. Below this range, nanogels would be partly and irreversibly dehydrated, which would significantly alter the drug release. Among the five sugars investigated at 3 different concentrations, sucrose, glucose and trehalose at concentrations $\geq 10\%$ w/v were found potentially compatible with our goal on the freeze-drying of blank (unloaded nanogels). These data were similar to those reported by others.(125) When the more rigid DOX-loaded nanogels were freeze-dried, glucose 20% allowed preserving all their physicochemical characteristics with a superior reproducibility to trehalose.

Finally, it is generally suggested that acidic media enhance the swelling of pH-responsive chitosan nanogels and, as a consequence, the drug release from these nanogels is enhanced at lower pH values.(156) This is indeed noteworthy as those systems could accelerate the

release of their loaded drugs into intratumoral space or even into the cytosol of tumor cells. However, this fact seems to be controversial when applied to ionically crosslinked chitosan/TPP-based nanogels. In presence of the sole TPP crosslinker, Jane *et al.* found that DOX was released in a very fast manner (≤ 15 min) in phosphate buffer pH 7.4.(150) We observed a similar trend in our results where 100% of DOX was released within the first four hours (Fig. 3). The crosslinking between the negatively charged TPP and HA and the positively-charged DOX and CH mainly depends on chitosan being kept positively charged with protonated amino groups available for ionic interactions. At neutral pH 7.4 this protonation as well as the crosslinking are less than in case of acidic pH, so the drug fails to be retained inside the nanogels.

▪ Conclusion

Ionic gelation method allowed the synthesis of NGs with desirable size and size distribution. Moreover the incorporation of polyanions such as TPP and HA offered the advantage of higher DOX-loading efficiency. Cryoprotection-accompanied freeze-drying did not alter the physicochemical characteristics of DOX-loaded NGs or DOX EE%. However, a stability study is required to investigate the long-term protection effect of freeze-drying on NGs storage. Also further studies are still required to confirm the pH responsiveness of NGs in which chitosan is ionically linked to TPP, particularly at pH 7.4.

Acknowledgements:

The technical support of Josée Desrochers (faculty of pharmacy, Université de Montréal) is thankfully acknowledged for DSC and FT-IR experiments.

References:

1. Arcamone F, Cassinelli G, Fantini G, Grein A, Orezzi P, Pol C, et al. Adriamycin, 14-Hydroxydaunomycin, a new antitumor antibiotic from *S. peuceetius* var. *caesius*. *Biotechnology and Bioengineering*. 2000;67(6):704-13.
2. O'Brien MER, Wigler N, Inbar M, Rosso R, Grischke E, Santoro A, et al. Reduced cardiotoxicity and comparable efficacy in a phase III trial of pegylated liposomal doxorubicin HCl (CAELYX™/Doxil®) versus conventional doxorubicin for first-line treatment of metastatic breast cancer. *Annals of Oncology*. 2004;15(3):440-9.
3. Rahman A, Carmichael D, Harris M, Roh JK. Comparative Pharmacokinetics of Free Doxorubicin and Doxorubicin Entrapped in Cardiolipin Liposomes. *Cancer Research*. 1986;46(5):2295-9.
4. Bigotte L, Olsson Y. Cytofluorescence localization of adriamycin in the nervous system. *Acta Neuropathol*. 1982;58(3):193-202.
5. Barenholz Y. Doxil® — The first FDA-approved nano-drug: Lessons learned. *Journal of Controlled Release*. 2012;160(2):117-34.
6. Greish K. Enhanced permeability and retention of macromolecular drugs in solid tumors: A royal gate for targeted anticancer nanomedicines. *Journal of Drug Targeting*. 2007;15(7-8):457-64.
7. Yu MK, Park J, Jon S. Targeting Strategies for Multifunctional Nanoparticles in Cancer Imaging and Therapy. *Theranostics*. 2012;2(1):3-44.
8. Ghaz-Jahani M, Abbaspour-Aghdam F, Anarjan N, Berenjian A, Jafarizadeh-Malmiri H. Application of Chitosan-Based Nanocarriers in Tumor-Targeted Drug Delivery. *Mol Biotechnol*. 2015;57(3):201-18.
9. Xiao S, Castro R, Maciel D, Gonçalves M, Shi X, Rodrigues J, et al. Fine tuning of the pH-sensitivity of laponite–doxorubicin nanohybrids by polyelectrolyte multilayer coating. *Materials Science and Engineering: C*. 2016;60:348-56.
10. Wang Y, Qin F, Tan H, Zhang Y, Jiang M, Lu M, et al. pH-responsive glycol chitosan-cross-linked carboxymethyl- β -cyclodextrin nanoparticles for controlled release of anticancer drugs. *International Journal of Nanomedicine*. 2015;10:7359-70.
11. Scheeren LE, Nogueira DR, Macedo LB, Vinardell MP, Mitjans M, Infante MR, et al. PEGylated and poloxamer-modified chitosan nanoparticles incorporating a lysine-based surfactant for pH-triggered doxorubicin release. *Colloids and Surfaces B: Biointerfaces*. 2016;138:117-27.
12. Chatelet C, Damour O, Domard A. Influence of the degree of acetylation on some biological properties of chitosan films. *Biomaterials*. 2001;22(3):261-8.
13. Almalik A, Donno R, Cadman CJ, Cellesi F, Day PJ, Tirelli N. Hyaluronic acid-coated chitosan nanoparticles: Molecular weight-dependent effects on morphology and hyaluronic acid presentation. *Journal of Controlled Release*. 2013;172(3):1142-50.
14. Lim C, Lee DW, Israelachvili JN, Jho Y, Hwang DS. Contact time- and pH-dependent adhesion and cohesion of low molecular weight chitosan coated surfaces. *Carbohydrate Polymers*. 2015;117:887-94.
15. Lee DW, Lim C, Israelachvili JN, Hwang DS. Strong adhesion and cohesion of chitosan in aqueous solutions. *Langmuir: the ACS journal of surfaces and colloids*. 2013;29(46):14222-9.

16. Jain A, Thakur K, Sharma G, Kush P, Jain UK. Fabrication, characterization and cytotoxicity studies of ionically cross-linked docetaxel loaded chitosan nanoparticles. *Carbohydrate Polymers*. 2016;137:65-74.
17. Jonassen H, Kjøniksen A-L, Hiorth M. Stability of Chitosan Nanoparticles Cross-Linked with Tripolyphosphate. *Biomacromolecules*. 2012;13(11):3747-56.
18. Soni G, Yadav KS. Nanogels as potential nanomedicine carrier for treatment of cancer: A mini review of the state of the art. *Saudi Pharmaceutical Journal*.
19. Abdelwahed W, Degobert G, Stainmesse S, Fessi H. Freeze-drying of nanoparticles: Formulation, process and storage considerations. *Advanced Drug Delivery Reviews*. 2006;58(15):1688-713.
20. Lee MK, Kim MY, Kim S, Lee J. Cryoprotectants for freeze drying of drug nano-suspensions: Effect of freezing rate. *Journal of Pharmaceutical Sciences*. 2009;98(12):4808-17.
21. Fonte P, Soares S, Costa A, Andrade JC, Seabra V, Reis S, et al. Effect of cryoprotectants on the porosity and stability of insulin-loaded PLGA nanoparticles after freeze-drying. *Biomatter*. 2012;2(4):329-39.
22. Kumar S, Gokhale R, Burgess DJ. Sugars as bulking agents to prevent nano-crystal aggregation during spray or freeze-drying. *Int J Pharm*. 2014;471(1–2):303-11.
23. Michael JP. Mechanisms of Protein Stabilization during Freeze-Drying and Storage. *Freeze-Drying/Lyophilization Of Pharmaceutical & Biological Products, Third Edition. Drugs and the Pharmaceutical Sciences: Informa Healthcare; 2004.*
24. Fonte P, Soares S, Sousa F, Costa A, Seabra V, Reis S, et al. Stability Study Perspective of the Effect of Freeze-Drying Using Cryoprotectants on the Structure of Insulin Loaded into PLGA Nanoparticles. *Biomacromolecules*. 2014;15(10):3753-65.
25. Kevin ST, Sarah MH, Erik MS. The effect of cryoprotection on the use of PLGA encapsulated iron oxide nanoparticles for magnetic cell labeling. *Nanotechnology*. 2013;24(12):125101.
26. Keusters L, Stolk LML, Umans R, van Asten P. Stability of solutions of doxorubicin and epirubicin in plastic minibags for intravesical use after storage at -20° C and thawing by microwave radiation. *Pharmaceutisch Weekblad Scientific Edition*. 1986;8(3):194-7.
27. Courant T, Roullin VG, Cadiou C, Callewaert M, Andry MC, Portefaix C, et al. Hydrogels Incorporating GdDOTA: Towards Highly Efficient Dual T1/T2 MRI Contrast Agents. *Angewandte Chemie International Edition*. 2012;51(36):9119-22.
28. . !!! INVALID CITATION !!! ().
29. Cielecka-Piontek J, Jelińska A, Zajac M, Sobczak M, Bartold A, Oszczapowicz I. A comparison of the stability of doxorubicin and daunorubicin in solid state. *Journal of Pharmaceutical and Biomedical Analysis*. 2009;50(4):576-9.
30. Siepman J, Siepman F. Mathematical modeling of drug delivery. *International Journal of Pharmaceutics*. 2008;364(2):328-43.
31. Artech Pujana M, Pérez-Álvarez L, Cesteros Iturbe LC, Katime I. pH-sensitive chitosan-folate nanogels crosslinked with biocompatible dicarboxylic acids. *European Polymer Journal*. 2014;61:215-25.
32. Saravanabhavan SS, Bose R, Skylab S, Dharmalingam S. Fabrication of Chitosan/TPP Nano Particles as a Carrier Towards the Treatment of Cancer. 2013. 2013;5(1):8.
33. Amidi M, Mastrobattista E, Jiskoot W, Hennink WE. Chitosan-based delivery systems for protein therapeutics and antigens. *Adv Drug Delivery Rev*. 2010;62(1):59-82.
34. Janes KA, Fresneau MP, Marazuela A, Fabra A, Alonso MaJ. Chitosan nanoparticles as delivery systems for doxorubicin. *Journal of Controlled Release*. 2001;73(2–3):255-67.
35. Nam J-P, Lee K-J, Choi J-W, Yun C-O, Nah J-W. Targeting delivery of tocopherol and doxorubicin grafted-chitosan polymeric micelles for cancer therapy: In vitro and in vivo evaluation. *Colloids and Surfaces B: Biointerfaces*. 2015;133:254-62.

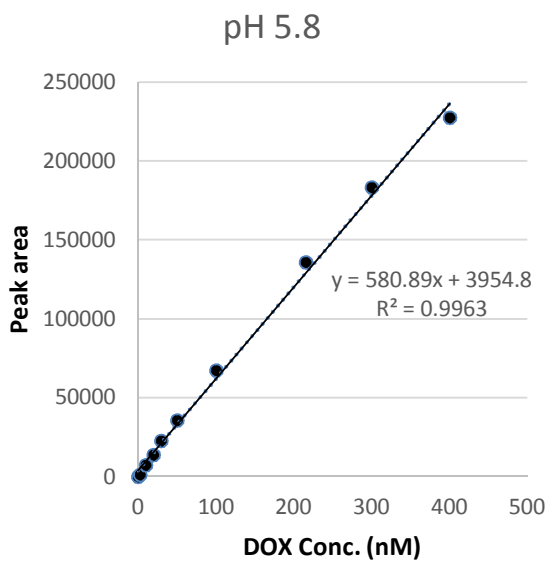
36. Jain NK, Jain SK. Development and In Vitro Characterization of Galactosylated Low Molecular Weight Chitosan Nanoparticles Bearing Doxorubicin. *AAPS PharmSciTech*. 2010;11(2):686-97.
37. Mitra S, Gaur U, Ghosh PC, Maitra AN. Tumour targeted delivery of encapsulated dextran–doxorubicin conjugate using chitosan nanoparticles as carrier. *Journal of Controlled Release*. 2001;74(1–3):317-23.
38. Elgadir MA, Uddin MS, Ferdosh S, Adam A, Chowdhury AJK, Sarker MZI. Impact of chitosan composites and chitosan nanoparticle composites on various drug delivery systems: A review. *Journal of Food and Drug Analysis*. 2015;23(4):619-29.
39. Al-Qadi S, Alatorre-Meda M, Martin-Pastor M, Taboada P, Remuñán-López C. The role of hyaluronic acid inclusion on the energetics of encapsulation and release of a protein molecule from chitosan-based nanoparticles. *Colloids and Surfaces B: Biointerfaces*. 2016;141:223-32.
40. Sadighian S, Hosseini-Monfared H, Rostamizadeh K, Hamidi M. pH-Triggered Magnetic-Chitosan Nanogels (MCNs) For Doxorubicin Delivery: Physically vs. Chemically Cross Linking Approach. *Advanced Pharmaceutical Bulletin*. 2015;5(1):115-20.
41. Feng C, Sun G, Wang Z, Cheng X, Park H, Cha D, et al. Transport mechanism of doxorubicin loaded chitosan based nanogels across intestinal epithelium. *European Journal of Pharmaceutics and Biopharmaceutics*. 2014;87(1):197-207.
42. Chen G, Wang W. Role of Freeze Drying in Nanotechnology. *Drying Technology*. 2007;25(1):29-35.
43. Manchun S, Dass CR, Sriamornsak P. Stability of freeze-dried pH-responsive dextrin nanogels containing doxorubicin. *Asian Journal of Pharmaceutical Sciences*.
44. Daoud-Mahammed S, Couvreur P, Gref R. Novel self-assembling nanogels: Stability and lyophilisation studies. *Int J Pharm*. 2007;332(1–2):185-91.

Supporting information

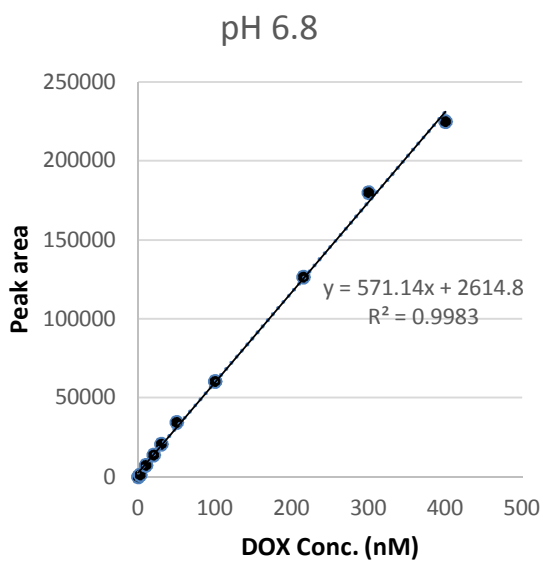
1- Calibration curves of DOX.

DOX was quantified in phosphate buffers of different pH (Table SX)..

(a)



(b)



(c)

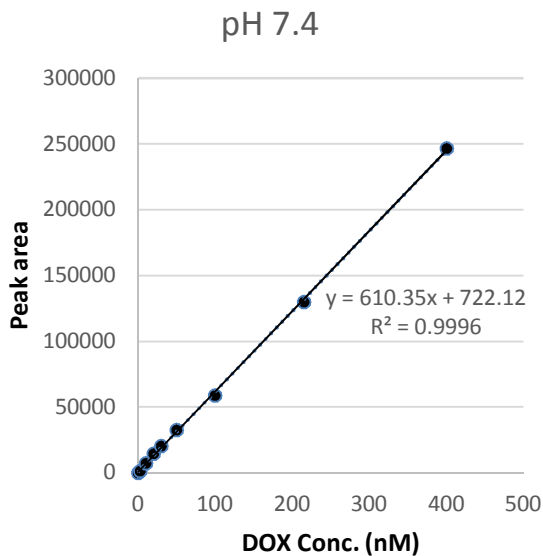


Figure S1: Calibration curves were generated for DOX concentrations between 0 and 400 nM repeated 3 times each and average results were used. The calibration curves were established at 3 different pH values a) 5.8, b) 6.8 and c) 7.4

Table S1: The appropriate volumes of 0.2M NaOH in mL were added to 50 mL KH_2PO_4 solution and volumes were completed to 200 mL with purified water in order to obtain the corresponding pH values.

pH	5.8	6.8	7.4
0.2M NaOH (mL)	3.6	22.4	39.1

2- DOX degradation in different pH media.

A known DOX concentration was placed in different pH media and protected from light. At regular intervals, DOX samples were withdrawn and quantified by HPLC-MS/MS, as described in Materials and Methods.

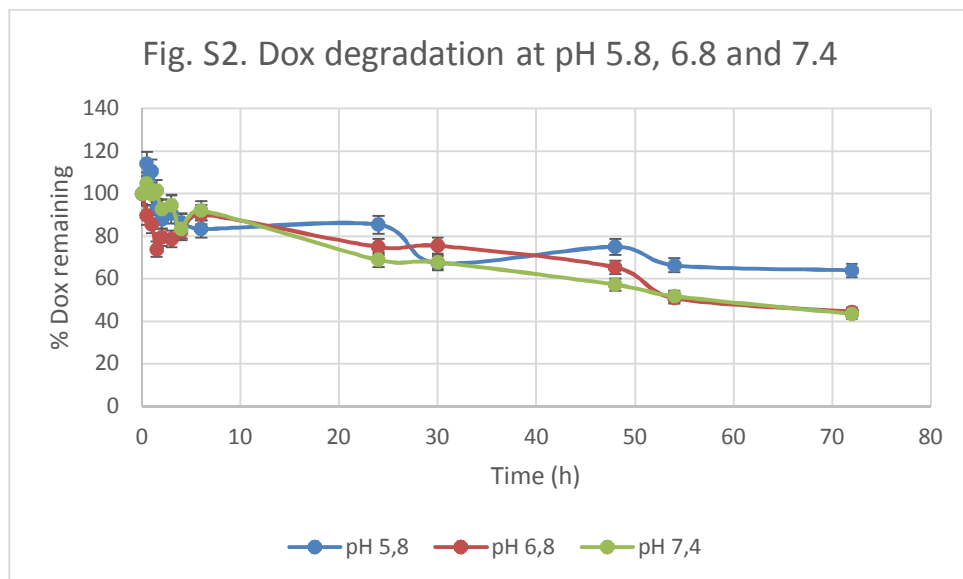


Figure S2. DOX degradation at different pH values (5.8, 6.8 & 7.4). Concentrations were thereafter calculated using K_d values retrieved in this experiment to correct apparent concentrations of released DOX in release kinetics studies.

Part two

Materials

Unless otherwise stated, starting materials were obtained from commercial suppliers and used without further purification. Citric acid was purchased from A&C (American Chemicals LTD, Montreal (Qc), Canada). Sodium tripolyphosphate (TPP) was purchased from Alfa Aesar (Ward Hill (MA), USA). All other chemicals, including doxorubicin HCl (DOX), were purchased from Sigma Aldrich (St. Louis, MO, USA). Milli-Q water was used for all experiments.

Method

1. Temozolomide encapsulation

TMZ-loaded NGs synthesis and physicochemical characterization. Cationic phase was prepared by using 9 mL of 10% (w/v) citric acid to solubilize 22.5 mg of LMW chitosan (CH) under magnetic stirring for 2 h until complete dissolution. The anionic phase was composed of an aqueous solution of 0.8 mg. mL⁻¹ HA, 1.2 mg. mL⁻¹, and 0.3 mg. mL⁻¹. 4.5 mL of this solution were added dropwise to 9 mL of the cationic phase while stirring and under sonication conditions as already reported elsewhere.(129)

Dynamic light scattering (DLS) was used for measurement of average hydrodynamic diameters (size) and polydispersity indexes (PDI) (Zetasizer Nano-ZS, Malvern Instruments, UK). Each sample was analyzed in triplicate at 20°C at a scattering angle of 173°. DLS data were expressed in % Intensity in order to detect the potential presence of aggregates in the nanoparticle suspensions. ζ-(zeta) potential (ZP) data were collected through electrophoretic light scattering (ELS) at 20°C, 150 V. The instrument was calibrated with a Malvern - 42 mV standard prior to each set of measurements. For both

kinds of measurements either purified water alone or purified water/citric acid mixture was used as a reference dispersing medium.

Quantification of TMZ. %EE of TMZ was determined indirectly using UV/Visible spectrophotometry. For that purpose resulted TMZ-loaded NGs were centrifuged at 16,000 g, 4°C (Eppendorf Centrifuge 5415 R) for 90 minutes. Supernatants were then separated and quantified for the amount of TMZ using UV/Vis (Cary 100 Agilent) at a wavelength of 320 nm. Equation 6 was used to calculate %EE of TMZ in NGs.

Equation 6:

$$EE\% = \frac{Initial[TMZ] - [TMZ]_{supernatant} \times 100}{Initial[TMZ]}$$

Typical example of TMZ quantification by UV/Vis is given in Figure 5 below.

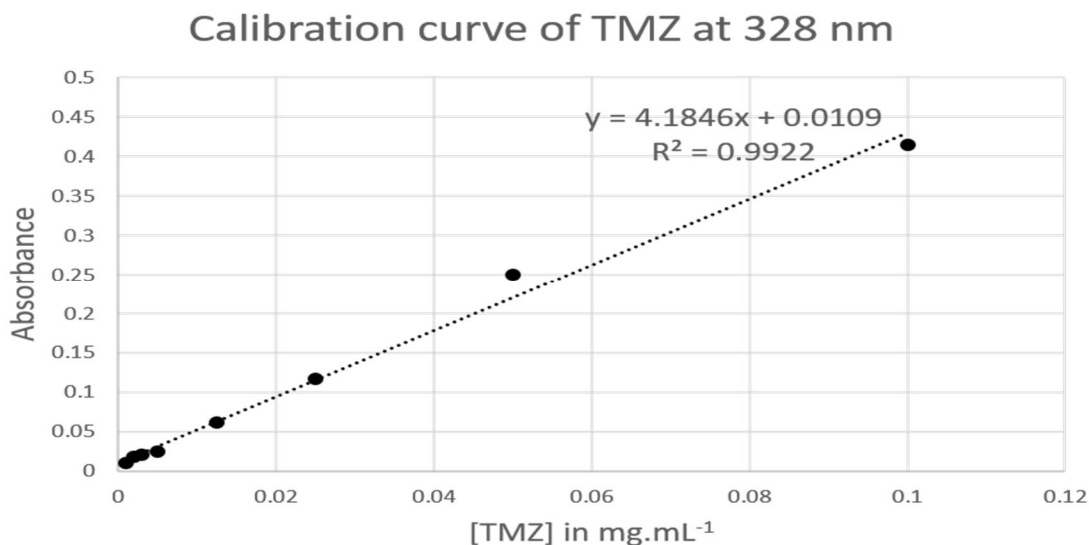


Figure 5: Calibration curve used to quantify TMZ using UV/Vis at 328 nm. TMZ was prepared in concentration range of (0.001 to 0.1 mg.mL⁻¹). TMZ was dissolved in water and NGs supernatants were used as blank.

2- USPIO encapsulation into CH-based NGs

A diagnostic contrast agent USPIO was tried for encapsulation into the CH-based NGs. Same procedure and concentrations of CH, HA and TPP as in formulating drug-loaded NGs were used. Only the stirring step was suppressed to avoid interference from the magnetized contrast agent, CA. Medium molecular weight chitosan was used and the formulated NGs were then characterized for their size, PdI and ZP using DLS/ELS technique (Malvern Zetasizer NanoZS).

3- Theranostic nanogel preparation

DOX/USPIO-loaded NGs. MMW chitosan was used in the same concentration as in DOX-loaded NGs. Both DOX and USPIO were added to the cationic phase of chitosan. HA and TPP concentrations were kept the same as in DOX-loaded NGs procedure. Stirring step was suppressed.

TMZ/USPIO-loaded NGs. LMW chitosan was used in the same concentration as in TMZ-loaded NGs. USPIO was added to the cationic phase of chitosan while TMZ was added to the anionic phase. HA and TPP concentrations were kept the same as in DOX-loaded NGs procedure. Stirring step was suppressed.

Formulated NGs were then characterized for their size, PdI and ZP using DLS/ELS technique techniques (Malvern Zetasizer NanoZS).

Results& discussion

1. Temozolomide encapsulation

TMZ-loaded NG physicochemical characterization. Size, PdI and ZP of the synthesized NGs were measured using DLS/ELS technique and are reported in table 5. Unlike DOX-loaded nanogels which were optimized when DOX was added to the chitosan phase, better results for TMZ-loaded nanogels were observed when TMZ was added to the TPP/HA phase. Also the CH molecular weight played an important role in optimizing TMZ-loaded NGs. For instance, TMZ-loaded nanogels optimal

results for all sizes, PDI and ZP were attained when using low molecular weight chitosan (LMW-CH). Only the PDI was slightly higher compared to what was obtained with DOX-loaded NGs. When higher molecular weight CH was used (e.g. medium MW), aggregates appeared.

Quantification of TMZ. Using the calibration curve equation to calculate %EE of TMZ into the nanogels synthesized, we found that achieved encapsulation rates were as high as $95 \pm 2\%$. These results revealed compatibility between TMZ and CH-based NGs from encapsulation perspectives. Despite the hydrophobicity of TMZ, $\log P = -0.66$ measured using octanol/water system,(161) the drug still favoured to stay in the NG core. Compared to the poor loading by PLGA nanoparticles, chitosan nanoparticles could be considered a better carrier for TMZ.(162)

Table 5: Results obtained for DLS/ELS characterization for TMZ-loaded nanogels, using HMW-CH, USPIO-loaded nanogels, USPIO/Dox- and USPIO/TMZ-loaded nanogels.

	TMZ-loaded nanogels	USPIO/CH/HA /TPP	DOX-USPIO/CH/HA/TPP using MMW CH	TMZ-USPIO/CH/HA/TPP using LMW CH
Size	233 ± 6	339 ± 3	338 ± 6	321 ± 4
PdI	0.31 ± 0.40	0.36 ± 0.23	0.31 ± 0.4	0.44 ± 0.11
ZP (mV)	47 ± 1	54 ± 1	49 ± 2	56 ± 1
%EE	95 ± 2%	Not available	Not available	Not available

2- USPIO encapsulation into CH-based NGs

Observed results from DLS/ELS for USPIO-loaded NGs are collected in table 5. The size of NGs loaded with USPIO became significantly higher for the first time. USPIO are supplied in the form of negatively-charged nanoparticles with an individual size around 10 nm, as measured by TEM. However, when we tried to evaluate this size by DLS, we noticed aggregates with an average mean diameters ranging from 30 to 60 nm. It is therefore possible that, despite the presence of ultrasound dispersing, those aggregates are fully encapsulated into the NGs, leading to a two-fold increase in the hydrodynamic diameter reported. Also the significant higher PdI values, relative to the previously formed NGs, were actually caused by the presence of two population peaks. One of these peaks was due to the newly formed USPIO-loaded NGs while the other one was caused by free USPIO (size around 10-20 nm), which failed to get encapsulated into the NGs. The surface charge of NGs remained positive indicating no –or very few-adsorption of USPIO onto the NG surface. Unfortunately, due to a lack of adequate instrumentation, these preliminary data were not confirmed by the quantification of USPIO encapsulation. Such an analysis would require a technique as ICP-OES or ICP-MS to actually dose the iron molecules trapped into the NG matrix.

Chitosan has been reported as a surface-coating material for USPIO. In general the chitosan-USPIO system can contribute to an efficient magnetic labelling of tumor cells. Other studies confirmed the efficient endosomal uptake as well as retention of chitosan-USPIO NPs.(163)

3- Theranostic nanogel preparation

Similarly to the USPIO encapsulation, results in table 5 show high values of all size, PDI and ZP after trying to co-encapsulate both USPIO with either TMZ or Dox into CH-based NGs. Regarding the PDI values, they are also high due to the presence of free USPIO in the measurement medium. Although these USPIO particles come in the form of nanoparticles that do not exceed 10 nm in diameter, they interfere with total PDI of the particles inside the measured sample. Size and ZP increased and even exceeded the specified limit, 200 nm and 55 mV, respectively.

Part three

General discussion

Relative low cost, biodegradability as well as biocompatibility of chitosan motivated us to select it as the major component of our nanogels.(164) Chitosan has characteristic amino groups in its structure (165) which get protonated in an acidic medium.(166) All this qualified chitosan chains for an ionic interaction, i.e. ionic gelation by negative binding sites in tripolyphosphate.(165) In addition to the basic ionic crosslinking mechanism, hyaluronic acid was also incorporated into the structure of chitosan-based nanogel for further structure support.(84) In fact the chemical structure of HA seemed to help the formation of hydrogen bonds with chitosan in particular. It is also thought that HA enhances uptake of nanogels and improve their target specificity.(84) For an optimal concentration selection of the NG ingredients, we first prepared several batches using the same concentrations, as well as the same procedure, reported by Courant T *et. al.*(129) The sonication step in the procedure allowed obtaining uniform NGs, PDI of 0.27 ± 0.04 , size after purification was 165 ± 3 nm.

To detect the effect of changes in acidity on the physicochemical characteristics of NGs, particularly size and ZP were measured at different pH values. These values started from around pH 2.6 and gradually increased up to 11. Regarding the size of the NGs, figure 6, they were optimal at pH 2.5 which is the normal pH of NG suspension during preparation. However, a decrease in acidity caused a significant particle aggregation and an increase in particle size detected ($>1,000$ nm).

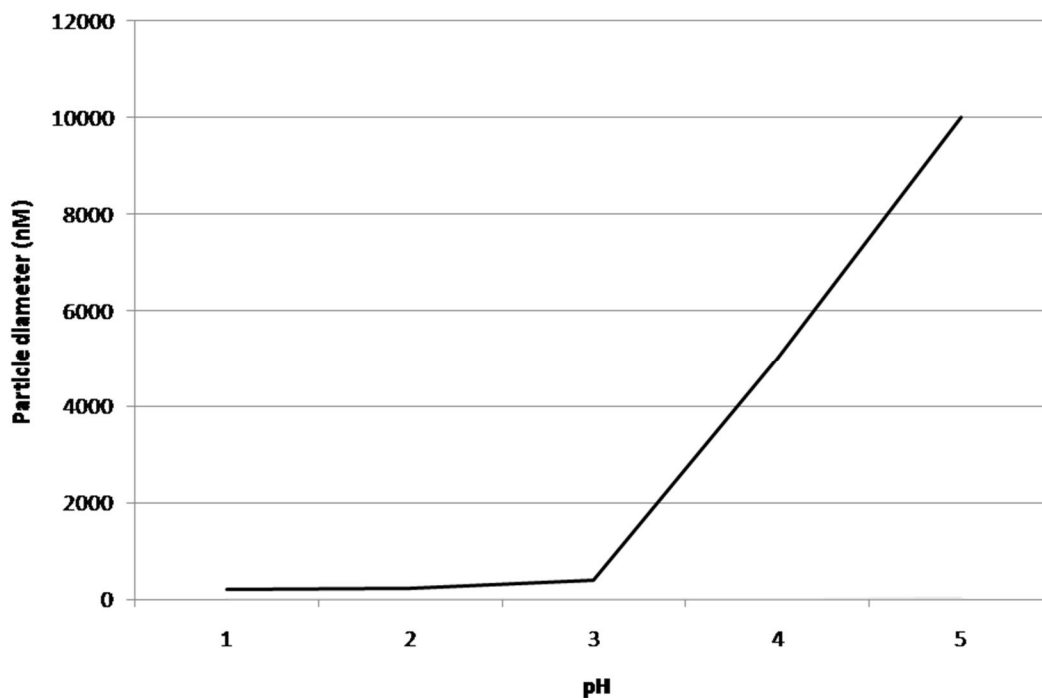


Fig. 6 Effect of decreasing acidity on the diameter of CH NGs Increasing pH values lead to a first gradual increase in the size of NPs followed by a significant sudden formation of aggregates.

The surface charge, figure 7, firstly decreased in direct proportion to the decrease in acidity, may be due to loss of positive charge at higher pH values, especially at the NG surface which interacts first with the environment. From the obtained results, the surface charge was neutralized to zero, isoelectric point reached, at a point between pH 4.7 - 5.1. The charge further decreased as the acidity decreased until it reached -7 at pH 6.3. Then a slight increase was noticed until the net charge was neutral again, 0 to 1, at pH 11.5. Variations in size and ZP in response to different pH values were compatible, to a great extent, with results from other literature.(167)

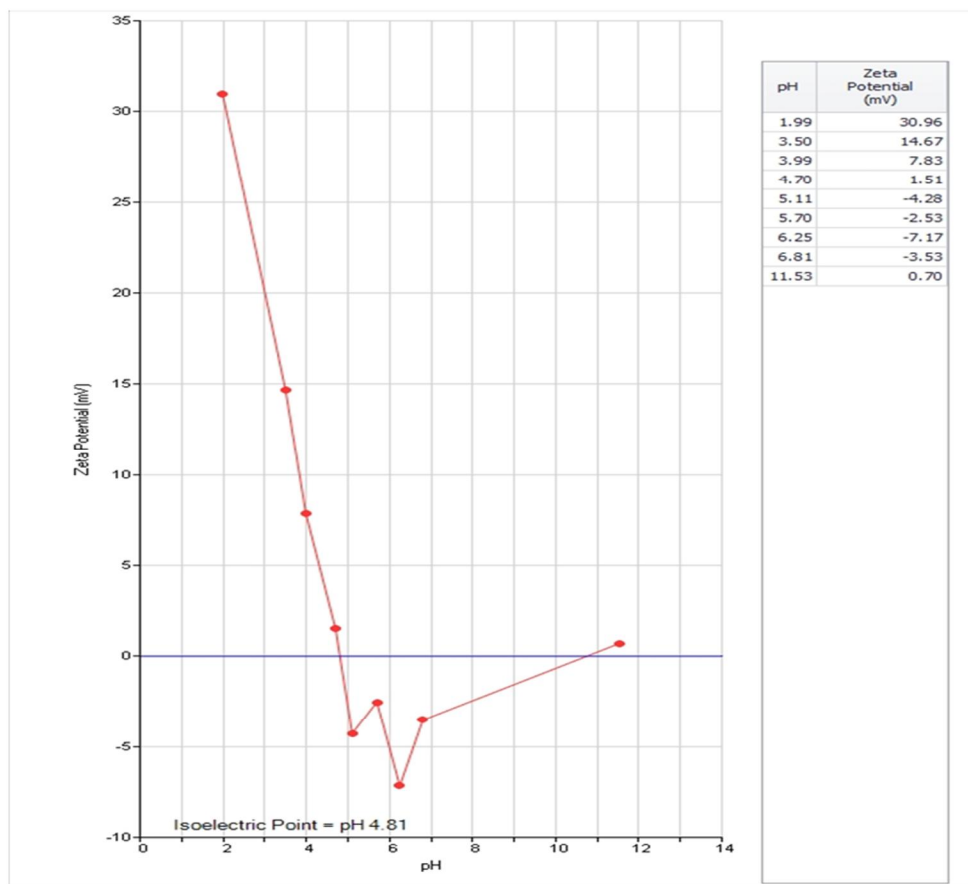


Fig. 7. Effect of increasing acidity on the surface charge of CH NGs. An increase in pH values of NGs medium caused a predominant decrease in surface charge to until it reached maximum negative value at pH 6.3. However, a further increase the net charge was slightly increased again.

After optimizing the blank NG formulation and confirming the reproducibility of the procedure, we repeated the same method except that we added a chemotherapeutic agent to the NG components. We set a goal to encapsulate temozolomide (TMZ) and doxorubicin (DOX) at concentrations of 0.1 and 0.125% w/v respectively. The quantity of encapsulated agent was determined indirectly using UV/Vis in case of TMZ and LC-MS/MS in case of DOX. Percentages

of encapsulation efficiency (EE%) were measured for both types of loaded NGs. The calculated EE% were in average 98% in case of TMZ-loaded NGs and 90% ±8 in case of DOX-loaded NGs.

Some challenges were encountered while developing a method of analysis for DOX. DOX has a pKa equals to 8.3(168) In this acidic range of pH the molecule exists as positively charged ion due to protonation of the amino group. Our assumption is that this probably caused a complex formation between DOX and the negatively charged phosphate groups of TPP, also present in the supernatant.(169) Trying to directly quantify DOX required alkalisation of the supernatant and increasing pH to be higher than 8.3, optimally 10.5 where DOX color changes from orange to violet. At that point all the DOX is transferred to the unionized form and probably was not complexed by TPP. This is a suggested explanation which still needs experimental confirmation.

Since the effectiveness of a drug delivery system is strongly related to its long-term stability, we tried to develop a method enabling the long term storage of NGs in the solid state. Freeze-drying has been always the procedure of choice to transfer solutions and suspensions into solid products of higher stability.(124) However, to protect against the harmful stresses of freeze-drying cryoprotection using sugars of variable types and concentrations was carried out.(124) Among all the sugars investigated, ideal results, *i.e.* almost no change in size or ZP, were obtained using trehalose at 20%w/v and glucose at 10 & 20%w/v. These findings were found consistent with findings reported by others.(170)

A release study was finally designed to monitor the release behaviour of DOX from the loaded NGs before (figure 3, in the article) and after freeze-drying (figure 4, article). This study was performed at 3 different pH values (5.8, 6.8 & 7.4). The release of DOX from fresh NGs (figure 3) shows a significant responsiveness to different pH values. It was obvious that pH-

responsiveness followed the expected rule by showing higher release rates at pH 5.8 than at 6.8. However, the unexpected, even higher, release at pH 7.4 could be explained due to the sudden unprotonation of chitosan at pH higher than its pKa. Crosslinking mechanism of chitosan depends mainly on the latter being kept positively charged. Thus, an ionic interaction with negatively charged TPP is feasible. Un-protonation of chitosan at high pH values consequently lead to sudden, not gradual, un-crosslinking of chitosan polymer. This resulted in a complete loss of NGs structure followed by a full drug release. This hypothesis still needs further experiments to be confirmed. However, the steepness of the slope in Figure 4 reinforces this hypothesis. Except for our findings at pH 7.4 other results were found similar to recent results obtained for pH-triggered chitosan-based NGs.(156)

Figure 3 (article) also showed a characteristic two-plateau-effect at the three different pH values. This could be due to two phases of drug release. The first phase is due to the chitosan degradation. Since this step is pH-responsive, the drug is released at different rates which explains the difference in degrees of steepness before reaching the first plateau. The second phase of release occurs mainly due to the dissociation of internal layers of NGs which is mainly composed of hyaluronic acid. Dissolution of this polymer depends mainly on the H-bond formation. This mechanism is not pH-dependent and takes place at the same rate in the three pH values. Thus, during this phase the drug is released at the same rate in all different pH values. Studying DOX release from freeze-dried NGs, figure 4 (article), it was noticed that the two-plateau-effect disappeared and a burst effect is reached faster, within 2 hours maximum. These two findings could be explained due to the increased porosity of the lyophilisate which facilitated the water diffusion and further drug solubilisation regardless other factors. This also did not prevent the NG sensitivity to different pH values.

References

1. Gromeier M, Lachmann S, Rosenfeld MR, Gutin PH, Wimmer E. Intergeneric poliovirus recombinants for the treatment of malignant glioma. *Proceedings of the National Academy of Sciences of the United States of America*. 2000;97(12):6803-8.
2. Liu Z, Yao Z, Li C, Lu Y, Gao C. Gene Expression Profiling in Human High-Grade Astrocytomas. *Comparative and Functional Genomics*. 2011;2011.
3. Louis DN, Ohgaki H, Wiestler OD, Cavenee WK, Burger PC, Jouvet A, et al. The 2007 WHO Classification of Tumours of the Central Nervous System. *Acta Neuropathologica*. 2007;114(2):97-109.
4. R. Stupp JCTonn. High-grade malignant glioma: ESMO Clinical Practice Guidelines for diagnosis, treatment and follow-up.
5. Jackson M, Hassiotou F, Nowak A. Glioblastoma stem-like cells: At the root of tumor recurrence and a therapeutic target. *Carcinogenesis*. 2014.
6. Mason WP, Maestro RD, Eisenstat D, Forsyth P, Fulton D, Laperrière N, et al. Canadian recommendations for the treatment of glioblastoma multiforme. *Current Oncology*. 2007;14(3):110-7.
7. M. Stephen Mahaley J, Curtis Mettlin, Nachimuthu Natarajan, Edward R. Laws J, Barbara B. Peace. National survey of patterns of care for brain-tumor patients. *Journal of Neurosurgery*. 1989;71(6):826-36.
8. Ohgaki H, Dessen P, Jourde B, Horstmann S, Nishikawa T, Di Patre P-L, et al. Genetic Pathways to Glioblastoma: A Population-Based Study. *Cancer Research*. 2004;64(19):6892-9.
9. Scherer HJ. Cerebral Astrocytomas and Their Derivatives. *The American Journal of Cancer*. 1940;40(2):159-98.
10. Ohgaki H, Kleihues P. The Definition of Primary and Secondary Glioblastoma. *Clinical Cancer Research*. 2013;19(4):764-72.
11. Narahara K, Kimura S, Kikkawa K, Takahashi Y, Wakita Y, Kasai R, et al. Probable assignment of soluble isocitrate dehydrogenase (IDH1) to 2q33.3. *Human Genetics*. 1985;71(1):37-40.
12. Turcan S, Rohle D, Goenka A, Walsh LA, Fang F, Yilmaz E, et al. IDH1 mutation is sufficient to establish the glioma hypermethylator phenotype. *Nature*. 2012;483(7390):479-83.
13. Balss J, Meyer J, Mueller W, Korshunov A, Hartmann C, von Deimling A. Analysis of the IDH1 codon 132 mutation in brain tumors. *Acta Neuropathologica*. 2008;116(6):597-602.
14. Watanabe T, Nobusawa S, Kleihues P, Ohgaki H. IDH1 Mutations Are Early Events in the Development of Astrocytomas and Oligodendrogliomas. *The American Journal of Pathology*. 2009;174(4):1149-53.
15. Yan H, Parsons DW, Jin G, McLendon R, Rasheed BA, Yuan W, et al. IDH1 and IDH2 Mutations in Gliomas. *New England Journal of Medicine*. 2009;360(8):765-73.
16. Nobusawa S, Watanabe T, Kleihues P, Ohgaki H. IDH1 Mutations as Molecular Signature and Predictive Factor of Secondary Glioblastomas. *American Association for Cancer Research*. 2009;15(19):6002-7.
17. Mellai M, Caldera V, Annovazzi L, Schiffer D. The Distribution and Significance of IDH Mutations in Gliomas 2013 2013-02-27.
18. Ohgaki H. Epidemiology of Brain Tumors. In: Verma M, editor. *Cancer Epidemiology. Methods in Molecular Biology*. 472: Humana Press; 2009. p. 323-42.
19. Canadian Cancer Society SC, Provincial territorial Cancer Registries, Public Health Agency of Canada. *Canadian Cancer Statistics 2012*.
20. Glioblastoma: Alberta Health Services, CLINICAL PRACTICE GUIDELINE CNS-001

version 3; 2012. 15 p.

21. Schwartzbaum JA, Fisher JL, Aldape KD, Wrensch M. Epidemiology and molecular pathology of glioma. *Nat Clin Pract Neuro*. 2006;2(9):494-503.
22. Sizoo EM, Braam L, Postma TJ, Pasman HRW, Heimans JJ, Klein M, et al. Symptoms and problems in the end-of-life phase of high-grade glioma patients. *Neuro-Oncology*. 2010;12(11):1162-6.
23. Posti JP, Bori M, Kauko T, Sankinen M, Nordberg J, Rahi M, et al. Presenting symptoms of glioma in adults. *Acta Neurologica Scandinavica*. 2015;131(2):88-93.
24. Brat DJ, Prayson RA, Ryken TC, Olson JJ. Diagnosis of malignant glioma: role of neuropathology. *Journal of Neuro-Oncology*. 2008;89(3):287-311.
25. David Oh, Richard A. Prayson. Evaluation of Epithelial and Keratin Markers in Glioblastoma Multiforme. *Archives of Pathology & Laboratory Medicine*. 1999;123(10):917-20.
26. Beer TW, Shepherd P, Theaker JM. Ber EP4 and epithelial membrane antigen aid distinction of basal cell, squamous cell and basosquamous carcinomas of the skin. *Histopathology*. 2000;37(3):218-23.
27. Goldman LW. Principles of CT: Multislice CT. *Journal of Nuclear Medicine Technology*. 2008;36(2):57-68.
28. Achiam MP, Løgager VB, Skjoldbye B, Møller JM, Lorenzen T, Rasmussen VL, et al. Preoperative CT versus diffusion weighted magnetic resonance imaging of the liver in patients with rectal cancer; a prospective randomized trial. *PeerJ*. 2016;4:e1532.
29. Brenner DJ, Hall EJ. Computed Tomography — An Increasing Source of Radiation Exposure. *New England Journal of Medicine*. 2007;357(22):2277-84.
30. Bongartz G. Technical principles of MSCT: European Guidelines for Multislice Computed Tomography; 2004 March 2004. 13 p.
31. Pooley RA. Fundamental Physics of MR Imaging. *RadioGraphics*. 2005;25(4):1087-99.
32. Scherzinger AL, Hendee WR. Basic Principles of Magnetic Resonance Imaging—An Update. *Western Journal of Medicine*. 1985;143(6):782-92.
33. Gustav J. Strijkers WJMM, Geralda A. F. van Tilborg and Klaas Nicolay. MRI Contrast Agents: Current Status and Future Perspectives. 15 p.
34. Aime S, Castelli DD, Crich SG, Gianolio E, Terreno E. Pushing the Sensitivity Envelope of Lanthanide-Based Magnetic Resonance Imaging (MRI) Contrast Agents for Molecular Imaging Applications. *Accounts of Chemical Research*. 2009;42(7):822-31.
35. Michel Lacroix, Dima Abi-Said, Daryl R. Fourney, Ziya L. Gokaslan, Weiming Shi, Franco DeMonte, et al. A multivariate analysis of 416 patients with glioblastoma multiforme: prognosis, extent of resection, and survival. *Journal of Neurosurgery*. 2001;95(2):190-8.
36. Julka PK. Postoperative treatment of glioblastoma multiforme with radiation therapy plus concomitant and adjuvant temozolomide : A mono-institutional experience of 215 patients. *Can Res Ther*. 2013;9:381-6.
37. Walker MD, Green SB, Byar DP, Alexander E, Batzdorf U, Brooks WH, et al. Randomized Comparisons of Radiotherapy and Nitrosoureas for the Treatment of Malignant Glioma after Surgery. *New England Journal of Medicine*. 1980;303(23):1323-9.
38. Weller M, Cloughesy T, Perry JR, Wick W. Standards of care for treatment of recurrent glioblastoma—are we there yet? *Neuro-Oncology*. 2013;15(1):4-27.
39. Yung WKA, Albright RE, Olson J, Fredericks R, Fink K, Prados MD, et al. A phase II study of temozolomide vs. procarbazine in patients with glioblastoma multiforme at first relapse. *British Journal of Cancer*. 2000;83(5):588-93.
40. Brada M, Hoang-Xuan K, Rampling R, Dietrich P-Y, Dirix LY, Macdonald D, et al. Multicenter phase II trial of temozolomide in patients with glioblastoma multiforme at first relapse. *Annals of Oncology*. 2001;12(2):259-66.
41. Reithmeier T, Graf E, Piroth T, Trippel M, Pinsker M, Nikkhah G. BCNU for recurrent glioblastoma multiforme: efficacy, toxicity and prognostic factors. *BMC Cancer*. 2010;10(1):30.

42. van den Bent MJ, Brandes AA, Rampling R, Kouwenhoven MCM, Kros JM, Carpentier AF, et al. Randomized Phase II Trial of Erlotinib Versus Temozolomide or Carmustine in Recurrent Glioblastoma: EORTC Brain Tumor Group Study 26034. *Journal of Clinical Oncology*. 2009;27(8):1268-74.
43. Brandes AA, Tosoni A, Amistà P, Nicolardi L, Grosso D, Berti F, et al. How effective is BCNU in recurrent glioblastoma in the modern era?: A phase II trial. *Neurology*. 2004;63(7):1281-4.
44. Wick W, Puduvalli VK, Chamberlain MC, van den Bent MJ, Carpentier AF, Cher LM, et al. Phase III Study of Enzastaurin Compared With Lomustine in the Treatment of Recurrent Intracranial Glioblastoma. *Journal of Clinical Oncology*. 2010;28(7):1168-74.
45. Happold C, Roth P, Wick W, Steinbach J, Linnebank M, Weller M, et al. ACNU-based chemotherapy for recurrent glioma in the temozolomide era. *Journal of Neuro-Oncology*. 2009;92(1):45-8.
46. Addeo R, Caraglia M, De Santi MS, Montella L, Abbruzzese A, Parlato C, et al. A new schedule of fotemustine in temozolomide-pretreated patients with relapsing glioblastoma. *Journal of Neuro-Oncology*. 2011;102(3):417-24.
47. Fan CH, Liu WL, Cao H, Wen C, Chen L, Jiang G. O6-methylguanine DNA methyltransferase as a promising target for the treatment of temozolomide-resistant gliomas. *Cell Death Dis*. 2013;4:e876.
48. Stupp R, Hegi ME, Mason WP, van den Bent MJ, Taphoorn MJB, Janzer RC, et al. Effects of radiotherapy with concomitant and adjuvant temozolomide versus radiotherapy alone on survival in glioblastoma in a randomised phase III study: 5-year analysis of the EORTC-NCIC trial. *The Lancet Oncology*. 2009;10(5):459-66.
49. Messaoudi K, Clavreul A, Lagarce F. Toward an effective strategy in glioblastoma treatment. Part I: resistance mechanisms and strategies to overcome resistance of glioblastoma to temozolomide. *Drug Discovery Today*. 2015;20(7):899-905.
50. Franceschi E, Omuro AMP, Lassman AB, Demopoulos A, Nolan C, Abrey LE. Salvage temozolomide for prior temozolomide responders. *Cancer*. 2005;104(11):2473-6.
51. Kong, Lee, Kim, Son, Lim, Kim, et al. A pilot study of metronomic temozolomide treatment in patients with recurrent temozolomide-refractory glioblastoma. *Oncology Reports*. 2006;16(5):1117-21.
52. Berrocal A, Perez Segura P, Gil M, Balaña C, Garcia Lopez J, Yaya R, et al. Extended-schedule dose-dense temozolomide in refractory gliomas. *Journal of Neuro-Oncology*. 2010;96(3):417-22.
53. Perry JR, Bélanger K, Mason WP, Fulton D, Kavan P, Easaw J, et al. Phase II Trial of Continuous Dose-Intense Temozolomide in Recurrent Malignant Glioma: RESCUE Study. *Journal of Clinical Oncology*. 2010;28(12):2051-7.
54. Kong D-S, Lee J-I, Kim JH, Kim ST, Kim WS, Suh Y-L, et al. Phase II trial of low-dose continuous (metronomic) treatment of temozolomide for recurrent glioblastoma. *Neuro-Oncology*. 2010;12(3):289-96.
55. Norden AD, Lesser GJ, Drappatz J, Ligon KL, Hammond SN, Lee EQ, et al. Phase 2 study of dose-intense temozolomide in recurrent glioblastoma. *Neuro-Oncology*. 2013;15(7):930-5.
56. Stupp R, Mason WP, van den Bent MJ, Weller M, Fisher B, Taphoorn MJB, et al. Radiotherapy plus Concomitant and Adjuvant Temozolomide for Glioblastoma. *New England Journal of Medicine*. 2005;352(10):987-96.
57. Arcamone F, Cassinelli G, Fantini G, Grein A, Orezzi P, Pol C, et al. Adriamycin, 14-hydroxydaimomycin, a new antitumor antibiotic from *S. Peucetius* var. *caesius*. *Biotechnology and Bioengineering*. 1969;11(6):1101-10.
58. Barenholz Y. Doxil® — The first FDA-approved nano-drug: Lessons learned. *Journal of Controlled Release*. 2012;160(2):117-34.
59. O'Brien MER, Wigler N, Inbar M, Rosso R, Grischke E, Santoro A, et al. Reduced cardiotoxicity and comparable efficacy in a phase III trial of pegylated liposomal doxorubicin HCl (CAELYX™/Doxil®) versus conventional doxorubicin for first-line treatment of metastatic breast cancer. *Annals of Oncology*. 2004;15(3):440-9.

60. PubChem Compound Database; [Internet]. [cited accessed Apr. 1, 2016].
61. Rahman A, Carmichael D, Harris M, Roh JK. Comparative Pharmacokinetics of Free Doxorubicin and Doxorubicin Entrapped in Cardiolipin Liposomes. *Cancer Research*. 1986;46(5):2295-9.
62. Bigotte L, Olsson Y. Cytofluorescence localization of adriamycin in the nervous system. *Acta Neuropathologica*.58(3):193-202.
63. Gerweck LE, Seetharaman K. Cellular pH Gradient in Tumor versus Normal Tissue: Potential Exploitation for the Treatment of Cancer. *Cancer Research*. 1996;56(6):8.
64. Greish K. Enhanced permeability and retention of macromolecular drugs in solid tumors: A royal gate for targeted anticancer nanomedicines. *Journal of Drug Targeting*. 2007;15(7-8):457-64.
65. Ananda S, Nowak AK, Cher L, Dowling A, Brown C, Simes J, et al. Phase 2 trial of temozolomide and pegylated liposomal doxorubicin in the treatment of patients with glioblastoma multiforme following concurrent radiotherapy and chemotherapy. *Journal of Clinical Neuroscience*. 2011;18(11):1444-8.
66. Yousefpour P, Atyabi F, Vasheghani-Farahani E, Movahedi A-AM, Dinarvand R. Targeted delivery of doxorubicin-utilizing chitosan nanoparticles surface-functionalized with anti-Her2 trastuzumab. *International Journal of Nanomedicine*. 2011;6:1977-90.
67. Kang JH, Adamson C. Novel chemotherapeutics and other therapies for treating high-grade glioma. *Expert Opinion on Investigational Drugs*.0(0):1-19.
68. Thomas AA, Brennan CW, DeAngelis LM, Omuro AM. EMerging therapies for glioblastoma. *JAMA Neurology*. 2014;71(11):1437-44.
69. Dresemann G. Imatinib and hydroxyurea in pretreated progressive glioblastoma multiforme: a patient series. *Annals of Oncology*. 2005;16(10):1702-8.
70. Brennan CW, Verhaak RGW, McKenna A, Campos B, Noushmehr H, Salama SR, et al. The Somatic Genomic Landscape of Glioblastoma. *Cell*. 2013;155(2):462-77.
71. Ettinghausen S, Rosenberg S. The adoptive immunotherapy of cancer using lymphokine activated killer cells and recombinant interleukin-2. *Springer Semin Immunopathol*. 1986;9(1):51-71.
72. Wei J, Barr J, Kong L-Y, Wang Y, Wu A, Sharma AK, et al. Glioma associated cancer-initiating cells induce immune suppression. *Clinical cancer research : an official journal of the American Association for Cancer Research*. 2010;16(2):461-73.
73. Forrester JV, Xu H, Lambe T, Cornall R. Immune privilege or privileged immunity? *Mucosal Immunol*. 2008;1(5):372-81.
74. Stupp R, Wong ET, Kanner AA, Steinberg D, Engelhard H, Heidecke V, et al. NovoTTF-100A versus physician's choice chemotherapy in recurrent glioblastoma: A randomised phase III trial of a novel treatment modality. *European Journal of Cancer*. 2012;48(14):2192-202.
75. Swanson KD, Lok E, Wong ET. An Overview of Alternating Electric Fields Therapy (NovoTTF Therapy) for the Treatment of Malignant Glioma. *Current Neurology and Neuroscience Reports*. 2016;16:8.
76. Leweke F, Damian MS, Schindler C, Schachenmayr W. Multidrug Resistance in Glioblastoma: Chemosensitivity Testing and Immunohistochemical Demonstration of P-Glycoprotein. *Pathology - Research and Practice*. 1998;194(3):149-55.
77. Tivnan A, Zakaria Z, O'Leary C, Kogel D, Pokorny JL, Sarkaria JN, et al. Inhibition of Multidrug resistance protein 1 (MRP1) improves chemotherapy drug response in primary and recurrent glioblastoma multiforme. *Frontiers in Neuroscience*. 2015;9.
78. Loscher W, Potschka H. Drug resistance in brain diseases and the role of drug efflux transporters. *Nat Rev Neurosci*. 2005;6(8):591-602.
79. McKinnon. *Towards Precriving Practice: The blood-brain barrier*. 6 ed2007. 5:6 p.
80. Uston C. NEUROwords Dr. Thomas Willis' Famous Eponym: The Circle of Willis. *Journal of the History of the Neurosciences*. 2005;14(1):16-21.

81. Abbott NJ, Patabendige AAK, Dolman DEM, Yusof SR, Begley DJ. Structure and function of the blood–brain barrier. *Neurobiology of Disease*. 2010;37(1):13-25.
82. De Jong WH, Borm PJA. Drug delivery and nanoparticles: Applications and hazards. *International Journal of Nanomedicine*. 2008;3(2):133-49.
83. Raemdonck K, Demeester J, De Smedt S. Advanced nanogel engineering for drug delivery. *Soft Matter*. 2009;5(4):707-15.
84. Soni G, Yadav KS. Nanogels as potential nanomedicine carrier for treatment of cancer: A mini review of the state of the art. *Saudi Pharmaceutical Journal*. 2016;24(2):133-9.
85. Caraglia. *Nanotech Revolution for the Anti-Cancer Drug Delivery through Blood- Brain-Barrier*. Bentham Science. 2012;12(3):186-96.
86. Reisch A, Runser A, Arntz Y, Mély Y, Klymchenko AS. Charge-Controlled Nanoprecipitation as a Modular Approach to Ultrasmall Polymer Nanocarriers: Making Bright and Stable Nanoparticles. *ACS Nano*. 2015;9(5):5104-16.
87. Shirsat AE, Chitlange SS. Application of quality by design approach to optimize process and formulation parameters of rizatriptan loaded chitosan nanoparticles. *Journal of Advanced Pharmaceutical Technology & Research*. 2015;6(3):88-96.
88. Brunel F, Véron L, Ladavière C, David L, Domard A, Delair T. Synthesis and Structural Characterization of Chitosan Nanogels. *Langmuir*. 2009;25(16):8935-43.
89. Kiang T, Wen J, Lim HW, Leong KW. The effect of the degree of chitosan deacetylation on the efficiency of gene transfection. *Biomaterials*. 2004;25(22):5293-301.
90. Wukasz RF. *Proceedings of the 49th Industrial Waste Conference Purdue University, May 1994*: Taylor & Francis; 1994.
91. Mironov V, Kasyanov V, Zheng Shu X, Eisenberg C, Eisenberg L, Gonda S, et al. Fabrication of tubular tissue constructs by centrifugal casting of cells suspended in an in situ crosslinkable hyaluronan-gelatin hydrogel. *Biomaterials*. 2005;26(36):7628-35.
92. Tan H, Chu CR, Payne KA, Marra KG. Injectable in situ forming biodegradable chitosan–hyaluronic acid based hydrogels for cartilage tissue engineering. *Biomaterials*. 2009;30(13):2499-506.
93. Lee H, Mok H, Lee S, Oh Y-K, Park TG. Target-specific intracellular delivery of siRNA using degradable hyaluronic acid nanogels. *Journal of Controlled Release*. 2007;119(2):245-52.
94. Mohanraj. Nanoparticles—a review. *Tropical Journal of Pharmaceutical Research*. 2006;5:561-73.
95. Yu MK, Park J, Jon S. Targeting Strategies for Multifunctional Nanoparticles in Cancer Imaging and Therapy. *Theranostics*. 2012;2(1):3-44.
96. Ghaz-Jahanian M, Abbaspour-Aghdam F, Anarjan N, Berenjian A, Jafarizadeh-Malmiri H. Application of Chitosan-Based Nanocarriers in Tumor-Targeted Drug Delivery. *Mol Biotechnol*. 2015;57(3):201-18.
97. Prabhakar U, Maeda H, Jain RK, Sevick-Muraca EM, Zamboni W, Farokhzad OC, et al. Challenges and key considerations of the enhanced permeability and retention (EPR) effect for nanomedicine drug delivery in oncology. *Cancer research*. 2013;73(8):2412-7.
98. Bae YH, Park K. Targeted drug delivery to tumors: Myths, reality and possibility. *Journal of Controlled Release*. 2011;153(3):198-205.
99. Di Marco M, Sadun C, Port M, Guilbert I, Couvreur P, Dubernet C. Physicochemical characterization of ultrasmall superparamagnetic iron oxide particles (USPIO) for biomedical application as MRI contrast agents. *International Journal of Nanomedicine*. 2007;2(4):609-22.
100. Lammers T, Koczera P, Fokong S, Gremse F, Ehling J, Vogt M, et al. Theranostic USPIO-Loaded Microbubbles for Mediating and Monitoring Blood-Brain Barrier Permeation. *Advanced functional materials*. 2015;25(1):36-43.
101. Liang X-J, Chen C, Zhao Y, Wang PC. Circumventing Tumor Resistance to Chemotherapy by Nanotechnology. *Methods in molecular biology (Clifton, NJ)*. 2010;596:467-88.

102. Merisko-Liversidge EM, Liversidge GG. Drug Nanoparticles: Formulating Poorly Water-Soluble Compounds. *Toxicologic Pathology*. 2008;36(1):43-8.
103. Lu J, Liong M, Zink JJ, Tamanoi F. Mesoporous Silica Nanoparticles as a Delivery System for Hydrophobic Anticancer Drugs. *Small*. 2007;3(8):1341-6.
104. Park JH, Saravanakumar G, Kim K, Kwon IC. Targeted delivery of low molecular drugs using chitosan and its derivatives. *Advanced Drug Delivery Reviews*. 2010;62(1):28-41.
105. Chan M, Almutairi A. Nanogels as imaging agents for modalities spanning the electromagnetic spectrum. *Materials Horizons*. 2016;3(1):21-40.
106. Sierra-Martin B, Fernandez-Barbero A. Multifunctional hybrid nanogels for theranostic applications. *Soft Matter*. 2015;11(42):8205-16.
107. Feng C, Sun G, Wang Z, Cheng X, Park H, Cha D, et al. Transport mechanism of doxorubicin loaded chitosan based nanogels across intestinal epithelium. *European Journal of Pharmaceutics and Biopharmaceutics*. 2014;87(1):197-207.
108. Azadi A, Rouini M-R, Hamidi M. Neuropharmacokinetic evaluation of methotrexate-loaded chitosan nanogels. *International Journal of Biological Macromolecules*. 2015;79:326-35.
109. Das D, Patra P, Ghosh P, Rameshbabu AP, Dhara S, Pal S. Dextrin and poly(lactide)-based biocompatible and biodegradable nanogel for cancer targeted delivery of doxorubicin hydrochloride. *Polymer Chemistry*. 2016.
110. Kapse-Mistry S, Govender T, Srivastava R, Yergeri M. Nanodrug delivery in reversing multidrug resistance in cancer cells. *Frontiers in Pharmacology*. 2014;5:159.
111. Unsoy G, Khodadust R, Yalcin S, Mutlu P, Gunduz U. Synthesis of Doxorubicin loaded magnetic chitosan nanoparticles for pH responsive targeted drug delivery. *European Journal of Pharmaceutical Sciences*. 2014;62:243-50.
112. Fang C, Wang K, Stephen ZR, Mu Q, Kievit FM, Chiu DT, et al. Temozolomide Nanoparticles for Targeted Glioblastoma Therapy. *ACS Applied Materials & Interfaces*. 2015;7(12):6674-82.
113. Kelkar SS, Reineke TM. Theranostics: Combining Imaging and Therapy. *Bioconjugate Chemistry*. 2011;22(10):1879-903.
114. Wang C, Ravi S, Garapati US, Das M, Howell M, MallelaMallela J, et al. Multifunctional Chitosan Magnetic-Graphene (CMG) Nanoparticles: a Theranostic Platform for Tumor-targeted Co-delivery of Drugs, Genes and MRI Contrast Agents. *Journal of materials chemistry B, Materials for biology and medicine*. 2013;1(35):4396-405.
115. Cavalli R, Argenziano M, Vigna E, Giustetto P, Torres E, Aime S, et al. Preparation and in vitro characterization of chitosan nanobubbles as theranostic agents. *Colloids and Surfaces B: Biointerfaces*. 2015;129:39-46.
116. Pecora R. Dynamic Light Scattering Measurement of Nanometer Particles in Liquids. *Journal of Nanoparticle Research*. 2000;2(2):123-31.
117. Goodman JW. Some fundamental properties of speckle*. *J Opt Soc Am*. 1976;66(11):1145-50.
118. Josefowicz J, Hallett FR. Homodyne Electrophoretic Light Scattering of Polystyrene Spheres by Laser Cross-Beam Intensity Correlation. *Appl Opt*. 1975;14(3):740-2.
119. Privalov PL, Potekhin SA. Scanning microcalorimetry in studying temperature-induced changes in proteins. *Methods Enzymol*. 1986;131:4-51.
120. Haines PJ, Reading M, Wilburn FW. Chapter 5 - Differential Thermal Analysis and Differential Scanning Calorimetry. In: Michael EB, editor. *Handbook of Thermal Analysis and Calorimetry*. Volume 1: Elsevier Science B.V.; 1998. p. 279-361.
121. Gill P, Moghadam TT, Ranjbar B. Differential Scanning Calorimetry Techniques: Applications in Biology and Nanoscience. *Journal of Biomolecular Techniques : JBT*. 2010;21(4):167-93.
122. Hariharan P, Hariharan P. 16 - Fourier Transform Spectroscopy. *Basics of Interferometry (Second edition)*. Burlington: Academic Press; 2007. p. 145-51.

123. Griffiths PR, De Haseth JA, Winefordner JD. *Fourier Transform Infrared Spectrometry*: Wiley; 2007.
124. Abdelwahed W, Degobert G, Stainmesse S, Fessi H. Freeze-drying of nanoparticles: Formulation, process and storage considerations. *Adv Drug Delivery Rev.* 2006;58(15):1688-713.
125. Lee MK, Kim MY, Kim S, Lee J. Cryoprotectants for freeze drying of drug nano-suspensions: Effect of freezing rate. *Journal of Pharmaceutical Sciences.* 2009;98(12):4808-17.
126. Fonte P, Soares S, Costa A, Andrade JC, Seabra V, Reis S, et al. Effect of cryoprotectants on the porosity and stability of insulin-loaded PLGA nanoparticles after freeze-drying. *Biomater.* 2012;2(4):329-39.
127. Kumar S, Gokhale R, Burgess DJ. Sugars as bulking agents to prevent nano-crystal aggregation during spray or freeze-drying. *Int J Pharm.* 2014;471(1–2):303-11.
128. Michael JP. *Mechanisms of Protein Stabilization during Freeze-Drying and Storage. Freeze-Drying/Lyophilization Of Pharmaceutical & Biological Products, Third Edition. Drugs and the Pharmaceutical Sciences: Informa Healthcare; 2004.*
129. Courant T, Roullin VG, Cadiou C, Callewaert M, Andry MC, Portefaix C, et al. Hydrogels Incorporating GdDOTA: Towards Highly Efficient Dual T1/T2 MRI Contrast Agents. *Angewandte Chemie International Edition.* 2012;51(36):9119-22.
130. Arcamone F, Cassinelli G, Fantini G, Grein A, Orezzi P, Pol C, et al. Adriamycin, 14-Hydroxydaunomycin, a new antitumor antibiotic from *S. peucetius* var. *caesius*. *Biotechnology and Bioengineering.* 2000;67(6):704-13.
131. Bigotte L, Olsson Y. Cytofluorescence localization of adriamycin in the nervous system. *Acta Neuropathol.* 1982;58(3):193-202.
132. Xiao S, Castro R, Maciel D, Gonçalves M, Shi X, Rodrigues J, et al. Fine tuning of the pH-sensitivity of laponite–doxorubicin nanohybrids by polyelectrolyte multilayer coating. *Materials Science and Engineering: C.* 2016;60:348-56.
133. Wang Y, Qin F, Tan H, Zhang Y, Jiang M, Lu M, et al. pH-responsive glycol chitosan-cross-linked carboxymethyl- β -cyclodextrin nanoparticles for controlled release of anticancer drugs. *International Journal of Nanomedicine.* 2015;10:7359-70.
134. Scheeren LE, Nogueira DR, Macedo LB, Vinardell MP, Mitjans M, Infante MR, et al. PEGylated and poloxamer-modified chitosan nanoparticles incorporating a lysine-based surfactant for pH-triggered doxorubicin release. *Colloids and Surfaces B: Biointerfaces.* 2016;138:117-27.
135. Chatelet C, Damour O, Domard A. Influence of the degree of acetylation on some biological properties of chitosan films. *Biomaterials.* 2001;22(3):261-8.
136. Almalik A, Donno R, Cadman CJ, Cellesi F, Day PJ, Tirelli N. Hyaluronic acid-coated chitosan nanoparticles: Molecular weight-dependent effects on morphology and hyaluronic acid presentation. *Journal of Controlled Release.* 2013;172(3):1142-50.
137. Lim C, Lee DW, Israelachvili JN, Jho Y, Hwang DS. Contact time- and pH-dependent adhesion and cohesion of low molecular weight chitosan coated surfaces. *Carbohydrate Polymers.* 2015;117:887-94.
138. Lee DW, Lim C, Israelachvili JN, Hwang DS. Strong adhesion and cohesion of chitosan in aqueous solutions. *Langmuir : the ACS journal of surfaces and colloids.* 2013;29(46):14222-9.
139. Jain A, Thakur K, Sharma G, Kush P, Jain UK. Fabrication, characterization and cytotoxicity studies of ionically cross-linked docetaxel loaded chitosan nanoparticles. *Carbohydrate Polymers.* 2016;137:65-74.
140. Jonassen H, Kjøniksen A-L, Hiorth M. Stability of Chitosan Nanoparticles Cross-Linked with Tripolyphosphate. *Biomacromolecules.* 2012;13(11):3747-56.
141. Soni G, Yadav KS. Nanogels as potential nanomedicine carrier for treatment of cancer: A mini review of the state of the art. *Saudi Pharmaceutical Journal.*

142. Fonte P, Soares S, Sousa F, Costa A, Seabra V, Reis S, et al. Stability Study Perspective of the Effect of Freeze-Drying Using Cryoprotectants on the Structure of Insulin Loaded into PLGA Nanoparticles. *Biomacromolecules*. 2014;15(10):3753-65.
143. Kevin ST, Sarah MH, Erik MS. The effect of cryoprotection on the use of PLGA encapsulated iron oxide nanoparticles for magnetic cell labeling. *Nanotechnology*. 2013;24(12):125101.
144. Keusters L, Stolk LML, Umans R, van Asten P. Stability of solutions of doxorubicin and epirubicin in plastic minibags for intravesical use after storage at -20° C and thawing by microwave radiation. *Pharmaceutisch Weekblad Scientific Edition*. 1986;8(3):194-7.
145. Cielecka-Piontek J, Jelińska A, Zajac M, Sobczak M, Bartold A, Oszczapowicz I. A comparison of the stability of doxorubicin and daunorubicin in solid state. *Journal of Pharmaceutical and Biomedical Analysis*. 2009;50(4):576-9.
146. Siepmann J, Siepmann F. Mathematical modeling of drug delivery. *Int J Pharm*. 2008;364(2):328-43.
147. Artech Pujana M, Pérez-Álvarez L, Cesteros Iturbe LC, Katime I. pH-sensitive chitosan-folate nanogels crosslinked with biocompatible dicarboxylic acids. *European Polymer Journal*. 2014;61:215-25.
148. Saravanabhavan SS, Bose R, Skylab S, Dharmalingam S. Fabrication of Chitosan/TPP Nano Particles as a Carrier Towards the Treatment of Cancer. 2013. 2013;5(1):8.
149. Amidi M, Mastrobattista E, Jiskoot W, Hennink WE. Chitosan-based delivery systems for protein therapeutics and antigens. *Adv Drug Delivery Rev*. 2010;62(1):59-82.
150. Janes KA, Fresneau MP, Marazuela A, Fabra A, Alonso MaJ. Chitosan nanoparticles as delivery systems for doxorubicin. *Journal of Controlled Release*. 2001;73(2-3):255-67.
151. Nam J-P, Lee K-J, Choi J-W, Yun C-O, Nah J-W. Targeting delivery of tocopherol and doxorubicin grafted-chitosan polymeric micelles for cancer therapy: In vitro and in vivo evaluation. *Colloids and Surfaces B: Biointerfaces*. 2015;133:254-62.
152. Jain NK, Jain SK. Development and In Vitro Characterization of Galactosylated Low Molecular Weight Chitosan Nanoparticles Bearing Doxorubicin. *AAPS PharmSciTech*. 2010;11(2):686-97.
153. Mitra S, Gaur U, Ghosh PC, Maitra AN. Tumour targeted delivery of encapsulated dextran-doxorubicin conjugate using chitosan nanoparticles as carrier. *Journal of Controlled Release*. 2001;74(1-3):317-23.
154. Elgadir MA, Uddin MS, Ferdosh S, Adam A, Chowdhury AJK, Sarker MZI. Impact of chitosan composites and chitosan nanoparticle composites on various drug delivery systems: A review. *Journal of Food and Drug Analysis*. 2015;23(4):619-29.
155. Al-Qadi S, Alatorre-Meda M, Martin-Pastor M, Taboada P, Remuñán-López C. The role of hyaluronic acid inclusion on the energetics of encapsulation and release of a protein molecule from chitosan-based nanoparticles. *Colloids and Surfaces B: Biointerfaces*. 2016;141:223-32.
156. Sadighian S, Hosseini-Monfared H, Rostamizadeh K, Hamidi M. pH-Triggered Magnetic-Chitosan Nanogels (MCNs) For Doxorubicin Delivery: Physically vs. Chemically Cross Linking Approach. *Advanced Pharmaceutical Bulletin*. 2015;5(1):115-20.
157. Guinesi LS, Cavalheiro ÉTG. The use of DSC curves to determine the acetylation degree of chitin/chitosan samples. *Thermochimica Acta*. 2006;444(2):128-33.
158. Chen G, Wang W. Role of Freeze Drying in Nanotechnology. *Drying Technology*. 2007;25(1):29-35.
159. Manchun S, Dass CR, Sriamornsak P. Stability of freeze-dried pH-responsive dextrin nanogels containing doxorubicin. *Asian Journal of Pharmaceutical Sciences*.
160. Daoud-Mahammed S, Couvreur P, Gref R. Novel self-assembling nanogels: Stability and lyophilisation studies. *Int J Pharm*. 2007;332(1-2):185-91.
161. Wang Y, Conway BR, Suppasansatorn P. Synthesis of temozolomide esters as potent anticancer pro-drugs for topical and transdermal applications in treatments of cancers. *Google Patents*; 2007.

162. Ananta JS, Paulmurugan R, Massoud TF. Temozolomide-loaded PLGA nanoparticles to treat glioblastoma cells: a biophysical and cell culture evaluation. *Neurological Research*. 2016;38(1):51-9.
163. Bakhru SH AE, Highley C, Delubac D, Suhan J, Hitchens TK, Ho C, Zappe S. Enhanced cellular uptake and long-term retention of chitosan-modified iron-oxide nanoparticles for MRI-based cell tracking. *International Journal of Nanomedicine*. 2012;2012(7):4613—23.
164. Zhao L-M, Shi L-E, Zhang Z-L, Chen J-M, Shi D-D, Yang J, et al. Preparation and application of chitosan nanoparticles and nanofibers. *Brazilian Journal of Chemical Engineering*. 2011;28:353-62.
165. Rampino A, Borgogna M, Blasi P, Bellich B, Cesàro A. Chitosan nanoparticles: Preparation, size evolution and stability. *International Journal of Pharmaceutics*. 2013;455(1–2):219-28.
166. Gulati N, Nagaich U, Saraf SA. Intranasal Delivery of Chitosan Nanoparticles for Migraine Therapy. *Scientia Pharmaceutica*. 2013;81(3):843-54.
167. Nallamuthu I, Devi A, Khanum F. Chlorogenic acid loaded chitosan nanoparticles with sustained release property, retained antioxidant activity and enhanced bioavailability. *Asian Journal of Pharmaceutical Sciences*. 2015;10(3):203-11.
168. Sanson C, Schatz C, Le Meins J-F, Soum A, Thévenot J, Garanger E, et al. A simple method to achieve high doxorubicin loading in biodegradable polymersomes. *Journal of Controlled Release*. 2010;147(3):428-35.
169. Masarudin MJ, Cutts SM, Evison BJ, Phillips DR, Pigram PJ. Factors determining the stability, size distribution, and cellular accumulation of small, monodisperse chitosan nanoparticles as candidate vectors for anticancer drug delivery: application to the passive encapsulation of [(14)C]-doxorubicin. *Nanotechnology, Science and Applications*. 2015;8:67-80.
170. Veilleux D, Nelea M, Biniecki K, Lavertu M, Buschmann MD. Preparation of Concentrated Chitosan/DNA Nanoparticle Formulations by Lyophilization for Gene Delivery at Clinically Relevant Dosages. *Journal of Pharmaceutical Sciences*. 2016;105(1):88-96.
171. Danhier F, Messaoudi K, Lemaire L, Benoit J-P, Lagarce F. Combined anti-Galectin-1 and anti-EGFR siRNA-loaded chitosan-lipid nanocapsules decrease temozolomide resistance in glioblastoma: In vivo evaluation. *Int J Pharm*. 2015;481(1–2):154-61.
172. Gautier J, Allard-Vannier E, Burlaud-Gaillard J, Domenech J, Chourpa I. Efficacy and Hemotoxicity of Stealth Doxorubicin-Loaded Magnetic Nanovectors on Breast Cancer Xenografts. *Journal of Biomedical Nanotechnology*. 2015;11(1):177-89.
173. Maxim S, Gabriele M. Recent Developments of Magnetic Nanoparticles for Theranostics of Brain Tumor. *Current Drug Metabolism*. 2016;17(8):737-44.

Conclusion

The following is an explanation of what have been achieved throughout this project based on a comparison with our objectives:

Objective 1: Synthesizing drug- (DOX)-loaded NGs and determining their physicochemical characteristics:

Both blank and DOX-loaded NGs were synthesized and optimized for their size, PDI and ZP. Where the synthesis process was done by the ionic gelation method and the characterization was done by DLS/ELS techniques. In other literature presenting loading of DOX into chitosan nanoparticles, DOX is either grafted to the polymeric backbone of chitosan,(151) or complexed within the nanogels. The two approaches produced efficient loadings but also resulted in various release kinetics ranging from a few minutes to several hours.(150, 152) A major risk of these systems is their lack of biocompatibility in each process step (use of toxic solvents or high amounts of emulsifiers for instance). In this view, ionic gelation is preferable since it involves mild aqueous conditions.(153) However, the sole use of chitosan and TPP does not allow the efficient retention of DOX into nanogels and a polyanion has to be included into the formulation.(150) Therefore we chose to investigate the encapsulation of DOX into chitosan / hyaluronic acid / TPP nanogels which were successfully used with other molecules.(154) The encapsulation of DOX through ionic gelation resulted in an increase in hydrodynamic diameter and surface charge, but almost no significant changes in the nanoparticle size distribution. The zeta potential results showed that a significant part of DOX is entrapped at the nanogel surface since after purification, a markedly more positive surface charge is observed. These physicochemical

characteristics were noticed to be higher than others reported recently and suggest better particle stability in terms of surface charge.(155) Generally, our NGs exhibited particle sizes which were smaller and also more uniform with a PDI of 0.27 after purification. Encapsulation efficiency values were found to be slightly higher than those obtained for chitosan/TPP alone (156) or chitosan/carboxymethyl chitosan nanogels.(107)

Preliminary less intensive studies were performed, at the end, to synthesize TMZ-loaded NGs and characterize them. TMZ was different from chitosan in that better results obtained when changing the sequence of addition and using LMW-CH instead of the MMW-CH used to synthesize DOX-loaded NGs. Higher loading efficiency results were observed when TMZ was added to the TPP/HA phase. Only the PDI was slightly higher compared to what was obtained with DOX-loaded NGs. When relatively higher molecular weight CH was used (e.g. medium MW), aggregates appeared. Compared to other literature we found that a recent study still preferred using LMW of chitosan to encapsulate TMZ.(171) Although this was for the purpose of not forming a stable complex with siRNA rather than to improve the physicochemical characteristics of TMZ-loaded NGs, the overall results were satisfactory in terms of size, PDI and Zp.

Objective 2: Studying release profile of DOX from NGs before and after freeze-drying:

Using both fresh and freeze-dried NGs, DOX release profiles from both of them were compared at three different pH values 5.8, 6.8 and 7.4. It is generally suggested that acidic media enhance the swelling of pH-responsive chitosan nanogels and, as a consequence, the drug release from these nanogels is enhanced at lower pH values.(156) This is a remarkable note as those systems could accelerate the release of their loaded drugs into intratumoral space or even into the cytosol of tumor cells. However, when it comes to the ionically crosslinked

chitosan/TPP-based nanogels this fact seems to be controversial. Using TPP solely as a crosslinker, Jane *et al.* found that DOX was released in a very fast manner (≤ 15 min) in phosphate buffer pH 7.4.(150) Similar trend was observed in our results where 100% of DOX was released within the first four hours (Fig. 3). The crosslinking between the negatively charged TPP and HA and the positively-charged DOX and CH mainly depends on chitosan being kept positively charged with protonated amino groups available for ionic interactions. At neutral pH 7.4 this protonation as well as the crosslinking are less than in case of acidic pH, so the drug fails to be retained inside the nanogels.

Objective 3: Preliminary trials to synthesize theranostic NGs:

Theranostic NGs seemed feasible to be synthesized, however less well optimized, by co-encapsulating a contrast agent USPIO either with DOX or TMZ into chitosan-based NGs. The synthesis was still done by ionic gelation technique and the resulting NGs were also characterized by DLS/ELS techniques. Larger size of NPs were observed when we tried to encapsulate USPIO, either alone or in combination with DOX or TMZ, into chitosan NGs. The co-existence of free un-encapsulated USPIO lead to significantly high PDI values. Comparing the size of our USPIO-loaded chitosan NGs to results from other literature we found that small sizes were obtained when trying to graft, by Schmidt chemical reaction, the USPIO NPs to the chitosan polymer. This approach mandates the use of hazardous materials like sodium azide and sulfuric acid.(163) We believe that optimal sizes can still be reached, while concurrently maintaining biocompatibility, by means of either concentration or molecular weight adjustment of the chitosan polymer. An increase in the sonication force have not yet been tried and can have an impact on both decreasing the size and PDI of USPIO-loaded chitosan NGs. Although the simultaneous delivery of both DOX

and a diagnostic agent was mainly synthesized as nanovectors rather than by encapsulation, the pegylation of SPIONs (supra para magnetic iron oxide nanoparticles), seems promising to our future work.(172) Since the core of chitosan-based nanoparticles is hydrophilic the pegylated surface of USPIO makes it more hydrophilic and favouring to stay inside the NGs core. Thus, increasing the loading efficiency as well as improving PDI results because less free USPIO will be left un-encapsulated. Theranostic NPs using TMZ and USPIO resulted in almost similar findings when we synthesized DOX/USPIO NPs. Results of TMZ/USPIO loaded NPs remained high in terms of size and PDI. Comparing this to other literature we found that good physicochemical characteristics, yet poor loading efficiencies were obtained when TMZ was coencapsulated with SPIOs into PLGA NPs rather than chitosan-based ones.(173) Further investigation of TMZ/USPIO theranostic chitosan NPs are necessary to achieve both high EE% and optimum physicochemical characteristics.

Prespectives

Many steps still await to be taken in order to unravel the capabilities of polymeric theranostic NGs among them are:

- 1- TMZ-loaded Chitosan NGs as well as theranostic NGs of USPIO with either DOX or TMZ still need in terms of their physicochemical characteristics.
- 2- The synthesized DOX-loaded NGs need to be tested for their cytotoxic effects using GBM cells.
- 3- USPIO-loaded NGs are to be tested for their diagnostic effects using relaxometric techniques.
- 4- Further studies required to understand the behaviour of DOX release at pH 7.4

- 5- Release kinetics to perform for TMZ-loaded NGs as well as any theranostic NGs to be synthesized in the future.